Aus der

Klinik und Poliklinik für Psychiatrie und Psychotherapie

Klinikum der Ludwig-Maximilians-Universität München

Untersuchung der oligodendroglialen Beiträge zu Störungen der weißen Substanz in der Schizophrenie mit Hilfe von patientenzentrierten, stammzellbasierten, neurobiologischen Testsystemen

Dissertation

zum Erwerb des Doktorgrades der Medizin

an der Medizinischen Fakultät

der Ludwig-Maximilians-Universität München

vorgelegt von

aus

Jan Benedikt Waldeck

Jahr

2026

Mit Genehmigung der Medizinischen Fakultät der
Ludwig-Maximilians-Universität München

Erstes Gutachten:	Prof. Dr. Andrea Schmitt
Zweites Gutachten:	Priv. Doz. Dr. Dietmar Spengler
Drittes Gutachten:	Prof. Dr. Dominik Paquet

Dekan: Prof. Dr. med. Thomas Gudermann

Tag der mündlichen Prüfung: 11.03.2026

Eidesstattliche Versicherung

Waldeck, Jan Benedikt

Name, Vorname

Ich erkläre hiermit an Eides statt, dass ich die vorliegende Dissertation mit dem Titel

Untersuchung der oligodendroglialen Beiträge zu Störungen der weißen Substanz in der Schizophrenie mit Hilfe von patientenzentrierten, stammzellbasierten, neurobiologischen Testsystemen

selbständig verfasst, mich außer der angegebenen keiner weiteren Hilfsmittel bedient und alle Erkenntnisse, die aus dem Schrifttum ganz oder annähernd übernommen sind, als solche kenntlich gemacht und nach ihrer Herkunft unter Bezeichnung der Fundstelle einzeln nachgewiesen habe.

Ich erkläre des Weiteren, dass die hier vorgelegte Dissertation nicht in gleicher oder in ähnlicher Form bei einer anderen Stelle zur Erlangung eines akademischen Grades eingereicht wurde.

München, 22.08.2025

Ort, Datum

Jan Benedikt Waldeck

Unterschrift Jan Benedikt Waldeck

LMU LUDWIG-MAXIMILIANS-UNIVERSITÄT MÜNCHEN

Dekanat Medizinische Fakultät
Promotionsbüro

Erklärung zur Übereinstimmung der gebundenen Ausgabe der Dissertation mit der elektronischen Fassung

Waldeck, Jan Benedikt

Name, Vorname

Hiermit erkläre ich, dass die elektronische Version der eingereichten Dissertation mit dem Titel:

Untersuchung der oligodendroglialen Beiträge zu Störungen der weißen Substanz in der Schizophrenie mit Hilfe von patientenzentrierten, stammzellbasierten, neurobiologischen Testsystemen

in Inhalt und Formatierung mit den gedruckten und gebundenen Exemplaren übereinstimmt.

München, 22.08.2025

Ort, Datum

Jan Benedikt Waldeck

Unterschrift Jan Benedikt Waldeck

Inhaltsverzeichnis

Abkürzungsverzeichnis

Ein Abkürzungsverzeichnis kann dem Leser dabei helfen, spezifische Abkürzungen besser zu verstehen und ggf. hier nachzuschlagen. Es empfiehlt sich vor allem dann, wenn zahlreiche Abkürzungen verwendet werden.

DTI = Diffusions-Tensor-Bildgebung

FA = Fraktionelle Anisotropie

GWAS = Genomweite Assoziationsstudien

hiPSC = human induzierte pluripotente Stammzellen

ICC = Immunzytochemie

iOLs = induzierte reife Oligodendrozyten

iOPCs = induzierte Oligodendrozyten-Vorläuferzellen

MAGMA = Multi-marker Analysis of GenoMic Annotation

MBP = myelin basic protein

MRT = Magnetresonanztomographie

O4 = surface antigen

OLs = reife Oligodendrozyten

OPCs = Oligodendrozyten-Vorläuferzellen

scRNAseq = single cell RNA sequencing

snRNAseq = single nucleus RNA sequencing

SON = Abbreviation for transcription factors including
S = SOX10 = SRY-box 10
O = OLIG2 = oligodendrocyte transcription factor 2
N = NKX6.2 = NK6 homeobox 2

SZ = Schizophrenie

WM = Weiße Substanz

Publikationsliste

Raabe FJ, Stephan M, **Waldeck JB**, …, Schmitt A, Falkai P, Rossner MJ. *Expression of Lineage Transcription Factors Identifies Differences in Transition States of Induced Human Oligodendrocyte Differentiation.* Cells. 2022; 11(2). doi:10.3390/cells11020241

Chang MH*, **Waldeck JB***, Stephan M, …, Falkai P, Rossner MJ, Raabe FJ. *iPSC-modelling reveals genetic associations and morphological alterations of oligodendrocytes in schizophrenia.* Translational Psychiatry. 2025;15(1):287. https://doi.org/10.1038/s41398-025-03509-x **(geteilter Erstautor)**

1. Einleitung

1.1 Hintergrund und Stand der Forschung

1.1.1 Hintergrund

Definition: Schizophrenie (SZ) ist eine schwerwiegende, chronische und in der Regel stark beeinträchtigende neuropsychiatrische Störung, von der schätzungsweise 0,3-0,8% der Weltbevölkerung betroffen sind (1). Sie stellt eine erhebliche Belastung für den Einzelnen, die Angehörigen und die Gesellschaft dar und gehört weltweit zu den häufigsten Ursachen für Behinderungen (2). Die mit der SZ verbundene wirtschaftliche Belastung ist beträchtlich, wobei die jährlichen Kosten je nach Land zwischen 94 Millionen und 102 Milliarden US-Dollar liegen (3). Das klinische Erscheinungsbild ist in der Regel heterogen und umfasst Positivsymptome wie Halluzinationen und Wahnvorstellungen, Negativsymptome wie Affektverflachung, Anhedonie und sozialen Rückzug sowie tiefgreifende kognitive Defizite, die Aufmerksamkeit, Gedächtnis und Exekutivfunktionen beeinträchtigen (4). Aktuelle antipsychotische Medikamente können die positiven Symptome effektiv verbessern (5), wohingegen die negativen und kognitiven Symptome weiterhin eine große therapeutische Herausforderung darstellen (6). Diese unbehandelten Symptome beeinträchtigen jedoch maßgeblich die Lebensqualität der Patienten, da sie deren Fähigkeit zur gesellschaftlichen Teilhabe und beruflichen Integration erheblich einschränken (7, 8).

Ätiologie: Trotz mehr als einem Jahrhundert intensiver Forschung sind die genaue Ätiologie und Pathophysiologie der SZ nach wie vor nicht vollständig geklärt (9). Konsens herrscht darüber, dass es sich um eine komplexe, multifaktorielle Störung handelt (10). Diese resultiert aus dem Zusammenspiel genetischer Prädispositionen sowie verschiedener Umwelteinflüsse, die über die gesamte Lebensspanne die Gehirnentwicklung und -funktion beeinträchtigen (4, 11-13) . Neben lange postulierten neuronalen Dysfunktionen deuten Befunde zunehmend auf die Beteiligung weiterer zellulärer Systeme und struktureller Veränderungen im Gehirn hin (10).

Ziel der vorliegenden Arbeit ist es, das zelluläre und neurobiologische Verständnis der Entstehung kognitiver Symptome bei Schizophrenie zu erweitern. Der Fokus liegt dabei auf Störungen der weißen Substanz und ihrer myelinbildenden Zellen, den Oligodendrozyten. Diese gelten neben neuronalen Mechanismen als mitursächlich für die genannten Symptome. Die Ergebnisse dieser Arbeit könnten die Entwicklung neuer therapeutischer Ansätze ermöglichen und so zu einer Verbesserung der Lebensqualität Betroffener beitragen.

1.1.2 Stand der Forschung

Imaging (DTI): Konvergierende Erkenntnisse aus Neuroimaging-Studien deuten darauf hin, dass Anomalien in der Struktur und Integrität der weißen Substanz (WM) des Gehirns ein zentrales neuropathologisches Merkmal der SZ sind (14, 15). Techniken wie die Diffusions-Tensor-Bildgebung (DTI) zeigen bei Personen mit SZ im Vergleich zu gesunden Kontrollpersonen eine in zahlreichen Faserbahnen beobachtete Verringerung der fraktionierten Anisotropie (FA) – ein Maß für die Kohärenz und Organisation der WM-Bahnen (15-18).

Wichtig ist, dass diese WM-Veränderungen bereits in einem frühen Stadium der Erkrankung auftreten, schon bei Patienten mit der ersten Episode nachweisbar sind und signifikant mit der Schwere der kognitiven Beeinträchtigungen korrelieren (19-21). So wurde in einer Vielzahl von Studien ein direkter Zusammenhang zwischen der mikro- und makrostrukturellen Integrität der WM und der Leistung bei verschiedenen kognitiven Aufgaben bei Menschen mit SZ festgestellt (18, 22-25). Es wird vermutet, dass die kognitiven Defizite auf eine verlangsamte Verarbeitungsgeschwindigkeit und Störungen der Mikro- und Makrokonnektivität unterschiedlicher Gehirnareale zurückzuführen sind (19, 26).

Die Konsistenz dieser Ergebnisse deutet darauf hin, dass die Störung der weißen Substanz ein entscheidendes neurobiologisches Substrat darstellt, das zur kognitiven Symptomatik der SZ beiträgt.

Weiße Substanz und Oligodendrozyten: Um die zellulären Grundlagen dieser Beeinträchtigung zu verstehen, muss die Struktur der weißen Substanz genauer betrachtet werden. Der Hauptbestandteil der weißen Substanz des zentralen Nervensystems ist Myelin, das von spezialisierten Gliazellen, den Oligodendrozyten (OLs), gebildet wird (27). OLs bilden Fortsätze aus, die sich um neuronale Axone wickeln und die mehrschichtige, lipidreiche Myelinscheide bilden. Diese Hülle fungiert als elektrischer Isolator, was die schnelle saltatorische Leitung von Aktionspotenzialen erleichtert und die Konnektivität sowie die effektive Informationsverarbeitung zwischen verschiedenen Gehirnregionen begünstigt (28).

Neben ihrer zentralen Funktion der Myelinisierung, beeinflussen Oligodendrozyten zudem den neuronalen Energiestoffwechsel, die neuronale Erregbarkeit und Plastizität (28-30). Durch diese Prozesse sind Oligodendrozyten maßgeblich an kognitiven Prozessen wie Lernen und Gedächtniskonsolidierung beteiligt (31).

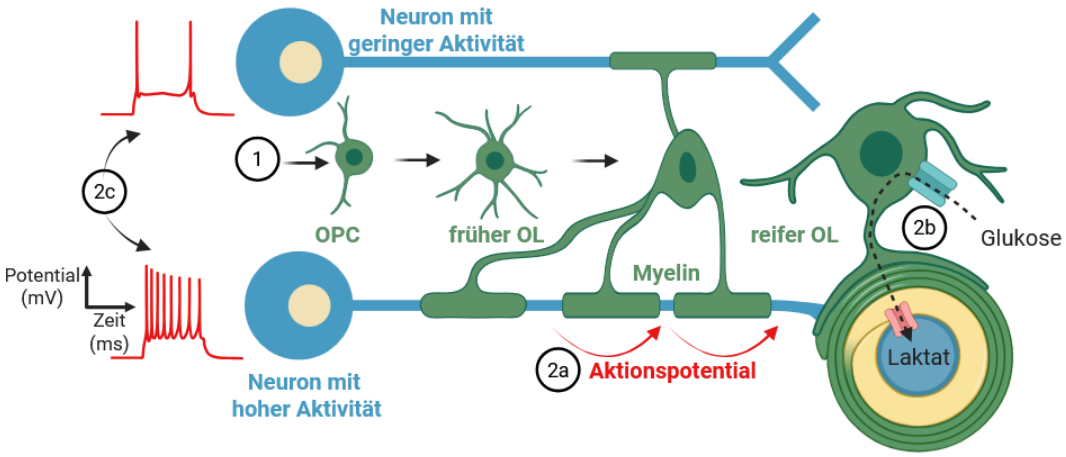

Abbildung 1: Differenzierung und Funktion von Oligodendroglia. (1) Schematischer Überblick der Entwicklung von einer Oligodendrozyten-Vorläuferzelle (OPC) über einen frühen Oligodendrozyten (OL) zu einem reifen, myelinisierenden Oligodendrozyten. Zu den Schlüsselfunktionen der reifen OL im zentralen Nervensystem gehören: (2a) Bildung und Aufrechterhaltung der Myelinscheide um Axone zur Ermöglichung effizienter Aktionspotentialleitung (2b) Metabolische Unterstützung von Axonen durch Laktatbereitstellung; (2c) Aktivitätsabhängige Anpassung der Myelinisierung (Myelinplastizität). Graphik erstellt mit biorender.com, inspiriert von (32, 33).

Die Entwicklung und Funktion von OLs unterliegen einer präzisen Regulation. OLs entstehen aus den Oligodendrozyten-Vorläuferzellen (OPCs). Diese müssen sich vermehren, an geeignete Stellen wandern, sich zu reifen OLs differenzieren und schließlich Myelinscheiden um die Zielaxone bilden (34). Dieser gesamte Lebenszyklus wird durch ein komplexes Zusammenspiel von intrinsischen genetischen Programmen und extrinsischen Signalen gesteuert (35). Es konnte in zahlreichen Studien nachgewiesen werden, dass eine Vielzahl von Transkriptionsfaktoren, Signalwegen und epigenetischen Mechanismen interagieren, um die OPC-Spezifikation, den Zeitpunkt der Differenzierung, die Expression von Myelin-Genen und die OL-Reifung zu regulieren (36-38). Die kritische Phase der Myelinisierung der Großhirnrinde in der späten Adoleszenz korreliert dabei mit dem typischen Erstmanifestationsalter der SZ (39, 40).

Die Komplexität dieses regulatorischen Netzwerks macht deutlich, dass die OL-Biologie an mehreren Stellen gestört werden kann. Zahlreiche Befunde deuten darauf hin, wie eine Beteiligung dieser Zelllinie zu Veränderungen der Myelinisierung, der WM-Struktur und folglich der Funktion der neuronalen Schaltkreise führt, die die Grundlage für kognitive Prozesse bilden. Diese Daten werden im Folgenden detaillierter vorgestellt.

Post-mortem Studien: Die Hypothese, dass eine Funktionsstörung der Oligodendrozyten mit der SZ in Zusammenhang steht, wird durch konvergierende Daten aus postmortalen Hirnstudien von verstorbenen SZ-Patienten gestützt (26, 41). Diese umfassen eine reduzierte Anzahl von OLs und deren Vorläuferzellen (OPCs), eine gestörte

Expression von OL-bezogenen Genen und Proteinen sowie morphologische Veränderungen der Zellen, z.B. verlängerte und mehr verzweigte Fortsätze, und letztlich eine veränderte Myelinisierung (42-46). Auffälligerweise konnte gezeigt werden, dass eine verminderte Anzahl von OLs im Hippocampus mit dem Volumen verbundener Gehirnregionen des Papez-Kreises und v.a. der kognitiven Leistung korreliert (47, 48). Diese Studien unterstreichen die Bedeutung von OLs und deren Vorläuferzellen in der Pathogenese der SZ und weisen auf deren zentrale Rolle für die kognitive Leistung hin.

Genetik: Die in Post-mortem-Studien festgestellten Dysfunktionen von Oligodendrozyten und die Veränderungen der weißen Substanz bei SZ werfen die Frage nach den zugrundeliegenden Mechanismen auf. Ein entscheidender Ansatz zur Klärung dieser Frage ist die Untersuchung genetischer Faktoren, deren Relevanz durch die hohe Erblichkeit der SZ zusätzlich unterstrichen wird. Meta-Analysen von Zwillingsstudien schätzen die Erblichkeit der Anfälligkeit für SZ durchgängig als bemerkenswert hoch ein, wobei die Angaben häufig zwischen 60 und 80% liegen (49-52).

Die genetische Architektur, welche dieser Erblichkeit zugrunde liegt, ist hochgradig komplex und polygen. Groß angelegte Genomweite Assoziationsstudien (GWAS) führten zu signifikanten Fortschritten in der Entschlüsselung dieser Architektur. Gemäß den jüngsten Forschungsergebnissen existieren über 280 genetische Risikoloci für SZ, wobei jeder einzelne Locus lediglich eine marginale Steigerung des Risikos bewirkt (53). Die Schwierigkeit besteht darin, diese Erkenntnisse in die daraus resultierenden funktionellen Mechanismen zu übersetzen (54, 55). Die Mehrheit dieser Loci ist in nicht-kodierenden Regionen lokalisiert, die eine signifikante Rolle in der Regulation der Neuroentwicklung durch eine veränderte Genexpression zu spielen scheinen (56, 57). Nachfolgende funktionelle Pathway- und Gene-Set-Enrichment-Analysen ergaben, dass die identifizierten Risikoloci zu großen Teilen auf gemeinsame Pathways der synaptischen Funktion und des Immunsystems konvergieren (55, 58, 59). Allerdings basieren diese Analysen oft auf humanen Post-mortem oder murinen Datensätzen mit inhärenten technischen Limitationen. So führt die häufig auf Zellkerne beschränkte Analyse (snRNAseq) zum Verlust zytoplasmatischer Transkripte (60).

Neben diesen Hauptbefunden wurde auch eine moderate Assoziation von SZ-Risikoloci mit Genen festgestellt, die in oligodendroglialen Zelllinien vermehrt exprimiert werden (61-63). Diese Ergebnisse legen nahe, dass Anomalien der Oligodendrozyten und des Myelins möglicherweise primäre Faktoren in der Ätiologie der SZ sind und nicht nur sekundäre Folgen (64, 65).

hiPSC-Forschung: Bis vor kurzem war die Erforschung der biologischen Ursachen psychiatrischer Störungen auf periphere Gewebe, korrelative Bildgebungsstudien, Genetik und molekulare oder histologische Analysen von postmortalen Gehirnproben beschränkt. Technische Herausforderungen schränken jedoch die Interpretation dieser

Ergebnisse ein. So basieren die verwendeten transkriptomischen Daten häufig auf menschlichen Postmortem-Proben, die möglicherweise nicht den relevantesten zellulären Zustand oder das Entwicklungsstadium widerspiegeln (Paper II). Mausmodelle können sich zudem in der Expression kritischer Gene von Menschen unterscheiden (53, 62).

Die Verwendung von humanen induzierten pluripotenten Stammzellen (hiPSCs) hat die Erforschung der biologischen Ursachen psychiatrischer Störungen revolutioniert (66). Diese Technologie ermöglicht die Differenzierung von hiPSCs in nahezu jeden neuronalen oder glialen Zelltyp und bietet einen innovativen Ansatz zur Überwindung vieler Einschränkungen der oben genannten Methoden (67). HiPSC-basierte Studien haben neuronale Dysfunktionen bei SZ aufgezeigt, aber nur wenige haben sich mit glialen Beeinträchtigungen befasst (68). Drei hiPSC-basierte Studien haben gliale Beeinträchtigungen bei SZ untersucht und weisen auf zellautonome Störungen der oligodendroglialen Entwicklung und Funktion hin.

Windrem et al. verwendeten hiPSCs von Patienten mit im Kindesalter auftretender SZ und zeigten, dass die daraus gewonnenen glialen Vorläuferzellen, transplantiert in Mäuse, eine abnormale Entwicklung und dysregulierte Genexpression aufwiesen, einhergehend mit Hypomyelinisierung und SZ-relevanten Verhaltensdefiziten (69). Weiterhin fanden McPhie et al. heraus, dass hiPSC-Linien von SZ-Patienten im Vergleich zu Kontrollen signifikant weniger O4-positive Oligodendrozyten produzierten, ein Befund, der mit dem in vivo mittels MRT gemessenen Myelin-Gehalt des Gehirns derselben Personen korrelierte (70). In ähnlicher Weise identifizierten de Vrij et al. unter Verwendung von hiPSCs und durch Vergleich der Ergebnisse mit In-vivo-Bildgebung, dass Mutationsträger einer seltenen familiären CSPG4-Mutation, eine Korrelation von zellulären Anomalien und reduzierten FA-Werten in der DTI aufweisen.

Zu den wichtigsten Einschränkungen dieser Studien gehören kleine Stichprobengrößen, die Konzentration auf bestimmte SZ-Subtypen (im Kindesalter auftretende oder familiäre Fälle mit seltenen Mutationen), die möglicherweise die Verallgemeinerbarkeit einschränken, die Abhängigkeit von langen Differenzierungsprotokollen (40-200 Tage), sowie die Notwendigkeit einer weiteren mechanistischen Aufklärung (25).

Unserer Kenntnis nach gibt es keine Studie, die systematisch die Mechanismen, die dem zelltypspezifischen Beitrag der Oligodendroglia zur Störung der WM in SZ zugrunde liegen, untersucht. Neue Erkenntnisse in diesem Bereich könnten wegweisend für die Entwicklung neuer therapeutischer Strategien sein, die darauf abzielen, die weiße Substanzstörung zu beheben und somit die kognitiven und funktionellen Defizite bei Patienten mit SZ zu lindern.

1.2 Darstellung des Forschungsvorhabens

1.2.1 Verbindende übergeordnete Fragestellung

Das Ziel dieses Promotionsvorhabens ist es, die Beiträge von Oligodendroglia zur Pathologie der weißen Substanz bei Schizophrenie zu untersuchen, indem die zellulären Auswirkungen der Schizophrenie-assoziierten Genetik auf die Entwicklung und Funktion der Oliogdendrozyten mit Hilfe von hiPSC in vitro analysiert werden.

Die zentrale Forschungsfrage, welche die beiden zugrundeliegenden Publikationen dieser kumulativen Arbeit verbindet, lautet:

Wie beeinflussen genetische Faktoren die Biologie von Oligodendrozyten in Schizophrenie-Patienten mit kognitiven Beeinträchtigungen und Störungen der weißen Substanz?

1.2.2 Meilensteine

Die übergeordnete Fragestellung soll mit Hilfe eines hiPSC-Modells beantwortet werden, das folgende Meilensteine umfasst:

Meilenstein 1: Etablierung eines effizienten Differenzierungsprotokolls

Ziel des ersten Meilensteins ist die Weiterentwicklung und Validierung eines Protokolls zur Differenzierung von hiPSCs in reife Oligodendrozyten (iOLs) durch die forcierte Expression spezifischer Transkriptionsfaktoren. Die Optimierung zielt darauf ab, eine hohe Effizienz (maximaler Anteil an reifen iOLs in Zellkultur), eine verbesserte Reproduzierbarkeit sowie eine verkürzte Differenzierungsdauer im Vergleich zu bisherigen Protokollen zu erreichen (71, 72).

Zur Validierung werden die resultierenden iOLs umfassend charakterisiert. Mittels Immunzytochemie (ICC) wird die morphologische Reife anhand von Zellgröße und Verzweigungsgrad beurteilt, sowie das molekulare Profil anhand spezifischer Oberflächenmarker analysiert und mit dem primärer humaner Oligodendrozyten verglichen.

Meilenstein 2: Generierung stabiler Fall-Kontroll-Zelllinien

Im Rahmen dieses Meilensteins wird das bereits etablierte Differenzierungsprotokoll auf insgesamt 15 hiPSC-Zelllinien angewendet. Diese Zelllinien stammen aus einer klinisch umfassend phänotypisierten Kohorte bestehend aus Schizophreniepatienten (n = 8) und gesunden Kontrollpersonen (n = 7) (73). Die Auswahl basierte auf neurokognitiven Profilen sowie bildgebenden Befunden zur Integrität der weißen Substanz. Hierbei wurden Patienten mit kognitiven Defiziten und reduzierten FA-Werten in der DTI ausgewählt, während die Kontrollgruppe durchschnittliche kognitive Leistungen und unauffällige DTI-Befunde aufwies.

Die Differenzierung der hiPSCs zu oligodendroglialen Zellen erfolgt mithilfe des in Meilenstein 1 etablierten basierten Protokolls und wird durch immunzytochemische Analysen überprüft. Ziel ist es, die erfolgreiche Differenzierung in reife Oligodendrozyten sicherzustellen, welche durch spezifische morphologische und molekulare Marker charakterisiert sind. Diese validierten Zellmodelle bilden die Grundlage für die nachfolgenden Fall-Kontroll-Analysen in Meilenstein 3.

Meilenstein 3: Fall-Kontroll-Studien

Aufbauend auf den in Meilenstein 2 generierten und validierten Patienten- und Kontroll-Zelllinien werden abschließend umfassende Fall-Kontroll-Studien durchgeführt. Ziel ist die Identifizierung zellulärer Unterschiede in der Morphologie, Reifung und dem Transkriptionsprofil von induzierten Oligodendrozyten-Vorläuferzellen (iOPCs) und reifen Oligodendrozyten (iOLs) zwischen Schizophreniepatienten und gesunden Kontrollpersonen.

Mittels ICC für O4, einem Oberflächenprotein zur Erkennung von iOPCs, und MBP, zur Erkennung von iOLs, sowie automatisierter Bildanalyse-Pipelines werden Entwicklungsstadien und wichtige morphologische Parameter quantifiziert. Diese Analysen sollen Unterschiede in der Reifungsdynamik und strukturellen Integrität zwischen den Gruppen aufdecken und zum besseren Verständnis der beobachteten Veränderungen der weißen Substanz bei Patienten beitragen.

1.2.3 Bedeutung

Durch das Erreichen der genannten Meilensteine soll dieses Promotionsvorhaben wertvolle Einblicke in die pathologischen Mechanismen der weißen Substanzstörung bei SZ ermöglichen. Die Untersuchung der zellulären Auswirkungen der SZ-Genetik auf Oligodendrozyten kann zu zwei wichtigen Erkenntnissen beitragen:

1. **Vertieftes Verständnis der SZ-assoziierten Pathologie der weißen Substanz:** Bislang sind die genauen molekularen Mechanismen, die der Störung der WM bei SZ zugrunde liegen, unvollständig geklärt. Dieses Projekt könnte neue Erkenntnisse über die zellulären und molekularen Prozesse liefern, die zu Veränderungen der Oligodendrozyten und der Myelinbildung bei SZ beitragen.
2. **Mögliche Grundlage für neue therapeutische Ansätze:** Ein detaillierteres Verständnis der Rolle von Oligodendrozyten bei der SZ könnte zukünftige Forschungsarbeiten zur Entwicklung neuer und wirksamerer Therapien zur Verbesserung der weißen Substanzpathologie und der damit verbundenen kognitiven Beeinträchtigungen bei Schizophreniepatienten unterstützen. Die Ergebnisse dieses Projekts könnten neue Zielstrukturen für pharmakologische Interventionen und innovative therapeutische Strategien auf Basis von Stammzelltherapien oder Gentherapie aufzeigen.

1.3 Abgedeckte Aspekte durch die jeweiligen Veröffentlichungen

1.3.1 Paper I

Die Veröffentlichung "Expression of Lineage Transcription Factors Identifies Differences in Transition States of Induced Human Oligodendrocyte Differentiation" von Florian J. Raabe et al., bei der ich dritter Ko-Autor bin, vergleicht systematisch verschiedene Protokolle zur gerichteten Differenzierung von hiPSCs in Oligodendrozyten mittels Transkriptionsfaktor-Überexpression. Konkret wurden die Transkriptionsfaktoren SOX10 (S) alleine sowie in Kombination mit OLIG2 (SO) und NKX6.2 (SON) hinsichtlich ihrer Effizienz zur Generierung von iOPCs und iOLs untersucht.

Im Einzelnen deckt dieses Paper mehrere zentrale Aspekte der kumulativen Dissertation ab:

1. Etablierung eines effizienten Differenzierungsprotokolls (Meilenstein 1):

Die Studie optimierte das Differenzierungsprotokoll dahingehend, eine hohe Ausbeute an O4+-iOPCs und MBP+-iOLs zu erzielen und gleichzeitig die Differenzierungsdauer zu verkürzen. Mittels ICC wurde gezeigt, dass die SON-Kombination die höchste Effizienz bei der Generierung reifer iOLs aufweist, welche zudem eine komplexere Morphologie zeigen als S-induzierte Zellen. Einzelzell-RNA-Sequenzierungen (scRNA-seq), inklusive RNA-Velocity-Analysen, bestätigten, dass SON-induzierte Zellen einen höheren Reifegrad erreichen als S-induzierte Zellen. Die SON-Differenzierung resultierte in einem höheren Anteil reifer iOL-Cluster und weniger Zellen, die sich ungewollterweise in einen neuronalen Phänotyp entwickeln.
Damit trägt das Paper erheblich zur Validierung und Weiterentwicklung des Differenzierungsprotokolls bei und erfüllt somit die Ziele von Meilenstein 1.

2. Generierung stabiler Zelllinien (Meilenstein 2):

Im Zuge des Papers konnte die Robustheit des Protokolls bestätigt werden, indem die Differenzierungsvariationen auf sechs verschiedene Donor-Zelllinien angewendet wurden, und mittels ICC die erfolgreiche Differenzierung gezeigt werden konnte. Diese Erkenntnisse sind entscheidend für die Anwendung des Protokolls auf die Zelllinien von Schizophreniepatienten und Kontrollpersonen, wie in Meilenstein 2 beschrieben.

3. Fall-Kontroll-Studien (Meilenstein 3):

Durch die vergleichende Analyse der Differenzierungsprozesse in S- vs. SON-differenzierten Zellen mittels ICC, scRNAseq und RNA velocity konnten erste Algorithmen etabliert werden, die Unterschiede in der Entwicklung und Reifung von Oligodendrozyten identifizieren können. Diese Methoden und Erkenntnisse sind direkt auf die geplanten Fall-Kontroll-Studien anwendbar, um die Unterschiede zwischen Patienten-

und Kontroll-Zelllinien zu untersuchen. Somit unterstützt dieses Paper die Durchführung und Validierung der Experimente, die in Meilenstein 3 beschrieben sind.

Insgesamt deckt die Veröffentlichung wesentliche methodische und experimentelle Aspekte der kumulativen Dissertation ab, indem sie in vitro-Modelle zur Untersuchung der Biologie von Oligodendrozyten mittels hiPSCs und Differenzierungsprotokolle basierend auf Transkriptionsfaktoren entwickelt und vergleicht. Sie liefert Erkenntnisse über die Dynamik und Heterogenität der induzierten Oligodendrozyten-Differenzierung und unterstreicht die Bedeutung der Wahl spezifischer genetischer Transkriptionsfaktoren (S vs. SON) für das Differenzierungsprotokoll, abhängig davon, ob frühe (OPC) oder späte (OL) Entwicklungsstadien im Fokus stehen. Dies bildet die Basis für nachfolgende Untersuchungen zu den Auswirkungen von Schizophrenie-assoziierten genetischen Faktoren.

Eine Zusammenfassung meines geleisteten Beitrags findet sich im entsprechenden Kapitel (2.1 Beitrag zu Paper I).

1.3.2 Paper II

Die Veröffentlichung "iPSC-modelling reveals genetic associations and morphological alterations of oligodendrocytes in schizophrenia" von Chang, Waldeck et al., an der ich als geteilter Erst-Autor beteiligt war, baut auf dem ersten Paper auf und adressiert direkt die übergeordnete Fragestellung der Dissertation, indem sie die zellulären Auswirkungen von SZ-assoziierten genetischen Faktoren auf die Biologie von Oligodendrozyten (OLs) untersucht. Hierfür wurde ein hiPSC-basiertes Modell von SZ-Patienten mit klinisch manifester Störung der weißen Substanz und kognitiven Defiziten sowie von gesunden Kontrollpersonen genutzt.

Das zweite Paper deckt folgende wesentliche Aspekte der einzelnen Meilensteine ab:

1. Etablierung eines effizienten Differenzierungsprotokolls (Meilenstein 1):

Das im ersten Paper entwickelte Differenzierungsprotokoll für hiPSCs zu Oligodendrozyten wird in dieser Studie angewendet und validiert. Durch die erfolgreiche Implementierung und Anwendung des SON-Protokolls (Sox10, Olig2, Nkx6.2) auf eine neue Kohorte, wird die Effizienz und Reproduzierbarkeit des Protokolls weiter bestätigt.

Ebenso wird die biologische Relevanz der mittels des etablierten SON-Protokolls generierten Zellen gezeigt, indem durch unüberwachtes Clustering von Transkriptomdaten gezeigt wird, dass hiPSC-abgeleitete iOPCs und iOLs eine hohe Ähnlichkeit mit menschlichen postmortem OPCs und OLs aufweisen. Dies bestätigt die Eignung des Modells für die Untersuchung oligodendroglialer Pathologien. Weiterhin untermauert das Paper die genetische Relevanz des Modells durch eine MAGMA-Gen-Set-Analyse, die eine Anreicherung von SZ-Risikogenen spezifisch in reiferen iOLs nachweist.

Somit trägt das Paper zur Validierung der Methode bei, die in Meilenstein 1 beschrieben ist.

2. Generierung stabiler Zelllinien (Meilenstein 2):

Das etablierte Differenzierungsprotokoll wurde erfolgreich auf die hiPSC-Linien der klinisch charakterisierten und mittels DTI-Bildgebung stratifizierten Kohorte (n=8 SZ-Patienten mit reduzierter FA, n=7 Kontrollen) angewendet. Die erfolgreiche Differenzierung zu O4+ iOPCs und MBP+ iOLs wurde immunzytochemisch bestätigt, womit die Grundlage für die Fall-Kontroll-Studien geschaffen wurde.

3. Fall-Kontroll-Studien (Meilenstein 3):

Dieses Paper bildet den Kern von Meilenstein 3, indem es die geplanten Fall-Kontroll-Vergleiche durchführt. Mittels automatisierter Bildanalyse wurden signifikante morphologische Unterschiede identifiziert: MBP+ iOLs von SZ-Patienten zeigten eine erhöhte Gesamtlänge der Fortsätze und eine höhere Anzahl an Verzweigungspunkten im Vergleich zu Kontrollen. Dies deutet auf eine veränderte zelluläre Struktur und möglicherweise gestörte Reifungsdynamik hin. Interessanterweise korrespondiert dieser Befund einer erhöhten morphologischen Komplexität mit Beobachtungen aus Post-mortem-Studien, in denen ebenfalls eine hypertrophe Morphologie von OPCs mit erhöhter Verzweigung und Länge bei SZ-Patienten beschrieben wurde (44). Parallel durchgeführte Bulk-RNA-Sequenzierung und anschließende Gen-Set-Anreicherungsanalyse (GSEA) identifizierten Unterschiede im Transkriptionsprofil. Insbesondere zeigten sie eine Hochregulierung von Signalwegen, die mit G-Protein-gekoppelten Rezeptoren (GPCRs) und Immunantworten assoziiert sind, sowie eine Herunterregulierung von Pathways, die für DNA-Replikation und Zellzyklus relevant sind. Diese Ergebnisse deuten auf molekulare Mechanismen hinter den beobachteten morphologischen Defiziten hin und unterstützten die Hypothese einer gestörten, möglicherweise vorzeitigen Reifung ("prematuration").

Zusammenfassend trägt dieses Paper maßgeblich zur Beantwortung der übergeordneten Forschungsfrage bei, indem es Störungen in iOLs von SZ-Patienten aufdeckt. Es zeigt, dass genetische Faktoren bei SZ mit morphologischen und transkriptomischen Veränderungen in Oligodendrozyten assoziiert sind, die einer gestörten, möglicherweise vorzeitigen Reifung entsprechen ("prematuration phenotype"). Diese Erkenntnisse liefern Einblicke in die Pathomechanismen der bei SZ beobachteten Störungen der weißen Substanz und der damit verbundenen kognitiven Defizite.

Eine Zusammenfassung meines geleisteten Beitrags findet sich im entsprechenden Kapitel (2.2 Beitrag zu Paper II).

2. Beitrag zu den Veröffentlichungen

Dieses Kapitel stellt meinen Beitrag zu den oben genannten Veröffentlichung deutlich dar, um die Grundlage für die Bewertung meiner kumulativen Dissertation zu schaffen.

2.1 Beitrag zu Paper I (Expression of Lineage Transcription Factors Identifies Differences in Transition States of Induced Human Oligodendrocyte Differentiation; Raabe et al.)

Im Rahmen des Papers "Expression of Lineage Transcription Factors Identifies Differences in Transition States of Induced Human Oligodendrocyte Differentiation" (Raabe et al.) trug ich zu folgenden zwei Teilbereichen bei.

1. Planung, Durchführung und Analyse der technischen Experimente

Ein wesentlicher Teil meiner Arbeit bestand in der Planung und Durchführung der technischen Experimente, die ich dank professioneller Unterstützung von Dr. Florian Raabe erfolgreich umsetzen konnte. Dazu zählen:

- **Zellkultur:** Ich war maßgeblich für die Kultivierung und Aufrechterhaltung der Zellkulturen im Rahmen des Validierungsexperiments verantwortlich, das die Grundlage für sämtliche nachfolgenden Analysen bildeten. Dies beinhaltete die Kultivierung der hiPSCs, deren effiziente Transfektion mit den lentiviralen Vektoren für die Expression der Transkriptionsfaktor-Kombinationen S und SON, die Durchführung des etablierten Protokolls zur neuralen Induktion sowie die anschließende gerichtete Differenzierung der neuralen Vorläuferzellen zu i-OPCs und reifen iOLs unter Zugabe von Doxycyclin. Diese experimentellen Arbeiten führte ich zur technischen Etablierung und Optimierung des Protokolls an sechs unterschiedlichen hiPSC-Linien durch, um die Robustheit und Reproduzierbarkeit der Methode zu demonstrieren. Die von mir generierten und charakterisierten Zellpopulationen dienten zudem als Ausgangsmaterial für die im Paper beschriebenen bulk- und single-cell RNA-Sequenzierungsanalysen.
- **Immunzytochemie und Fluoreszenzmikroskopie:** Zur Charakterisierung der differenzierten Zellen führte ich umfassende immunzytochemische Färbungen durch. Dabei wurden stadienspezifische Markerproteine, wie O4 für iOPCs und MBP für reife iOLs, markiert. Die Detektion und Visualisierung dieser Proteine erfolgten mittels Fluoreszenzmikroskopie. Um eine objektive Bildaufnahme zu gewährleisten und einen möglichen Selektionsbias zu reduzieren, implementierte ich hierfür einen semi-automatisierten Arbeitsablauf zur systematischen Erfassung der Mikroskopiebilder an vordefinierten Positionen.

- **Automatisierte Bildanalyse:** Für die quantitative Auswertung der gewonnenen Fluoreszenzmikroskopiebilder entwickelte und programmierte ich ein spezifisches Makro für die Bildanalysesoftware Fiji (ImageJ). Dieses maßgeschneiderte Werkzeug ermöglichte eine automatisierte, objektive und reproduzierbare Quantifizierung relevanter Parameter, wie z.B. der prozentuale Anteil Marker-positiver Zellen der differenzierten Oligodendrozyten.
- **Statistische Auswertung:** Die mittels automatisierter Bildanalyse erhobenen quantitativen Daten wurden von mir unter Verwendung der statistischen Programmiersprache R ausgewertet. Diese statistische Analyse war entscheidend, um signifikante Unterschiede in der Differenzierungseffizienz und den phänotypischen Eigenschaften (z.B. Reifegrad, morphologische Komplexität) der Zellen, die unter Einfluss der verschiedenen Transkriptionsfaktor-Kombinationen generiert wurden, zu identifizieren und quantitativ zu belegen.

2. Erstellung von Teilen des Manuskripts

Über die experimentellen Arbeiten hinaus war ich an der Verfassung und Überarbeitung des Publikationsmanuskripts beteiligt. Mein Beitrag zur Manuskripterstellung beinhaltete:

- **Methodenabschnitt:** Ich habe zur Verfassung des Methodenabschnitts beigetragen, insbesondere bei der detaillierten Beschreibung der verwendeten Zellkulturtechniken, der hiPSC-Kultivierung, der neuralen Induktion und der oligodendroglialen Differenzierungsprotokolle (siehe Paper Abschnitte 2.2–2.6).
- **Statistische Analyse:** Den Abschnitt zur statistischen Analyse in dem die angewandten statistischen Methoden und die Ergebnisse der Analyse beschrieben werden, habe ich ebenfalls erstellt (siehe Paper 2.8.).
- **Abbildungen:** Ich leistete einen wesentlichen Beitrag zur Erstellung und Aufbereitung mehrerer Abbildungen für die Publikation. Dies umfasste die Generierung von Diagrammen zur Visualisierung der quantitativen Daten aus der Bildanalyse und den statistischen Auswertungen sowie teilweise die sorgfältige Auswahl und Bearbeitung repräsentativer Mikroskopiebilder zur Illustration der zellulären Phänotypen (siehe Paper: Fig 1, C & D; Fig 2; Fig 6, H & I; Fig S2).
- **Review und Editing:** Schließlich war ich umfassend in den Prozess des Reviews und Editings des Manuskriptentwurfs involviert. Meine Tätigkeit umfasste hierbei das kritische Korrekturlesen, die inhaltliche Prüfung auf Schlüssigkeit und wissenschaftliche Korrektheit sowie die sprachliche Optimierung, um die Klarheit, Präzision und Gesamtqualität der Publikation sicherzustellen.

2.2 Beitrag zu Paper II (iPSC-modelling reveals genetic associations and morphological alterations of oligodendrocytes in schizophrenia; Chang, Waldeck et al.)

Im Rahmen des Papers "iPSC-modelling reveals genetic associations and morphological alterations of oligodendrocytes in schizophrenia" (Chang, Waldeck et al.) war ich als geteilter Erstautor maßgeblich an der Planung, Umsetzung und Auswertung der Studie beteiligt. Im Detail umfasste mein Beitrag zu dem Paper:

1. Planung, Durchführung und Analyse der technischen Experimente

Ein wesentlicher Teil meiner Arbeit bestand in der Planung und Durchführung der technischen Experimente. Dazu zählen:

- **Theoretische Konzeption:** Gemeinsam mit Florian habe ich die grundlegende Idee und das Design der Studie entwickelt, was entscheidend war, um die Forschungsfrage klar zu definieren und die methodischen Ansätze festzulegen.
- **Erzeugung stabiler differenzierter Zelllinien von Patienten und gesunden Kontrollen:** Aufbauend auf den Ergebnissen und Methoden aus Paper I war ich verantwortlich für die Anwendung des optimierten Differenzierungsprotokolls auf die ausgewählte Kohorte von hiPSC-Linien. Ich nutzte die Transkriptionsfaktor-Kombination SON (SOX10, OLIG2, NKX6.2), welche in Paper I die höchste Effizienz zur Generierung reifer iOLs zeigte, um iOLs aus hiPSC-Linien von SZ-Patienten (N=8) und gesunden Kontrollen (N=7) zu differenzieren. Um experimentelle Variabilität und potenzielle Batch-Effekte zu kontrollieren, wurden diese anspruchsvollen und langwierigen Differenzierungen sorgfältig geplant und parallel bzw. gestaffelt durchgeführt.
- **Immunzytochemie und Fluoreszenzmikroskopie:** Analog zu Paper I führte ich die Immunfärbungen durch, um stadienspezifische Markerproteine der Oligodendrozyten-Linie (insbesondere O4 für späte iOPCs und MBP für reife iOLs) in den Kulturen zu detektieren. Für die standardisierte Aufnahme der Fluoreszenzmikroskopiebilder nutzte ich den in Paper I etablierten semi-automatisierten Workflow.
- **Automatisierte Bildanalyse:** Um die große Anzahl an Bilddaten objektiv und quantitativ auszuwerten, adaptierte und verbesserte ich das Fiji (ImageJ)-Makro, das ich für Paper I entwickelt hatte. Die Optimierungen betrafen insbesondere die Segmentierung und morphologische Charakterisierung von MBP-positiven iOLs. Diese weiterentwickelte automatisierte Analyse ermöglichte eine robuste und reproduzierbare Quantifizierung der Zellzahl, Zellgröße sowie komplexerer morphologischer Parameter wie der Gesamtlänge der Fortsätze (branch length) und der Anzahl an Verzweigungspunkten (junction number).

- **Statistische Auswertung SZ vs. HC:** Die aus der automatisierten Bildanalyse gewonnenen quantitativen morphologischen Daten wertete ich mittels statistischer Methoden in R aus. Ein zentraler Fokus lag auf dem Vergleich der morphologischen Parameter von O4- und MBP-positiven Zellen zwischen der SZ- und der Kontrollgruppe unter Verwendung von Mixed-Effects-Modellen, um die hierarchische Datenstruktur (mehrere Bilder pro Zelllinie, mehrere Zelllinien pro Gruppe) zu berücksichtigen. Zusätzlich analysierte ich die FA-Werte aus den DTI-Daten der klinischen Kohorte, um die Unterschiede in der Integrität der weißen Substanz zwischen den für die iPSC-Studie ausgewählten SZ-Patienten und Kontrollen statistisch zu bestätigen.

2. Beitrag zur Erstellung des Manuskripts

Als geteilter Erstautor war ich intensiv an der Abfassung und Überarbeitung des Manuskripts beteiligt. Mein Beitrag zur Manuskripterstellung beinhaltete:

- **Methodenabschnitt:** Ich verfasste wesentliche Teile des Methodenteils. Dies umfasste detaillierte Beschreibungen der Zellkultur, der neuralen Induktion und oligodendroglialen Differenzierung, der Immunzytochemie, der automatisierten Bildanalyse und der angewandten statistischen Verfahren.
- **Abschnitt – Ergebnisse:** Zum Verfassen des Ergebnisteils trug ich maßgeblich bei, insbesondere zu den Abschnitten, die die Resultate der quantitativen morphologischen Analysen der O4- und MBP-positiven Zellen darstellen und interpretieren.
- **Visualisierung:** Die Erstellung aussagekräftiger wissenschaftlicher Grafiken und Diagramme mittels R zur Visualisierung der komplexen morphologischen Daten und statistischen Ergebnisse war ein weiterer wichtiger Teil meines Beitrags. Dies umfasste beispielsweise die Erstellung der Boxplots und repräsentativen Bilddarstellungen in den Abbildungen 4, 5 und den Supplementärabbildungen S4 und S5.
- **Review & Editing:** Über den gesamten Schreib- und langen Reviewprozess hinweg war ich aktiv und intensiv in die Diskussion, Überarbeitung und das Editieren des Manuskripts involviert. Dies beinhaltete mehrere Revisionsrunden, die Einarbeitung von Feedback der Ko-Autoren und die Sicherstellung der wissenschaftlichen Stringenz, Klarheit und sprachlichen Präzision des finalen Manuskripts.

2.3 Begründung geteilte Erstautorenschaft – Paper II

Die geteilte Erstautorenschaft zwischen Man-Hsin Chang und mir basiert auf unseren gleichwertigen und komplementären Beiträgen zu dieser umfangreichen Forschungsarbeit. Die Entscheidung zur geteilten Erstautorenschaft reflektiert die intensive und synergetische Zusammenarbeit, in der beide Erstautoren unverzichtbare Leistungen in unterschiedlichen, jedoch für den wissenschaftlichen Erfolg und die Qualität des Papers gleichermaßen kritischen Schlüsselbereichen erbracht haben.

Die Arbeitsteilung in diesem Projekt war klar definiert und nutzte unsere jeweiligen ergänzenden Fähigkeiten, Expertisen und zeitlichen Ressourcen:

Die Hauptverantwortung meinerseits umfasste die Planung und Durchführung der gesamten experimentellen Laborarbeiten im Bereich der hiPSC-Kultivierung, der komplexen Differenzierung der Zelllinien-Kohorte und der anschließenden ICC und Fluoreszenzmikroskopie. Darauf aufbauend lag ein weiterer Schwerpunkt meiner Arbeit in der Entwicklung, Anwendung und Optimierung der automatisierten quantitativen Bildanalyse sowie der dazugehörigen statistischen Auswertung der morphologischen Daten und der Visualisierung dieser Ergebnisse.

Die wesentliche Verantwortung von Man-Hsin Chang umfasste die Koordination der Manuskripterstellung, Erstellung des ersten Entwurfs (Writing – First Draft) sowie Erstellung und Überarbeitung einer Vielzahl von Abbildungen. Darüber hinaus übernahm sie die zentrale Leitung bei der Durchführung wichtiger Experimente im Rahmen der Manuskriptrevision. Diese beinhalteten die Planung, Umsetzung und bioinformatische Analyse der bulk-RNA-Sequenzierungsdaten, welche einen weiteren zentralen experimentellen und analytischen Bestandteil der Studie darstellten.

Die intensive Zusammenarbeit wurde durch regelmäßige (Online-)Treffen sowie die Nutzung kollaborativer Tools geprägt. Dies ermöglichte eine effiziente Abstimmung und Synchronisation der Arbeitsbereiche und war für den Erfolg des interdisziplinären Projekts entscheidend.

Durch diese enge Verzahnung aller Arbeitsbereiche haben Man-Hsin Chang und ich in identischem Umfang und auf komplementäre Weise zum Gelingen des Papers beigetragen. Die jeweiligen Beiträge waren für die wissenschaftliche Substanz, die methodische Breite und die Gesamtqualität der Publikation gleichermaßen unverzichtbar. Diese gleichwertigen und synergetischen Leistungen bilden die fundierte Grundlage für die geteilte Erstautorenschaft.

3. Zusammenfassung:

Schizophrenie (SZ) ist eine komplexe neuropsychiatrische Erkrankung, die durch positive, negative und kognitive Symptome gekennzeichnet ist. Während antipsychotische Medikamente bei Positivsymptomen wirksam sein können, bleiben kognitive Defizite eine große therapeutische Herausforderung. Diese Defizite, die oft mit Anomalien der weißen Substanz (WM) im Gehirn einhergehen, beeinträchtigen die soziale und berufliche Teilhabe der Betroffenen erheblich.

Forschungsfrage: Es gibt zunehmend Evidenz dafür, dass eine Dysfunktion der Oligodendrozyten (OLs), die Myelin-bildenden Zellen des zentralen Nervensystems, eine Rolle bei der Entstehung von SZ spielt. GWAS haben Risikogene identifiziert, die in OLs exprimiert werden, und post-mortem-Studien zeigen Veränderungen in OLs von SZ-Patienten. Ziel dieser Arbeit ist es, zu untersuchen, wie genetische Faktoren Veränderungen von OLs bei SZ-Patienten mit kognitiven Beeinträchtigungen und Störungen der weißen Substanz beeinflussen.

Methoden: Um diese Forschungsfrage zu beantworten, wurde ein hiPSC-Modell verwendet. Es wurde ein effizientes Differenzierungsprotokoll etabliert, um hiPSCs in reife OLs zu differenzieren. Dieses Protokoll, basierend auf der Überexpression der Transkriptionsfaktoren SOX10, OLIG2 und NKX6.2 (SON), ermöglicht eine schnelle und effiziente Generierung von OLs. Anschließend wurde dieses Protokoll auf eine umfassend phänotypisierte Kohorte von hiPSC-Linien von SZ-Patienten (n=8) mit kognitiven Defiziten und reduzierter fraktioneller Anisotropie (FA) sowie gesunden Kontrollpersonen (n=7) angewendet. Die generierten Zellen wurden mittels ICC und RNA-Sequenzierung untersucht.

Ergebnisse: Das erste Paper dieser kumulativen Dissertation etablierte und validierte das SON-Protokoll zur effizienten Differenzierung von hiPSCs in reife OLs. Es wurde gezeigt, dass diese Methode im Vergleich zu anderen Protokollen zu einer höheren Ausbeute und komplexeren Morphologie von OLs führt.

Das zweite Paper nutzte dieses etablierte Protokoll, um OLs aus der SZ-Kohorte und den Kontrollpersonen zu generieren und zu vergleichen. Die Ergebnisse zeigten signifikante Veränderungen in den OLs von SZ-Patienten. Insbesondere wurde eine erhöhte morphologische Komplexität (verlängerte und stärker verzweigte Fortsätze) in den MBP-positiven iOLs der SZ-Patienten festgestellt. Des Weiteren zeigten Bulk-RNA-Sequenzierungsanalysen differentielle Genexpressionsmuster, wobei in den Patienten-iOLs Signalwege des Zellzyklus und der DNA-Replikation herunterreguliert waren. Diese Kombination von Befunden wurde als "Prämaturations-Phänotyp" interpretiert, der auf eine beschleunigte, aber möglicherweise fehlgeleitete Differenzierung hindeutet.

Diskussion: Diese Arbeit leistet einen stammzellbasierten Beitrag zum wachsenden Verständnis der SZ als Entwicklungsstörung des Gehirns mit signifikanter Beteiligung glialer Pathologien. Die Ergebnisse stützen die Hypothese, dass Anomalien der WM, wie sie in vivo mittels Bildgebung bei SZ-Patienten beobachtet werden, zumindest teilweise auf intrinsische, genetisch bedingte Defekte in OLs zurückzuführen sind. Die Identifizierung spezifischer morphologischer und transkriptomischer Veränderungen in patienteneigenen Zellen liefert zelluläre Korrelate für die mittels GWAS identifizierte Assoziation von SZ-Risikogenen mit OL-relevanten Genen und Pathways. Der beobachtete "Prematuration"-Phänotyp bietet eine erweiterte Perspektive auf die OL-Pathologie bei SZ, die über eine reine Hypomyelinisierung oder einen Verlust von OLs hinausgeht und eine qualitativ gestörte Reifung in den Vordergrund rückt.

Limitationen und Ausblick: Trotz der signifikanten Ergebnisse unterliegt die vorliegende Arbeit einigen Limitationen. Das hiPSC-Modell stellt naturgemäß eine Vereinfachung dar; es fehlt die komplexe dreidimensionale Struktur und das zelluläre Mikromilieu des Gehirns. Des Weiteren fokussiert sich die Analyse primär auf zellintrinsische OL-Eigenschaften; funktionelle Aspekte wie die tatsächliche Myelinisierungskapazität wurden nicht direkt untersucht. Die forcierte Expression von Transkriptionsfaktoren beschleunigt zwar die Differenzierung, weicht jedoch von der natürlichen Entwicklung ab und erschwert die Analyse des Beitrags dieser Faktoren, für die eine Dysregulation bei SZ beobachtet wurde. Die moderate Kohortengröße (n=8 vs. n=7) limitiert die Generalisierbarkeit der Befunde und die statistische Power. Zukünftige Forschung sollte sich auf die funktionelle Validierung des beobachteten "Prämaturations-Phänotyps" konzentrieren, z.B. durch Untersuchung der Myelinisierungsfähigkeit in Co-Kulturen. Ebenso ist die Replikation der Befunde in größeren und diverseren Kohorten essenziell. Des Weiteren sollten zukünftige Studien auch umweltbedingte Risikofaktoren in das hiPSC-Modell integrieren, um relevante Gen-Umwelt-Interaktionen auf Ebene der Oligodendroglia zu untersuchen.

Schlussfolgerung: Diese kumulative Dissertation liefert Einblicke in die zelluläre Pathologie der Oligodendroglia bei SZ durch die Etablierung und Anwendung eines patientenspezifischen hiPSC-Modells. Die Entdeckung eines potenziellen "Prämaturations-Phänotyps" unterstreicht nicht nur die Bedeutung von OLs in der Pathophysiologie der SZ, sondern verdeutlicht auch die kritische Relevanz, den jeweils passenden Zelltyp im korrekten Entwicklungsstadium und unter präzisen Kulturbedingungen zu untersuchen, um die komplexe Biologie der SZ valide zu erforschen. Dies eröffnet neue Perspektiven für zukünftige Forschungsarbeiten zur Entwicklung zielgerichteter therapeutischer Strategien zur Verbesserung der WM-Integrität und der kognitiven Funktionen bei SZ-Patienten.

4. Abstract (English):

Schizophrenia (SZ) is a highly complex neuropsychiatric disorder characterized by positive, negative and cognitive symptoms. While antipsychotic medication can be effective for positive symptoms, cognitive deficits remain a major therapeutic challenge. These deficits, which are often associated with white matter (WM) abnormalities in the brain, significantly impair the social and occupational participation of those affected.

Research question: There is increasing evidence that dysfunction of oligodendrocytes (OLs), the myelin-generating cells of the central nervous system, plays a role in the development of SZ. GWAS have identified risk genes expressed in OLs and postmortem studies show changes in OLs of SZ patients. The aim of this work is to investigate how genetic factors influence changes in OLs in SZ patients with cognitive impairment and white matter disorders.

Methods: To answer this research question, a hiPSC model was used. An efficient differentiation protocol was established to differentiate hiPSCs into mature OLs. This protocol, based on the overexpression of the transcription factors SOX10, OLIG2 and NKX6.2 (SON), enables a fast and efficient generation of OLs. Subsequently, this protocol was applied to a comprehensively phenotyped cohort of hiPSC lines from SZ patients (n=8) with cognitive deficits and reduced fractional anisotropy (FA) and healthy controls (n=7). The generated cells were analyzed by immunocytochemistry and RNA sequencing.

Results: The first paper of this cumulative dissertation established and validated the SON protocol for efficient differentiation of hiPSCs into mature OLs. It was shown that this method leads to a higher yield and more complex morphology of OLs compared to other protocols.

The second paper used this established protocol to generate and compare OLs from the SZ cohort and control subjects. The results showed significant changes in the iOLs of SZ patients. Increased morphologic complexity (longer branch length and increased junction numbers) was observed in the MBP-positive iOLs of SC patients. Furthermore, bulk RNA sequencing analyses revealed differential gene expression patterns, with cell cycle and DNA replication signaling pathways downregulated in the patient iOLs. This combination of findings was interpreted as a “prematuration phenotype” indicating accelerated but possibly misguided differentiation.

Discussion: This work contributes to the growing understanding of SZ as a neurodevelopmental disorder of the brain with significant involvement of glial pathologies. The results support the hypothesis that WM abnormalities, as observed in vivo by brain imaging in SZ patients, are at least partially due to intrinsic, genetically determined defects in OLs. The identification of specific morphological and transcriptomic changes

in patient-derived cells provides cellular correlates for the association of SZ risk genes with OL-relevant genes and pathways identified by GWAS. The observed “prematuration” phenotype provides a broader perspective on OL pathology in SZ that goes beyond mere hypomyelination or loss of OLs and emphasizes qualitatively impaired maturation.

Limitations and outlook: Despite the significant results, the present work is subject to some limitations. The hiPSC model is by nature a simplification; it lacks the complex three-dimensional structure and the cellular microenvironment of the brain. Furthermore, the analysis focuses primarily on cell-intrinsic OL properties; functional aspects such as the actual myelination capacity were not directly investigated. While the forced expression of transcription factors has been observed to accelerate differentiation, this approach deviates from natural development. Additionally, it complicates the analysis of these factors' contributions, for which dysregulation has been observed in SZ. The moderate cohort size (n=8 vs. n=7) limits the generalizability of the findings and the statistical power. Future research should focus on the functional validation of the observed “prematuration phenotype”, e.g. by investigating myelination capacity in co-cultures. Moreover, it is essential to replicate the findings in larger and more diverse cohorts. Furthermore, future studies should also integrate environmental risk factors (e.g. early stress, inflammation) into the hiPSC model to investigate relevant gene-environment interactions at the oligodendroglial level.

Conclusion: This cumulative dissertation provides insights into the cellular pathology of oligodendroglia in SZ through the establishment and application of a patient-specific hiPSC model. The identification of a potential “prematuration phenotype” not only emphasizes the importance of OLs in the pathophysiology of SZ but also highlights the critical importance to study the appropriate cell type at the correct developmental stage and under precise culture conditions to validly study the complex biology of SZ. This opens new perspectives for future research to develop targeted therapeutic strategies to improve WM integrity and cognitive function in SZ patients.

5. Paper I

Expression of Lineage Transcription Factors Identifies Differences in Transition States of Induced Human Oligodendrocyte Differentiation

Florian J. Raabe [1,2], Marius Stephan [1,2,3], Jan Benedikt Waldeck [1], Verena Huber [1], Damianos Demetriou [1], Nirmal Kannaiyan [1,3], Sabrina Galinski [1,3], Laura V. Glaser [4], Michael C. Wehr [1,3], Michael J. Ziller [5,6], Andrea Schmitt [1,7], Peter Falkai [1] and Moritz J. Rossner [1,3,*]

[1] Department of Psychiatry and Psychotherapy, University Hospital, LMU Munich, 80336 Munich, Germany
[2] International Max Planck Research School for Translational Psychiatry (IMPRS-TP), 80804 Munich, Germany
[3] Systasy Bioscience GmbH, 81669, Munich, Germany.
[4] Department of Computational Molecular Biology, Max Planck Institute for Molecular Genetics, 14195 Berlin, Germany
[5] Max Planck Institute of Psychiatry, 80804 Munich, Germany
[6] Department of Psychiatry, University of Münster, 48149 Münster, Germany
[7] Laboratory of Neurosciences (LIM-27), Institute of Psychiatry, University of São Paulo (USP), São Paulo-SP 05403-903, Brazil

***** Correspondence: Moritz.Rossner@med.uni-muenchen.de

cells

IMPACT FACTOR 5.2

Indexed in: PubMed

CITESCORE 10.5

Article

Expression of Lineage Transcription Factors Identifies Differences in Transition States of Induced Human Oligodendrocyte Differentiation

Florian J. Raabe, Marius Stephan, Jan Benedikt Waldeck, Verena Huber, Damianos Demetriou, Nirmal Kannaiyan, Sabrina Galinski, Laura V. Glaser, Michael C. Wehr, Michael J. Ziller et al.

Topic Collection

Stem Cell-Based Therapy, Disease Modeling and Drug Discovery

Edited by

Prof. Xiaowen Bai

MDPI

https://doi.org/10.3390/cells11020241

cells

MDPI

Article

Expression of Lineage Transcription Factors Identifies Differences in Transition States of Induced Human Oligodendrocyte Differentiation

Florian J. Raabe [1,2], Marius Stephan [1,2,3], Jan Benedikt Waldeck [1], Verena Huber [1], Damianos Demetriou [1], Nirmal Kannaiyan [1,3], Sabrina Galinski [1,3], Laura V. Glaser [4], Michael C. Wehr [1,3], Michael J. Ziller [5,6], Andrea Schmitt [1,7], Peter Falkai [1] and Moritz J. Rossner [1,3,*]

1 Department of Psychiatry and Psychotherapy, University Hospital, LMU Munich, 80336 Munich, Germany; Florian.Raabe@med.uni-muenchen.de (F.J.R.); marius.stephan@med.uni-muenchen.de (M.S.); Benedikt.Waldeck@med.uni-muenchen.de (J.B.W.); Venena.Huber@med.uni-muenchen.de (V.H.); Damianos.Demetriou@med.uni-muenchen.de (D.D.); Nirmal.Kannaiyan@med.uni-muenchen.de (N.K.); Sabrina.Galinski@med.uni-muenchen.de (S.G.); Michael.Wehr@med.uni-muenchen.de (M.C.W.); Andrea.Schmitt@med.uni-muenchen.de (A.S.); Peter.Falkai@med.uni-muenchen.de (P.F.)
2 International Max Planck Research School for Translational Psychiatry (IMPRS-TP), 80804 Munich, Germany
3 Systasy Bioscience GmbH, 81669 Munich, Germany
4 Department of Computational Molecular Biology, Max Planck Institute for Molecular Genetics, 14195 Berlin, Germany; glaser@molgen.mpg.de
5 Max Planck Institute of Psychiatry, 80804 Munich, Germany; michael_ziller@psych.mpg.de
6 Department of Psychiatry, University of Münster, 48149 Münster, Germany
7 Laboratory of Neurosciences (LIM-27), Institute of Psychiatry, University of São Paulo (USP), São Paulo 05403-903, Brazil
* Correspondence: Moritz.Rossner@med.uni-muenchen.de

check for updates

Citation: Raabe, F.J.; Stephan, M.; Waldeck, J.B.; Huber, V.; Demetriou, D.; Kannaiyan, N.; Galinski, S.; Glaser, L.V.; Wehr, M.C.; Ziller, M.J.; et al. Expression of Lineage Transcription Factors Identifies Differences in Transition States of Induced Human Oligodendrocyte Differentiation. *Cells* **2022**, *11*, 241. https://doi.org/10.3390/cells11020241

Academic Editor: Xiaowen Bai

Received: 21 December 2021
Accepted: 7 January 2022
Published: 11 January 2022

Publisher's Note: MDPI stays neutral with regard to jurisdictional claims in published maps and institutional affiliations.

Abstract: Oligodendrocytes (OLs) are critical for myelination and are implicated in several brain disorders. Directed differentiation of human-induced OLs (iOLs) from pluripotent stem cells can be achieved by forced expression of different combinations of the transcription factors SOX10 (S), OLIG2 (O), and NKX6.2 (N). Here, we applied quantitative image analysis and single-cell transcriptomics to compare different transcription factor (TF) combinations for their efficacy towards robust OL lineage conversion. Compared with S alone, the combination of SON increases the number of iOLs and generates iOLs with a more complex morphology and higher expression levels of myelin-marker genes. RNA velocity analysis of individual cells reveals that S generates a population of oligodendrocyte-precursor cells (OPCs) that appear to be more immature than those generated by SON and to display distinct molecular properties. Our work highlights that TFs for generating iOPCs or iOLs should be chosen depending on the intended application or research question, and that SON might be beneficial to study more mature iOLs while S might be better suited to investigate iOPC biology.

Keywords: directed differentiation; oligodendrocytes; human pluripotent stem cells; hiPSC; scRNAseq; RNA velocity

1. Introduction

Myelinating oligodendrocytes (OLs) are essential for saltatory nerve conduction in the central nervous system and are involved in the metabolic support of neurons and modulation of neuronal excitability [1,2]. OLs are derived from oligodendrocyte precursor cells (OPCs) and both cell types are considered heterogeneous populations with regional specifications and functionally different states [3–6]. Moreover, OL dysfunction is associated with several major neurological diseases, e.g., multiple sclerosis, leukodystrophy, stroke, and schizophrenia [1,7]. The advent of human-induced pluripotent stem cells (hiPSCs)

paved the way for generating hiPSC-derived OPCs (hiPSC OPCs) and hiPSC-derived OLs (hiPSC OLs) that improved our understanding of human biology and enabled dissection of pathophysiological mechanisms, including cell-based therapies [8,9].

Initial protocols applied small molecules and peptides but took 75 to 200 days to generate hiPSC OPCs and hiPSC OLs [8,9], thus limiting larger-scaled studies such as compound screens or large cohort investigations [10]. A subsequent, more rapid strategy used overexpression of lineage-specific transcription factors (TFs), which forces oligodendroglial differentiation and allows generation of induced OPCs (iOPCs) and iOLs within 20 to 30 days [8,9]. Most protocols identified overexpression of SRY-box 10 (SOX10) as sufficient for iOL generation [11–13] and overexpression of SOX9 alone was also recently shown to be an efficient approach [14]. Garcia-León et al., suggested that SOX10 (referred to as S) alone is most efficient for iOL generation [13]. In contrast, Ehrlich et al., showed that the combination SON–consisting of S, oligodendrocyte transcription factor 2 (OLIG2, referred to as O), and the NK6 homeobox 2 (NKX6.2, referred to as N)–enriched the yield of iOLs [11] and allowed direct reprogramming of human fibroblasts [15]. In addition, Pawlowski et al., applied the combination SO to generate iOLs from embryonic stem cells [12]. Nonetheless, iOLs displayed transcriptional similarities to primary OLs and allowed axonal myelination in vitro and in vivo [11,13]. Despite these functional and morphological similarities between studies, several experimental conditions beyond the different TF combinations varied, preventing direct comparison of the findings. First, the neural patterning strategies applied before initiating TF overexpression differed: Garcia et al., performed neural induction on a monolayer [13], whereas Ehrlich et al., performed free-floating embryoid body formation with neural patterning and applied different combinations of small molecules [11]. Second, different configurations of the TF-expressing lentivirus constructs were applied: Ehrlich et al., expressed all TFs as multicistronic units, however, Garcia et al., used combinations of individual TFs expressing lentiviral constructs, which likely reduced the efficacy of multi-TF combinations in generating iOLs compared with that of single TFs. Moreover, to date, no studies have addressed the fate and heterogeneity of individual iOPCs and iOL populations.

Therefore, we systematically compared S-, SO- and SON-directed differentiation of individual oligodendroglial lineage cells by using a streamlined protocol in which all TF combinations were expressed from an identical lentivirus backbone and all cell culture conditions were standardized. We show that S-, SO- and SON-directed differentiation were all sufficient to generate high yields of $O4^+$ iOPCs, however, SON provided significant more yield than SO and S. Further investigations with S and SON show that SON allows an earlier generation of MBP^+ iOLs with higher yields and more complex morphology. Subsequent scRNAseq experiments including RNA velocity analysis reveals a fastened directed oligodendroglial differentiation using SON and higher maturation stages of SON-iOLs compared to S-iOLs. We show that scRNAseq including RNA analysis is not limited to dissecting a static stage but allows to dissect the time-dependent dynamics of directed differentiation and highlights that SON-directed differentiation might be better suited for research with a focus on more mature iOL.

2. Materials and Methods

2.1. Lentiviral Vectors

The cDNA sequences of human SOX10 (S), SOX10-P2A-OLIG2 (SO) and SOX10-P2A-OLIG2-T2A-NKX6.2 (SON) were synthesized as plasmids (GenScript, Piscataway, NJ, USA), with each open reading frame flanked by attB1 and attB2 sites for Gateway recombination cloning. Synthesized genes were recombined into pDONR/Zeo (Thermo Fisher Scientific, Waltham, MA, USA, #12535035) to yield Entry clones. Entry clones were finally recombined into pINDUCER21-puro_Gateway-3xFLAG (Addgene, Watertown, MA, USA, plasmid #172981). HEK293 cells (ATCC) were used for lentivirus production. S-, SO- and SON-lentiviral vectors (12 µg of each) were transfected with packaging plasmids psPAX2 (Addgene plasmid #12260, 9 µg) and pMD2.G (Addgene plasmid #12259, 4 µg)

with 4 µg polyethylenimine per 1 µg plasmid-DNA (Polysciences, Warrington, FL, USA, #9002-98-6). Then, 48 h after lentiviral transfection, the culture medium was collected, filtered through a 0.45 µM PVDF filter, precipitated with PEG-it (System Biosciences, Palo Alto, CA, USA, #LV810A-1) according to the manufacturer's instructions, resuspended in DPBS, and stored at −80 °C for further use.

2.2. HiPSC Lines, HiPSC Cultivation and Lentiviral Transfection

hiPSC were derived from the hiPSC biobank at the Department of Psychiatry and Psychotherapy, University Hospital, LMU Munich, Munich, Germany. hiPSC were generated from PBMCs according to a previous protocol [16]. Conventional hiPSC verification included validation of pluripotency by immunocytochemistry (Tra1-60, NANOG, OCT4, SOX2), genomic integrity by digital karyotyping [17] (pipeline available at https://gitlab.mpcdf.mpg.de/luciat/cnv_detection.git, last accessed 28 June 2021), and successful differentiation into all three germ layers [18]. hiPSC were tested negative for HIV, HCV, CMV (by Synlab, Munich, Germany) and free of Mycoplasma infections (by Eurofins, Ebersberg, Germany). All used hiPSC lines and passaging numbers are annotated in Table S1. Technical experiments were performed with line PSYLMUi001-A, SON-directed oligodendroglial differentiation efficiency was replicated with six independent hiPSC lines as annotated in Table S1.

hiPSCs were cultivated in feeder-free conditions with iPS-Brew (Miltenyi Biotec, Bergisch Gladbach, Germany, #130-104-368) on Vitronectin (Thermo Fisher Scientific, Waltham, MA, USA, #A14700). Lentiviral transfection was performed in iPS-Brew, supplemented with 1 µM Y-27632 (Rock-Inhibitor, Selleckchem, Houston, USA, #S 1049) and plated with 5×10^4 cells/cm^2. Selection with 1 ug/mL puromycin (Thermo Fisher Scientific, Waltham, MA, USA, #A1113803) was performed 48 h after transfection. We performed the first passage after transfection with Accutase (Sigma-Aldrich, St. Louis, USA, #A6964) and single cells. Subsequent passaging for expansion or maintenance was performed as hiPSC clump passaging with 0.5 µM EDTA (Thermo Fisher Scientific, Waltham, MA, USA, #15575-020). An overview of used materials is annotated in Table S2. Independent experiments were based on independent lentiviral infections.

2.3. Neural Induction

Neural induction and oligodendroglial differentiation were performed according to published protocols [13,19] with the modification that lentiviral transduction was performed before and not after neural induction (Figure 1A). At least one passage before neural induction, the hiPSC medium was changed to mTeSR1 (StemCell, Vancouver, Canada, #85850). Two days before neural induction, hiPSCs were singularized with Accutase, resuspended in mTeSR1, supplemented with 1× RevitaCell (Thermo Fisher Scientific, Waltham, MA, USA, #A2644501), and plated at a cell density of 2×10^4 cells/cm^2 on 12- and 24-well plates (Corning, New York, NJ, USA, #CORN3513 and #CORN3526) coated with Matrigel (BD Bioscience, San Jose, CA, USA, #354277). Two days after cultivation in mTESR1, neural induction was initiated by medium exchange to N2B27, which consists of DMEM/F-12 with GlutaMAX™ (Gibco, brand of Thermo Fisher Scientific, Waltham, MA, USA, #31331028), 1× N2 (Gibco, #17502048), 1× NEAA (Gibco, #11140035), 50 µM Mercaptoethanol (Gibco, #21985023) and 25 µg/mL Insulin (Sigma, #I9278), supplemented with 10 µM SB431542 (StemCell, Vancouver, Canada, #72232), 1 µM LDN193189 (StemCell, Vancouver, Canada, #72147) and 0.1 µM retinoic acid (RA)(Sigma-Aldrich, St. Louis, MO, USA, #R2625-50MG). A daily full media change of 0.5 mL per 24 wells and 1 mL per 12 wells was performed and media volume was doubled after day 4 of neural induction. From day 8 after neural induction, daily media change was performed with N2B27 supplemented with 0.1 µM RA and 1 µM SAG (Millipore, Burlington, MA, USA, #566660) until day 12.

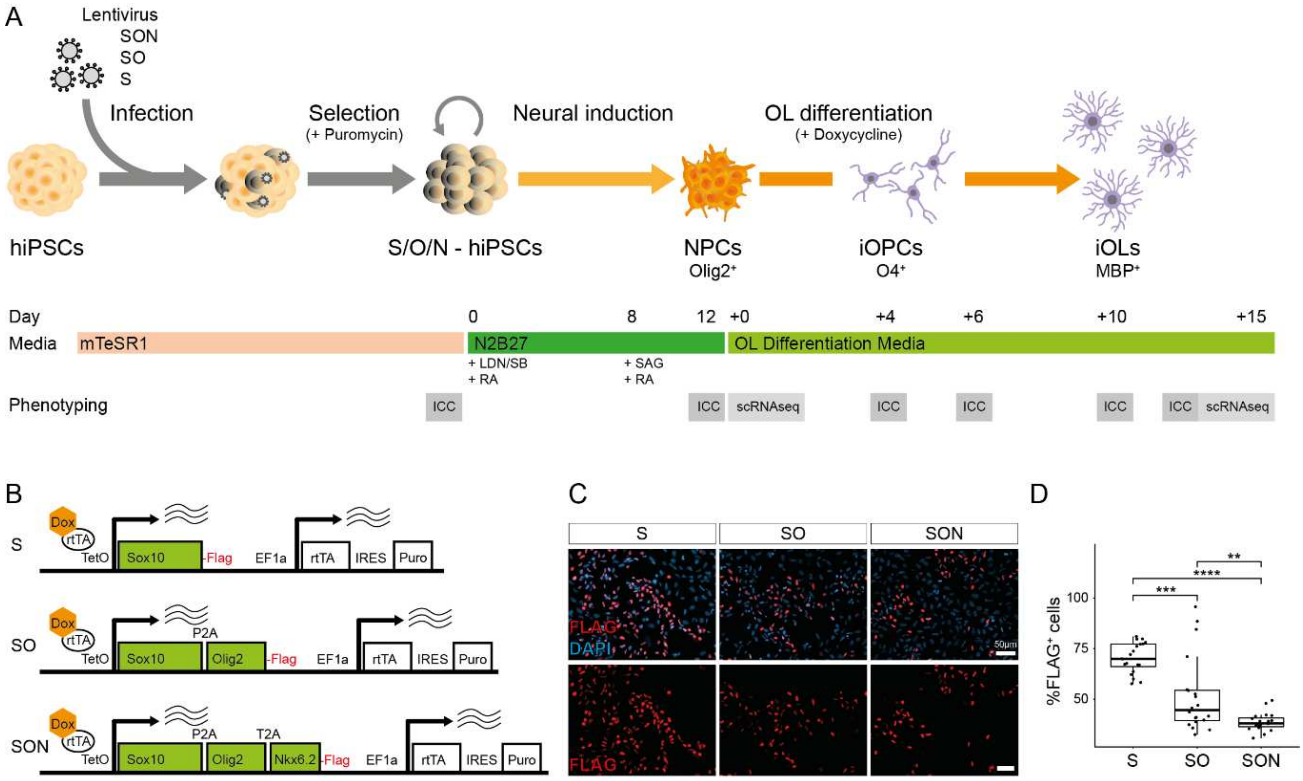

Figure 1. Experimental overview and applied constructs. (**A**) Experimental overview of directed differentiation of induced oligodendrocytes (iOLs) and their precursor cells (iOPC) from human induced pluripotent stem cells (hiPSCs). (**B**) Scheme of lentiviral vectors expressing the transcription factors (TF) SON (SOX10-OLIG2-NKX6.2), SO (SOX10-OLIG2) and S (SOX10). (**C**) Representative images of FLAG$^+$ hiPSCs 48 h after doxycycline induction. Scale bar: 50 µm. (**D**) Quantification of the percentage of FLAG$^+$ cells 48 h after doxycycline induction. Mean ± SD of FLAG$^+$ cells: 70.3% ± 7.5% in S-hiPSCs, 51.6% ± 18.7% in SO-hiPSCs and 38.7% ± 4.5% in SON-hiPSCs. Illustrated with box (quartiles) and whisker (largest/smallest observation within hinge ± 1.5× interquartile range) plot. Each dot represents one analyzed field of view (n = 20 per condition) from one independent experiment. Statistical analysis by Kruskal–Wallis test ($p < 0.0001$) and post hoc Mann–Whitney U test. ** $p < 0.01$, *** $p < 0.001$, **** $p < 0.0001$.

2.4. Oligodendroglial Differentiation

Twelve- or twenty-four-well plates were coated with PLO/Laminin. First, 50 µg/mL poly-L-ornithine (Sigma, P4957) in DPBS (ThermoFisher Scientific, Waltham, MA, USA, #1419009400) was coated overnight at 37 °C. Then, 3× washing steps were performed with DPBS, and plates were incubated overnight with 10 µg/mL mouse laminin (Sigma, #L2020) at 37 °C. Day 12 NPCs were passaged as single cells upon Accutase treatment and were seeded at a density of 150,000 cells/cm^2 in N2B27 supplemented with 0.1 µM RA, 1 µM SAG (Millipore, #566660), and 1× RevitaCell. The next day, directed OL differentiation was initiated by adding OL differentiation medium (OL-DM), which consists of N2B27 supplemented with 10 ng/mL PDGF-AA (PeproTech, brand of Thermo Fisher Scientific, Waltham, MA, USA, #100-13A), 10 ng/mL IGF1 (PeproTech, #100-11), 5 ng/mL HGF (PeproTech, #100-39), 10 ng/mL NT3 (Peprotech, #AF-450-03), 0.1 ng/mL Biotin (Sigma, #B4639), 1 mM dbcAMP (Sigma, #D0627), 60 ng/mL T3 (Sigma, #T6397) and 1 µg/mL doxycycline (Clontech, brand of Takara Bio, Shiga, Japan, #NC0424034). Full media change was performed every second day and puromycin selection was performed from Day + 2 to Day + 4 by supplementing media with 1 µg puromycin (ThermoFisher Scientific, Waltham, MA, USA, #A1113803). Cells were passaged at Day + 10 or cryopreserved for further use. Singularized cells were resuspended in OL-DM, supplemented with 1× RevitaCell and

mixed 1:1 with cooled ProFreeze CDM (Lonza, Basel, Switzerland, #BEBP12-769E) for freezing purposes. Cells were stored overnight in a freezing container (Nalgene Mr. Frosty) at −80 °C and subsequently placed in liquid nitrogen.

2.5. O4 Microbeads Purification

To select $O4^+$ cells, we performed microbead purification with anti-O4 microbeads (Miltenyi Biotec, #130-096-670) according to the manufacturer's instructions.

2.6. Immunofluorescence Staining and Imaging Analysis

Before fixation, cells were washed with PBS. Then, they were fixed with 4% PFA for 10 min at room temperature (RT). Subsequently, 3× washing with PBS was performed. Permeabilization and blocking were performed with 0.1% Triton and 5% goat serum in PBS for 60 min at RT. Triton was omitted for O4 staining. Primary antibodies were added in PBS supplemented with 0.1% Triton and 1% goat serum and incubated overnight at 4 °C. On the next day, the primary antibody solution was removed by 3× PBS washing. The respective secondary antibodies in PBS were added and the cells were incubated for 60 min at RT. The secondary antibody solution was removed by 3× PBS washing and nuclei were counterstained with DAPI, which was added during the second washing step. Finally, samples were washed 1× with water and mounted onto microscope slides. Imaging was performed on an Axio Observer.Z1 (Zeiss) inverted microscope and fields of view (FOV) were taken at randomly defined but fixed positions for each well at 20× magnification. Image analysis was performed with the Fiji [20] and its plugin Simple Neurite Tracer [21]. Average values per FOV were used for subsequent statistical analysis.

2.7. Single-Cell RNA Sequencing and Data Analysis

2.7.1. Sample Processing

Cells were detached and singularized with Accutase supplemented with DNAse1 (Merck, Darmstadt, Germany, #DN25-1G), cell aggregates were removed with 30 µm Pre-Separation Filters (Miltenyi Biotec, Bergisch-Gladbach, Germany #130-041-407), and cells were kept on ice in cold PBS with 1% BSA. Small aliquots of the samples were stained with trypan blue and cell density, viability, and multiplet rate were determined in an improved Neumann counting chamber. The density was adjusted to 2500 cells/µL. The multiplet rate was less than 7% in all samples.

2.7.2. Library Preparation

The single-cell libraries were prepared with the SureCell WTA 3′ Kit (Illumina, San Diego, CA, USA) on a ddSEQ Single-Cell Isolator (Bio-Rad, Hercules, USA) in accordance with the manufacturer's protocol. Library quality and yield were evaluated with a high-sensitivity DNA kit on a Bioanalyzer 2100 (Agilent, Santa Clara, CA, USA) according to the manufacturer's specifications.

2.7.3. Sequencing

Libraries for scRNAseq experiments were sequenced on a NextSeq550 (Illumina) in paired-end mode with 69 cycles in Read1 and 80 cycles in Read2. Subsequently, the sequencing data were demultiplexed with bcl2fastq (Illumina).

2.7.4. Upstream Analysis of scRNAseq Data

Reads were quality-checked with FastQC (v0.11.9). Barcodes in Read1 were identified, added to the Read2 BAM file as an XC tag, and quality-checked with the ddSeeker tool [22], which found that 91% of barcodes were good quality in all samples. The tagged BAM files were further processed with Drop-seq tools (v2.3.0). A metabundle was created with the Ensembl annotation release 100 of the GRCh38 human genome (*create_Drop-seq_reference_metadata*). A non-human fragment (3′LTR and WPRE) and the 3xFLAG-Tag

region of the expression constructs were added to the genome FASTA and GTF to determine the construct expression levels. The data were filtered for rejected barcodes. The reads were sorted by query name, and the BAM files were converted back to FASTQ for mapping. Read2 was mapped by using the STAR aligner (v2.7.5) with default settings. Aligned data were merged with the unaligned but barcode-tagged data. Functional annotation was added and any remaining substitution and synthesis errors in the cell barcodes were repaired to create the final BAM file. Digital gene expression data were extracted (*Digital Expression*) for the 2000 most abundant cell barcodes in each sample. The threshold was chosen to be well beyond the cut-off suggested by the knee plot generated by ddSeeker's *make_graphs.R*.

In the RNA velocity analysis pipeline, to acquire separate count matrices for spliced and unspliced reads we estimated counts with DropEst (v0.8.6) instead of Drop-seq's *Digital Expression*. The following command was used, in accordance with the suggestions of the developers of Velocyto [23]: *dropest -m -V -b -f -g%GTF file from Drop-seq metabundle% -L eiEIBA -m -c %FILEPATH%/dropEst/configs/drop_seq_velocyto.xml.* Note that the barcode tag was changed from *BC* to *XC* in *drop_seq_velocyto.xml* to make the Drop-seq output compatible with Dropest.

2.7.5. Downstream Analysis of scRNAseq Data

The scRNAseq data were further processed with the R (v4.0.4) package *Seurat* (v4.0.1) [24]. The UMI count tables were imported in R, and Seurat objects were created for each sample. We filtered for features expressed in at least three cells in each dataset and for cells with at least 200 features in the first step. Mitochondrial RNA content was determined by grepping for "^*MT-*" (*PercentageFeatureSet*). We filtered the cells further for barcodes with less than 5% mitochondrial RNA content, at least 1700 UMI counts in the NPC and SON sample and 1000 counts in the S sample, and a minimum of 1000 detected features. After these filtering steps, 1194 cells were left in total.

2.7.6. Normalization of scRNAseq Data

All datasets were merged into one object. To check for artifacts potentially introduced by merging, we additionally performed all analyses on each sample dataset individually. The data were normalized by the single-cell transform procedure (*SCTransform*) [25], which regressed out the percentage of mitochondrial transcripts.

2.7.7. Dimension Reduction and Clustering of scRNAseq Data

Dimension reduction was performed as a principal component analysis (*RunPCA*). The previously identified 3000 most variable features (*FindVariableFeatures*) were used as input. The first 30 principal components were computed. Based on an elbow plot, as suggested in Macosko et al., 2015, we decided to use the first 15 principal components for downstream analysis. We performed SNN graph-based clustering with a resolution of 0.23 (*FindNeighbors, FindClusters*); this clustering returned 5 distinct clusters of cells. Next, we computed a UMAP embedding (*RunUMAP;* wrapper function for integration of the *Python* library *umap-learn*; [26]). Later in the project, we revisited the clustering and increased the resolution to 0.28, which split the iOPC cluster into two subclusters, which we then used for differential expression analysis.

2.7.8. Integration with Bulk RNAseq Data

To integrate our data with publicly available bulk RNA-seq data, we followed the procedure from Ng et al. [14]. We used a primary cell dataset from mouse brain tissue because human datasets are commonly based on postmortem samples. The dataset is available on the Gene Expression Omnibus website under the accession number GSE52564 [27]. Briefly, we created an average expression table and excluded features that were expressed in less than 10% of all cells in our dataset. The filtering step was introduced to avoid artifacts resulting from bad coverage inherent to single-cell RNA-seq data and low expres-

sion. The resulting list was then filtered for variably expressed genes in our dataset; such genes were computed as differential expression with a minimum log2-fold change of 0.25 (*FindAllMarkers)*. This step improved the signal-to-noise ratio and reduced potential batch effects. Next, we filtered the reference dataset and our dataset for mouse/human homologs. Finally, a list of about 3000 features was entered into the analysis. From our datasets, we excluded all iOPC cells in the NI Day + 0 sample because of their low number and their high probability of being misclustered NPCs. From the reference dataset neurons, we retained myelinating oligodendrocytes (MO), newly formed oligodendrocytes (NFO), and oligodendrocyte progenitor cells (OPC). First, we calculated feature variability (*rowVars*) with the *DESeq2 R* package [28] for variance stabilization (*VarianceStabilizingTransformation;* vst). Then, we used the 2000 most variable features for the downstream analysis. A principal component analysis (PCA) was performed to check for batch effects and other artifacts, and Manhattan distances were calculated between samples and features. These distances were used for hierarchical clustering and shown in heatmaps. Additionally, Spearman correlation coefficients were calculated to ensure that our data correlated appropriately with the reference data.

2.7.9. Differential Expression Analysis

Differential gene expression was analyzed with *Seurat v3* [29]. Genes were selected for expression in a minimum of 10% of all cells included in the analysis and for variability between groups. The data used were normalized but not integrated because the integration procedure smoothens expression differences, which leads to the underestimation of transcriptional differences. The results were tested in a Wilcoxon rank-sum test, and p values were adjusted with the Bonferroni procedure. Marker genes for characterization of the clusters were identified with a minimum log2-fold change in average expression (avg_log2FC) of 0.25 between the respective cluster and background (*FindAllMarkers()*). In pairwise comparisons between clusters, an avg_log2FC threshold of 1 was chosen because the lower threshold used for marker identification produced a high level of noise in downstream analyses.

2.7.10. Analysis of Maturation Marker Load and Construct Expression

Construct counts based on the 3′LTR-WPRE sequence were included in the *sctransform* regression model for normalization (see Section 2.7.6.) and used for construct expression equivalent. The FLAG tag region was not detected in the sequencing data.

For the maturation marker load, a set of genes with increasing levels of expression during oligodendrocyte-lineage differentiation [9] and that were detected with scRNAseq was chosen, specifically: *CNP*, *CD9*, *CLDN11*, *GALC*, *PLP1*, *MAG*, *MAL*, *MBP*, *MOBP*, and *MYRF*. The normalized expression level of these genes was then summarized for each cell. A Spearman correlation factor between construct expression level and marker load was computed and tested for S and SON Day + 15 samples.

2.7.11. Hypergeometric Gene Ontology Term Enrichment Analysis

For hypergeometric enrichment analyses of gene ontology (GO) terms, we used the GOrilla online tool [30]. Unranked gene lists were compared, of which one comprised all genes that entered the respective differential expression analysis (background) and the other identified differentially expressed genes (target). Only process terms went into the analysis. Enriched terms were filtered with an FDR-adjusted q-value threshold of 10^{-3} and a B value of less than 500.

2.7.12. RNA Velocity Analysis

For RNA velocity analysis, we first created a loom file for each sample from the Dropest output by using the command line *Python* implementation of the *velocyto* (v0.17.17) [23]. Next, we combined these loom files for downstream analysis. Additionally, we analyzed each sample independently to make sure that merging the samples

had not introduced major artifacts. We used the *scVelo Python* library [31] for the rest of the pipeline. We imported the combined loom file as anndata with the *anndata* library [32] and imported the cellIDs, UMAP coordinates, and cluster assignment from the *Seurat* pipeline. The cells were filtered for these IDs and their UMAP coordinates, and clusters were assigned. Further, the cells were filtered and normalized by using the default parameters with *pp.filter_and_normalize()*. Briefly, highly variable genes were selected, and the data were normalized by total library size and subsequently transformed to a logarithmic scale. For quality control, the fraction of unspliced transcripts was determined and found to be 13%, which is well within the lower range of 10% to 25% that is typically found in scRNAseq data. A fraction of this size is to be expected from a 3′ UTR-enriched RNA-seq dataset and is sufficient for RNA velocity estimation [31,33]. Moments were calculated and a full dynamic model was fitted to the data [31] (*tl.recover_dynamics()*, *tl.velocity(mode = "dynamical")*. This model was used to compute the velocity graph (*tl.velocity_graph()*).

2.7.13. Latent Time and PAGA Analysis

In addition, the gene-shared latent time was computed (*tl.latent_time()*) to create a pseudo-timeline that was used to inform cell-to-cell transition inference. A PAGA analysis was computed to find cluster-to-cluster transitions (*tl.paga_plot()*) [34]. Latent times were reimported in R to be used as a measure for maturity and were tested between samples with a Wilcoxon rank-sum test.

2.8. Statistics

Data were first tested for normal distribution with a Shapiro–Wilk test. We used both parametric (Student's *t*-test, ANOVA) and nonparametric analyses (two-sample Wilcoxon's rank-sum test, Kruskal–Wallis test, chi-squared test, Fisher's exact test), depending on the specific distribution properties of the data. Significance was set at * $p < 0.05$, ** $p < 0.01$, *** $p < 0.001$ and **** $p < 0.0001$.

3. Results

3.1. Generation of Stable S-/SO-/SON-Expressing hiPSCs and Neural Induction

To investigate TF-based differences of directed differentiation of iOPCs and iOLs with S [13], SO [12] and SON [11], we applied these TF combinations in accordance with the neural induction and differentiation protocol adapted from Garcia-Leon et al. [13,19] (Figure 1A). To allow a direct comparison, we cloned the three TFs combinations of S, SO, and SON into the same lentiviral backbone containing constitutive expression units for the reversed tetracycline transactivator (rtTA) [35] and a puromycin selection cassette (see Methods for details) (Figure 1B and Figure S1A). The human coding regions of *SOX10*, *OLIG2*, and *NKX6.2*, which were linked by the self-cleavage sites P2A and T2A, were under the control of the doxycycline-inducible operator (tetO) harboring a C-terminal FLAG-tag (Figure 1B and Figure S1A). We demonstrated the functionality of the constructs 48 h after doxycycline induction by examining infected hiPSCs with immunostainings, which showed higher numbers of $FLAG^+$ cells with S than with SO and SON (Figure 1C,D), likely reflecting the size of the different constructs and reduced protein expression upon P2A- and T2A-mediated cleavage. According to our protocol (Figure 1A), infection was performed on the hiPSC level; subsequent puromycin selection was performed to enrich for S-, SO-, or SON-hiPSC and followed by neural induction to generate $PAX6^+$ and $OLIG2^+$ neural precursor cells (NPCs) (Figure S1B).

3.2. Graded Efficiency to Generate iOPCs by S-, SO- and SON-Directed Differentiation

We next tested whether S-, SO- and SON-directed differentiation differs in their potential to generate O4-positive ($O4^+$) iOPCs as assessed by immunocytochemistry (ICC). All TF combinations generated high yields of $O4^+$ cells + 4 and + 6 days after induction of oligodendroglial differentiation. SON provided higher yields than SO and S at both time

points (Figure 2A–D). At day + 4, 38.1% ± 14.6% of all cells stained positive for $O4^+$ with SON-directed differentiation, compared with 33.9% ± 13.3% with SO-directed and 28.6% ± 8.9% with S-directed differentiation (Figure 2B). At day + 6, 83.9% ± 14.6% of SON-directed, 74.4% ± 7.7% of SO-directed and 73.6% ± 8.1% of S-directed cells were $O4^+$ (Figure 2D). These results clearly show a graded potential (SON > SO > S) to generate oligodendroglial lineage cells.

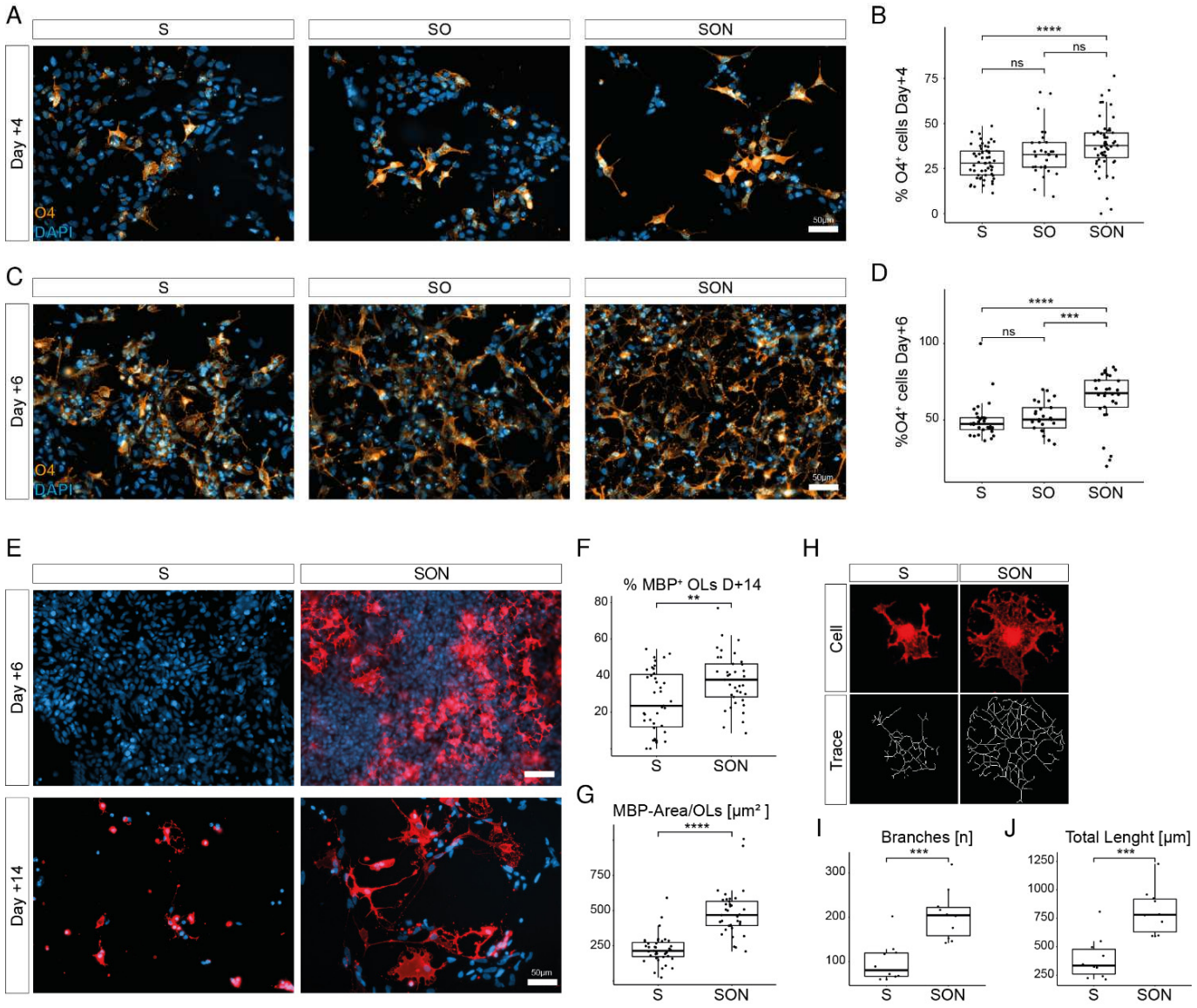

Figure 2. SON-directed differentiation leads to accelerated differentiation and morphologically highly ramified oligodendrocytes as compared with S-directed differentiation. (**A**) $O4^+$ (orange) iOPCs at Day + 4 of oligodendrocyte differentiation with S, SO and SON. Scale bar: 50 µm. (**B**) Quantification of $O4^+$ cells at Day + 4 illustrated with box-and-whisker plot. Each dot represents one analyzed field of view (n = 30–55 per condition) from two independent experiments. Statistical analysis by ANOVA ($F = 8.02$, $p = 0.00051$) and post hoc Tukey test. **** $p < 0.001$, ns = $p > 0.05$. (**C**) $O4^+$ (orange) iOPCs at Day + 6 of OL differentiation with S, SO and SON TFs. Scale bar: 50 µm. (**D**) Quantification of $O4^+$

cells at Day + 6 illustrated with a box-and-whisker plot. Each dot represents one analyzed field of view (n = 25–29 per condition) from two experiments. Statistical analysis by Kruskal–Wallis test (p = < 0.0001) and post hoc Mann–Whitney U test, *** $p < 0.001$, **** $p < 0.0001$, ns = $p > 0.05$. (**E**) MBP$^+$ iOLs appear at Day + 6 with SON-directed differentiation; no MBP$^+$ iOLs are detectable at this timepoint in the S condition. At Day + 14, SON- and S-MBP$^+$ cells are morphologically different. Representative images from two independent experiments. (**F**) Quantification of MBP$^+$ iOLs at Day + 14 illustrated with a box-and-whisker plot. Each dot represents one analyzed field of view (n = 37–39 fields of view per condition). Statistical analysis by Mann–Whitney U test. ** $p < 0.01$. Representative data from two independent experiments. (**G**) Quantification of average cell size of MBP$^+$ SON-iOLs compared with S-iOLs at Day + 14 of differentiation. Box-and-whisker plot; Each dot represents one analyzed field of view (n = 37–39 fields of view per condition). Statistical analysis by Mann–Whitney U test. **** $p < 0.0001$. Representative data from two independent experiments. (**H**) Illustration of representative individual cell assessments of S-iOLs and SON-iOLs with the Neurite simple tracer. (**I**) Quantification of the number of branches per MBP$^+$ cell (n = 10 analyzed cells per condition) illustrated by box-and-whisker plot. Statistical analysis by Mann–Whitney U test. *** $p < 0.001$. (**J**) Quantification of the total traced length per MBP$^+$ cell (n = 10 analyzed cells per condition) illustrated by box-and-whisker plot. Statistical analysis by Mann–Whitney U test. *** $p < 0.001$.

3.3. SON-Directed Differentiation Is Robust and Generates Mature iOLs More Efficiently Than S

To validate the robustness of our approach in generating O4$^+$ cells, we applied SON-directed differentiation from six independently generated iPSC lines from different donors (Figure S2). The analysis revealed comparable efficiencies for all samples, and we could highlight that an additional intermediate puromycin selection from day + 2 until day + 4 enriches the yield of O4$^+$ cells without the need for a mechanical purification step (Figure S2).

Given that the greatest differences were detected between SON and S, we compared these conditions in the subsequent analyses. Thus, we investigated the efficiency of SON- and S-directed differentiation in their potential to generate mature iOLs expressing the late-stage marker myelin basic protein (MBP). Compared with S-directed differentiation, SON-directed differentiation forced an earlier generation of MBP$^+$ iOLs (at day + 6) and yielded higher numbers at day + 14 (37.5% $\pm$ 14.7% vs. 26.0% $\pm$ 17.0%) (Figure 2E,F). SON generated iOLs that were highly significantly larger and had a more complex ramified OL morphology (Figure 2G–J).

3.4. Individual Transcriptomic Profiles Reveal a Higher Level of Maturation of iOLs upon SON Differentiation

To reveal the transcriptional architecture of individual induced cells, we applied single-cell RNA sequencing (scRNAseq) after completion of neural induction (NI Day + 0) and 15 days after S (S Day + 15) and SON (SON Day + 15) induction (Figure 1A). All samples were analyzed individually (NI Day + 0: n = 217 cells, S Day + 15: n = 577 cells, SON Day + 15: n = 400 cells) and for analyses purposes all 1194 cells were fused together to enable direct comparisons. Shared nearest neighbor (SNN) graph-based clustering identified separate populations of NPCs and neuronal cells, one iOPC cluster, and two distinct iOL clusters, iOL1 and iOL2 (Figure 3A,B). Subsequent statistical analysis revealed a highly significant ($p < 2.2 \times 10^{-16}$) cell cluster composition between the baseline sample NI Day + 0 (n = 217 cells) compared to differentiated samples S Day + 15 (n = 577 cells) and SON Day + 15 (n = 400 cells) as well as between the differentiated samples (Figure 3C, Table S5). This underlines the effect of the directed oligodendroglial differentiation per se as well as the impact on cell cluster composition when different combinations of directing transcription factors were applied (Figure 3A–C, Tables S4 and S5).

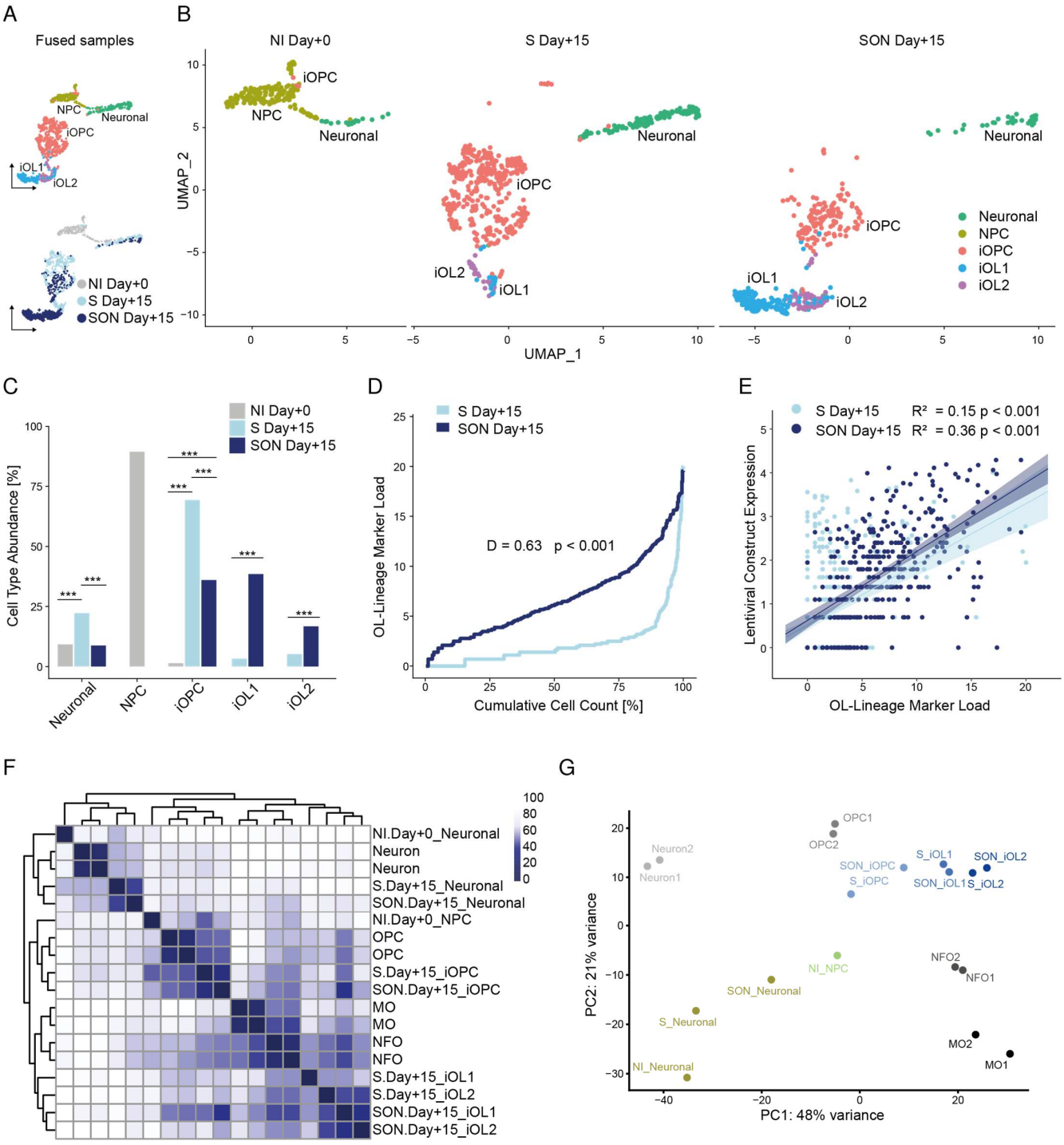

Figure 3. scRNAseq reveals higher level of maturation of oligodendroglial lineage cells, increased level of lentivirus dependent lineage commitment in SON-differentiation and co-clustering with primary OPCs and OLs. (**A**) UMAP embedding of integrated scRNAseq data of baseline sample (Day + 0) after neural induction (NI, *n* = 217 cells) and samples + 15 days after directed differentiation by SOX10 (S, *n* = 577 cells) and SOX10-OLIG2-NKX6.2 (SON, *n* = 400 cells). Top: UMAP dimension plot illustrates clusters of neural precursor cells (NPC, brown), neuronal cells (green), induced oligodendrocyte precursor cells (iOPCs, red), induced oligodendrocyte cluster 1 (iOL1, blue), and

induced oligodendrocyte cluster 2 (iOL2, violet). Bottom: UMAP dimension plot illustrated sample composition after neural induction (NI Day + 0, grey), 15 days after directed differentiation by SOX10 (S Day + 15, light blue), and SOX10-OLIG2-NKX6.2 (SON Day + 15, dark blue). (**B**) UMAP dimension plot, split by sample, showing clusters of neural precursor cells (NPC, brown), neuronal cells (green), induced oligodendrocyte precursor cells (iOPCs, red), induced oligodendrocyte cluster 1 (iOL1, blue), and induced oligodendrocyte cluster 2 (iOL2, violet). (**C**) Percentage of cells (*y*-axis) in each cluster (*x*-axis) from scRNAseq samples NI Day + 0 (grey), S Day + 15 (light blue), SON Day + 15 (dark blue) from B. Significant differences (*** $p < 0.001$) of the cell cluster abundance between annotated samples based on Fisher's exact tests. (**D**) Cumulative iOL lineage marker load (*y*-axis) across the ranked cells (*x*-axis) after + 15 days of directed differentiation by SOX10 (S Day + 15, light blue) and SOX10-OLIG2-NKX6.2 (SON Day + 15, dark blue). *p*-value indicates a significance difference in iOL lineage marker load distribution (Kolmogorov–Smirnov test, *p*-value < 0.001) across the cell population from the scRNAseq experiments after S- and SON-directed oligodendroglial differentiation with higher load in SON-expressing cells (Wilcoxon's rank-sum test, W = 44916, $p < 0.001$. (**E**) Linear regression model of the relationship between lentiviral construct expression (*y*-axis) and iOL lineage marker load (*x*-axis) across the cell populations of S- and SON-directed oligodendroglial differentiation from corresponding scRNAseq data. Spearman's R^2 coefficient of determination and respective significance value of the regression model is indicated in the plot. (**F**) Comparison of transcriptomes of samples from this study with published primary murine cells [27]. Heatmap of Manhattan sample distances and dendrograms from the corresponding unsupervised hierarchical clustering. Abbreviations for primary reference samples: MO, myelinating oligodendrocytes; NFO, newly formed oligodendrocytes; OPC, oligodendrocyte precursor cells. (**G**) Principal component analysis dimension plot showing the first two principal components. scRNAseq data points are colored, whereas reference murine samples are shown in black and grey scale, as indicated.

The most abundant cell types in the baseline neural induction Day + 0 sample were NPCs (89.4%) and neuronal cells (9.2%); a few cells were assigned to the iOPC cluster (1.4%) but no iOLs were detected (Figure 3A–C). The S-directed culture was dominated by the iOPC cluster (69.3%), and the proportion of iOL1 (3.3%) and iOL2 (5.2%) cells was much lower. In contrast, the sample from the SON-directed differentiation comprised a high fraction of iOL1 (38.5%) and iOL2 cells (16.8%), representing a significant ($p < 0.001$) 11- and 3-fold enrichment, respectively, over the S condition (Figure 3C). In contrast, the iOPC cluster was larger in S- compared to SON-directed oligodendroglial differentiation ($p < 0.001$; Figure 3C, Tables S4 and S5).

Next, we investigated the effect of S- versus SON-directed differentiation on the maturation state across the corresponding cell clusters. When plotting the cumulative OL-lineage marker load as a step function of the marker load rank, we observed that the SON-directed populations exhibited a different distribution of OL-lineage marker load (Kolmogorow-Smirnow-Test, *p*-value < 0.001) with generally higher load in SON-expressing cells (Wilcoxon's rank-sum test, W = 44916, $p < 0.001$, Figure 3D). Of note, in both directed differentiation approaches OL-Lineage marker load was significantly associated with the lentiviral construct expression ($p < 0.001$, Figure 3E). The correlation was higher in SON-directed differentiation ($R^2 = 0.36$) compared to S ($R^2 = 0.15$) indicating a stronger oligodendroglial determination using SON-directed differentiation (Figure 3E).

In both S- and SON-directed oligodendroglial differentiation, a small fraction of cells escaped the oligodendroglial lineage and differentiated towards a neuronal identity. However, this neuronal population was 2.5 times ($p < 0.001$) less abundant with SON-directed (8.8%) than with S-directed differentiation (22.2%) (Figure 3A–C).

3.5. Co-Clustering of S- and SON-Differentiated iOPCs and iOLs with Primary OPCs and OLs

To compare iOPCs and iOLs with primary OPCs and OLs, we calculated the average gene expression in each cluster and sample (Table S6) and performed unsupervised clustering of each sample's clusters with reference transcriptomic data that were obtained from FACS purified primary cells [27]. In the resulting dendrogram, we found three main clusters: One cluster grouped the iOL1 and iOL2 profiles together with newly formedmurine oligodendrocytes (NFO) and myelinating oligodendrocytes (MO) [27], a second cluster contained the iOPCs and NPCs together with the reference OPC samples (Figure 3F) and in the third cluster the neuronal cells clustered together with primary neurons. When we looked at the 50 most variable features in this unsupervised clustering, we found that 26 of those genes formed a gene set that separated the oligodendroglial samples from the neuronal cells (Figure S3). In this gene set, all iOL cluster profiles closely resembled the NFO and the expression profile MO of the reference sample. In a principal component analysis, the first principal component explained 48% of the total variance, and the samples were aligned in the presumable flow of differentiation, findings that underline the high similarity between the S-/SON-directed hiPSC-derived cells and primary oligodendroglial cells (Figure 3G).

3.6. Dedicated Gene Expression Profiles of Marker Genes Support Identities of Subclusters and Differential Efficiency of S and SON Conditions towards the Oligodendroglial Lineage

To further characterize cluster identities, we compared the expression and abundance of marker genes [9] in the dedicated NPC, iOPC, and iOL1 and iOL2 subclusters (Figure 4 and Figure S4, Tables S4–S7). The neural stem cell marker *PAX6* was highly expressed not only in a large proportion of NPCs but also in a substantial proportion of iOPCs. S-derived iOPCs expressed *PAX6* at higher frequencies as compared to SON iOPCs ($p < 0.001$) (Figure 4A–C). This enrichment towards NPC/S-iOPC was supported by violin plots showing the distribution of the averaged expression levels which was higher in S iOPCs over SON iOPCs ($p < 0.001$, Figure 4D). An overall similar profile was observed for an additional progenitor marker, *SOX3* (Figure S4A–D, Tables S4–S7). *SOX9*, an OPC stage-enriched TF, was predominantly expressed in S- and SON-iOPCs with no substantial differences within the respective clusters but a significantly higher number of *SOX9* expressing cells in the S-directed cluster compared to the SON condition ($p < 0.001$, Figure 4E–H). An overall similar, OPC-biased profile was obtained with *ST8SIA1* (the gene product stained with the prototypical OPC marker A2B5, Figure S4E–H, Tables S4–S7). *MBP* was selected as a marker for mature OLs and showed a strong increase in expression comparing iOPC and iOL1 clusters ($p < 0.001$) reaching the highest expressing levels in the iOL2 cluster ($p < 0.001$, Tables S4–S7). Moreover, SON iOPCs express low levels of *MBP* in contrast to S iOPCs ($p < 0.001$), but in S-derived cells, *MBP* was almost exclusively detected in iOL1 and iOL2 clusters (Figure 4I–L). Notably, some myelin genes expressed at the late stage, such as myelin-associated oligodendrocyte basic protein (*MOBP*), were robustly expressed only in the SON-derived iOL2 cell population and almost absent in S-derived cells (Figure 4M–P, Tables S4–S7). The higher level of expression of *MBP* and many other myelin marker genes, such as proteolipid protein 1 (*PLP1*) and galactosylceramidase (*GALC*, Figure S4I–P, Tables S4–S7), indicates that the iOL2 subcluster represents the most matured fraction of iOLs.

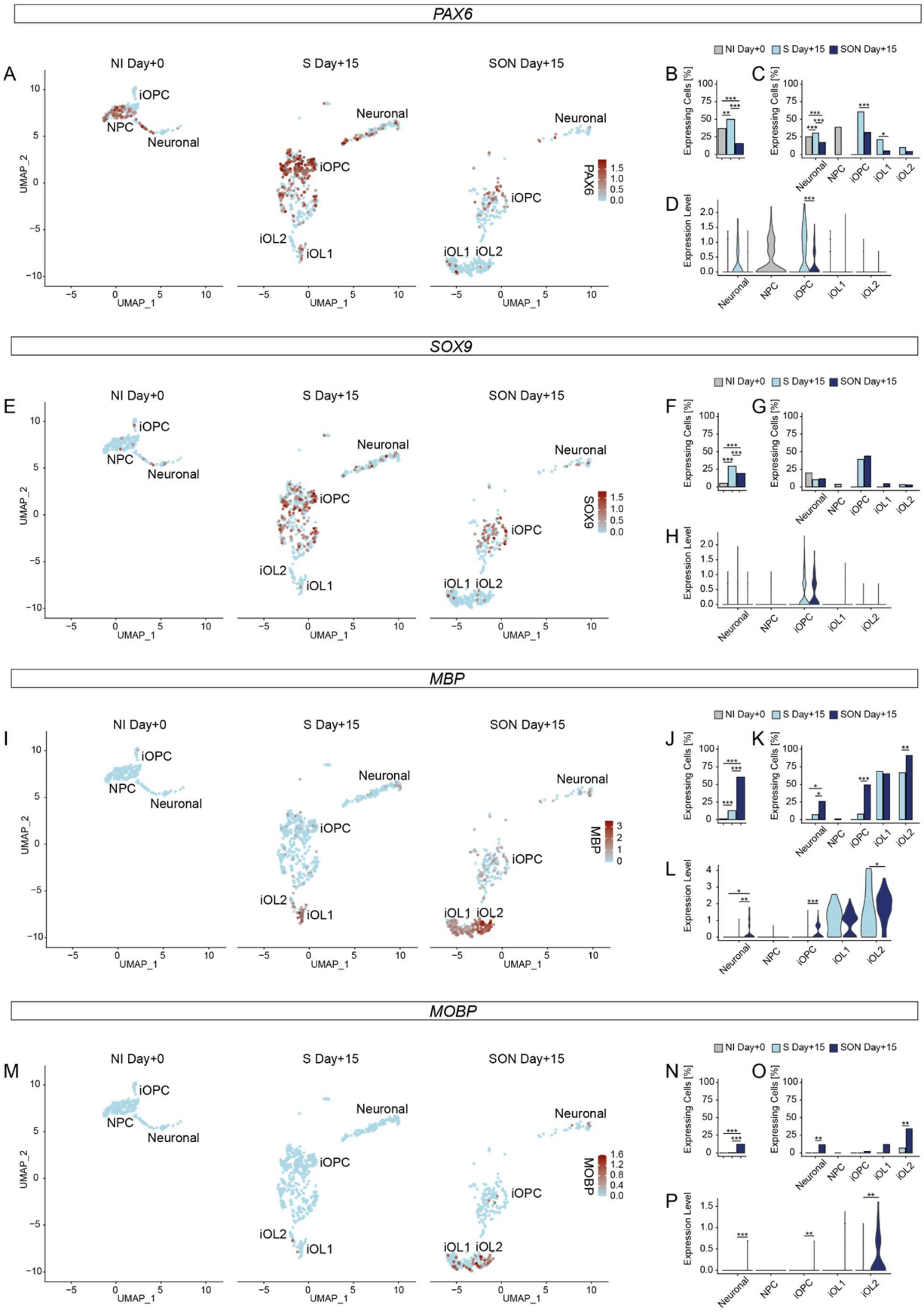

Figure 4. Marker gene expression verifies cluster identities and shows a mature oligodendrocyte phenotype in SON. (**A**,**E**,**I**,**M**) UMAP representation showing single-cell expression of selected marker

genes (**A**) *PAX6*, (**E**) *SOX9*, (**I**) *MBP*, (**M**) *MOBP* from scRNAseq of baseline sample after neural induction (NI Day + 0, n = 217 cells, one independent experiment) and samples after 15 days of directed differentiation by SOX10 (S Day + 15, n = 577 cells, one independent experiment) and SOX10-OLIG2-NKX6.2 (SON Day + 15, n = 400 cells, one independent experiment) with annotated cell clusters of neural precursor cells (NPC), neuronal cells, induced oligodendrocyte precursor cells (iOPCs), induced oligodendrocyte cluster 1 (iOL1) and induced oligodendrocyte cluster 2 (iOL2). Expression value per cell plotted according to the color intensity of the respective scale bar as indicated. (**B**,**F**,**J**,**N**) Bar plots illustrate the abundance of expressing cells for each sample. ** (p-value < 0.01), *** (p-value < 0.001) based on Fisher's exact tests (details provided in Table S5). (**C**,**G**,**K**,**O**) Bar plots illustrate the abundance of expressing cells for each cluster split by sample. * (p-value < 0.05), ** (p-value < 0.01), *** (p-value < 0.001) based on Fisher's exact tests (details provided in Table S5). (**D**,**H**,**L**,**P**) Violin plots of the normalized expression per sample within the respective cell type cluster. * (p-value < 0.05), ** (p-value < 0.01), *** (p-value < 0.001) based on Wilcoxon signed-rank test (details provided in Table S7).

3.7. RNA Velocity Reveals Divergent Dynamics of Fate Decisions upon Induced Oligodendroglial Differentiation

To examine the transcriptional dynamics underlying the different processes and outcomes of S- and SON-directed differentiation, we applied the RNA velocity approach to model the splicing kinetics as a proxy of the status of individual cells along the differentiation trajectories [23]. Briefly, the direction and speed of transcriptional changes in single cells are estimated from the ratio of detected unspliced to detected spliced transcripts. This allows for the prediction of the future transcriptional state of a specific gene in a given cell. A higher than expected ratio of unspliced to spliced mRNAs signifies upregulation over steady-state expression levels because of the temporal delay between an increase in transcriptional rate and an increase in the amount of mature mRNAs as end products of splicing [23]. In turn, a lower than expected unspliced to spliced ratio indicates downregulation because of the temporal delay between a decrease in the transcriptional rate and degradation of mature mRNAs. The 'velocity' vectors represent the direction and speed of the transcriptional changes in each cell and estimate future cell kinetics by indicating the movement of the cell through transcriptional space during differentiation.

In our data, we first determined the proportion of detectable unspliced transcripts to ensure their suitability for this type of analysis. This value typically depends on the protocol used, data processing, read length, and cell types present in the sample [31,33]. In our samples, the overall proportion of unspliced counts was 13% (Figure S5A), which was well within the expected range [33]. We found small differences among clusters (Figure S5B) and between samples (Figure S5C) but the differences were all within a range of 11% (iOL1) to 16% (NPC).

When the 'velocity' vectors were superimposed on the UMAP dimension plot (Figure 3A), two main streams of cells—an oligodendroglial and a neuronal stream—emerged along differentiation pathways in our cultures (Figure 5A). Moreover, we looked at the gene-shared latent time, a recent pseudo-time concept that uses only transcriptional kinetics instead of a diffusion-based approach [31]. Here, we found two endpoints, one pathway in the direction of the neuronal cluster and one in the direction of the iOL2 cluster, again indicating the presence of two distinct lineages in the pooled S and SON samples (Figure 5B). Additionally, we used partition-based graph abstraction (PAGA) to identify transitions between clusters [34] (Figure 5C). These transitions confirmed the two major differentiation pathways in our samples: One pathway represented the oligodendroglial lineage, in which the cells transitioned from an OPC state to an early OL identity in the iOL1 cluster and then moved on to the more mature iOL2 cluster, and the other led to a neuronal identity. In this stream, cells in the neural induction baseline sample differentiated directly towards this direction. In contrast, in the S

and SON samples, where no NPCs were left, iOPCs transdifferentiated to a neuronal identity. These escaping iOPCs were also clearly visible in the vector plot (Figure 5A).

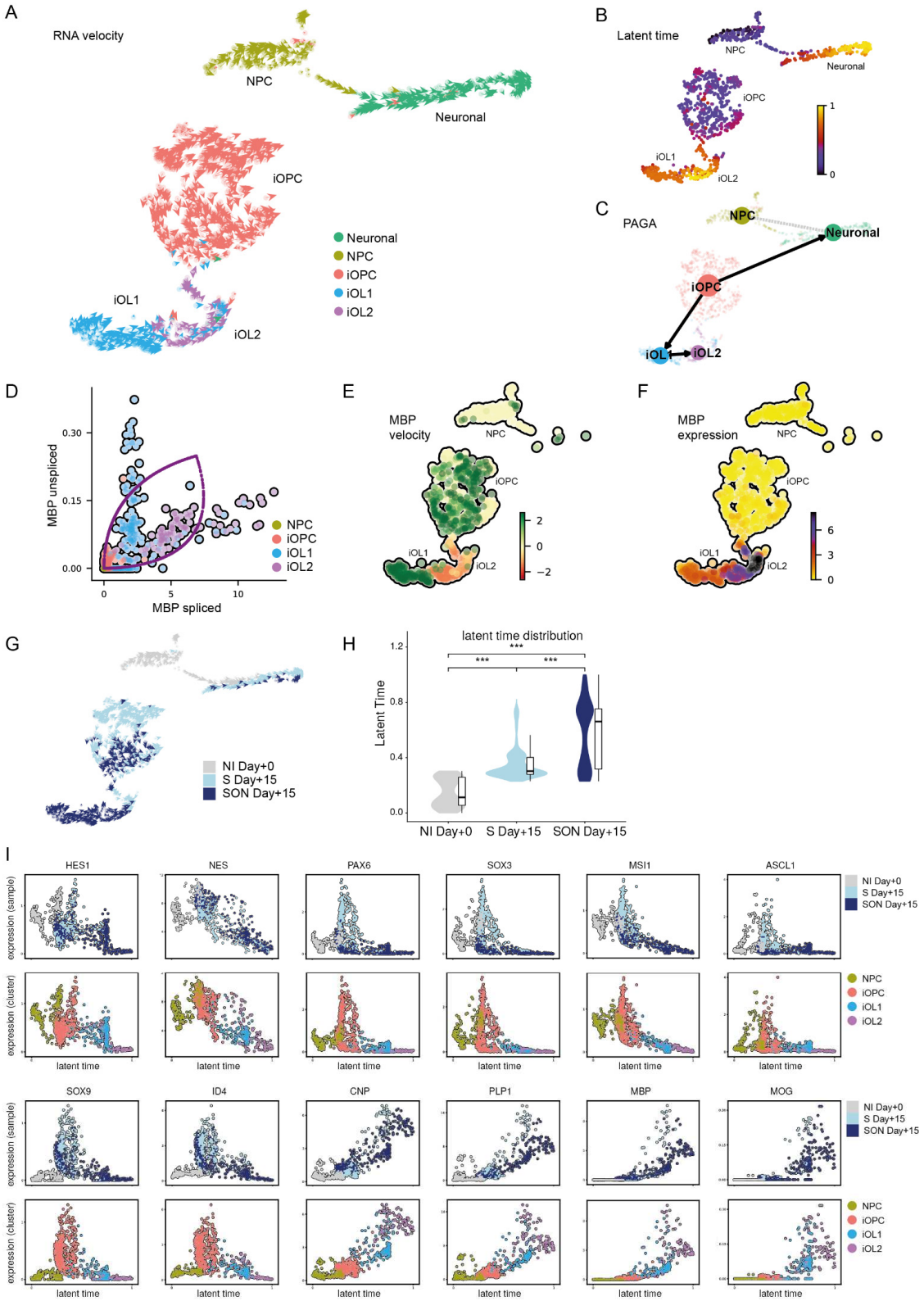

Figure 5. RNA velocity reveals the dynamics of fate decisions upon induced oligodendroglial differentiation. (**A**) RNA velocity vectors projected on the single-cell UMAP-based dimension plot

indicate direction and speed of individual cells in transcriptional space. (**B**) The gene-shared latent time identifies two endpoints of differentiation in the scRNAseq samples: One in the induced oligodendrocyte cluster 2 (iOL2) cluster and one in the neuronal cluster. (**C**) Partition-based graph abstraction (PAGA) plot visualizing transitions between clusters superimposed on the UMAP embedding reveals two differentiation paths: (1) the oligodendroglial lineage, in which the cells transition from iOPC to iOL1 to iOL2, and (2) the neuronal lineage from NPCs and iOPCs that escape the TF-directed oligodendroglial differentiation. (**D**) Dynamic model of MBP's transcriptional kinetics plotted on top of the scatter plot of unspliced and spliced transcript expression. (**E**) MBP velocity estimates indicating MBP mRNA induction (green) and repression (red). (**F**) MBP expression level. (**G**) Velocity vectors on UMAP embedding with sample color code: Sample after neural induction (NI Day + 0) in grey, S-directed differentiation (S Day + 15) in light blue and SON-directed differentiation (SON Day + 15) in dark blue, as indicated. (**H**) Latent time distribution between baseline (NI Day + 0), S-directed differentiation (S Day + 15), and SON-directed differentiation (SON Day + 15), illustrated with a violin and box- and-whisker plot. Pairwise comparisons were tested with Wilcoxon's rank-sum test. *** $p < 0.001$. (**I**) Latent time versus gene expression of stage-specific genes during oligodendrocyte differentiation. Individual cells colored by cluster and sample.

In addition, we analyzed the dynamic model and RNA velocity of individual 'velocity genes' (Figure 5I). An interesting example of a strong 'velocity gene' is *MBP*. The phase portrait visualizes unspliced and spliced transcripts overlayed with the corresponding dynamic model (Figure 5D). When examining the phase portrait of *MBP*, we noticed that most iOL1 cells were in an on state, i.e., upregulating *MBP* transcription, as indicated by a high positive ratio of unspliced to spliced transcripts (Figure 5E). In contrast, most iOL2 cells were close to a steady-state or negative velocity value, reflecting the endpoint of *MBP* upregulation (Figure 5E). However, the somewhat counterintuitive RNA velocity-derived model for the oligodendroglial differentiation path iOPC to iOL1 to iOL2 (Figure 5C,E) was in line with the elevated levels of spliced *MBP* mRNA level along this trajectory (Figure 5F,I).

We also detected clear differences in the differentiation processes between the S Day + 15 and SON Day + 15 samples (Figure 5G). Notably, the population of iOPCs moving towards the neuronal cluster was much more prominent in S-directed than in SON-directed oligodendroglial differentiation (Figure 5G, upper light blue half of the iOPC cluster). Moreover, the gene-shared latent time scores of each cell could be used as an indicator of maturity because in both samples the cells took a similar path in their differentiation to OLs. This was confirmed in an individual RNA velocity analysis of both samples, which eliminated the possibility that one sample could be interfering with the other (Figure S5D). When comparing the latent time scores between samples, the oligodendroglial lineage in the SON-expressing culture (median = 0.66; MAD = 0.31; $n = 365$) was found to be significantly more mature than that in the S-expressing culture (median = 0.30; MAD = 0.05; $n = 449$) [W = 42640; $p = 2.2 \times 10^{-16}$] (Figure 5H). This result was in line with the higher abundance of iOL1 and iOL2 cells in SON Day + 15.

Finally, we identified a series of differentiation marker genes from a previously published study [9] expressed in our samples and illustrated their transcriptional kinetics during OL differentiation as a gene expression level dependent on latent time (Figure 5I). This allowed us to show again the high overlap of a late gene-shared latent time point, the SON sample, and the iOL cluster identities (Figure 5I).

3.8. Characterisation of iOPC Subclusters

The RNA velocity analysis enabled us to clearly identify two distinct differentiation streams within the iOPC cluster that were moving in different directions (Figure 5G), a feature that was not detected in the first shared nearest neighbor (SNN)-based clustering result (Figure 3A,C). One subcluster followed the oligodendroglial lineage and was present in both S- and SON-directed differentiation and another partly escaped towards a neuronal lineage and was almost exclusively found in the S-directed differentiation (Figure 5G). Because of this observation, we increased the resolution of the SNN clustering to empir-

ically identify subpopulations in the sample. This approach allowed us to identify two iOPC subclusters that were illustrated in an RNA velocity plot color coded for the iOPC subclusters (Figure 6A and Figure S6A,B). The iOPC2 subcluster, which occurred in both conditions (18.2% in S Day + 15 and 32.0% in SON Day + 15), comprised mainly the iOPC population of the OPC-OL differentiation pathway (Figure 6A). In contrast, the iOPC1 subcluster was almost exclusively observed in S Day + 15 (51.1% in S Day + 15 and 4.2% in SON Day + 15) and comprised the stream of cells escaping towards the neuronal cluster, which likely represented a more volatile iOPC stage under the given culture condition (Figure 6A and Figure S6A,B). Of note, we analyzed the expression of the exogenous lentiviral construct via the scRNAseq-detecTable 3′LTR site (Figure S6C,D). Expression levels of exogenous constructs were higher and more homogenous in iOL1 and iOL2 compared to iOPC1, iOPC2, and the neuronal cluster. Furthermore, within iOPC1, iOPC2, iOL1, and iOL2, S-, or SON-construct expression were comparable.

To identify molecular signatures of the two iOPC stages, we compared the differential average gene expression in the S-iOPC1, S-iOPC2, and SON-iOPC2 subclusters (Figure 6B–F, Table S8). We found substantial differences in significantly deregulated genes between the iOPC1 and iOPC2 clusters in the comparisons of S-iOPC1 with S-iOPC2 (Figure 6B) and S-iOPC1 with SON-iOPC2 (Figure 6C). Notably, the progenitor markers PAX6 and SOX3 were expressed at a lower level in the iOPC2 cluster, indicating a higher maturation level (Figure 6B,C). In contrast, only very few genes were found to be differentially expressed in S-iOPC2 and SON-iOPC2, indicating that the iOPC2 cluster identity was independent of the condition and that it represents a rather homogenous entity (Figure 6D). This assumption was corroborated by the broad overlap of differentially expressed genes in both comparisons (Figure 6E,F). A comparison of SON-iOPC1 and SON-iOPC2 was deemed not advisable because of the low number of cells in the SON-iOPC1 cluster, which can be independently interpreted as an indicator of an increased drive of iOPC maturation mediated by SON compared with iOPC maturation mediated by S alone. This finding underlines that the directed OL differentiation driven by S was similar in both conditions, whereas the efficiency was higher with SON than with S. Furthermore, we performed a gene ontology term-based hypergeometric enrichment analysis for the comparisons of iOPC1 and iOPC2 (Table S9). Thereby we identified gene-sets relevant for the organization of the extracellular matrix as most significantly altered (Figure 6G), a result that is in line with several genes of the collagen family that were detected as being upregulated in the gene-by-gene analysis (Figure 6B,C).

These findings prompted us to hypothesize that structural differences may also be visible between S- and SON-generated iOPCs. Therefore, for both conditions we performed microbead purification to enrich $O4^+$ iOPCs at day + 10 and morphological analysis of $O4^+$ cells at day + 16. We thereby observed substantial morphological differences between S- and SON-directed $O4^+$ cells (Figure 6D) and a larger average cell size of SON-derived $O4^+$ cells compared with S-derived $O4^+$ cells (Figure 6H).

Overall, our results show that different combinations of TFs have a substantial effect on iOPC and iOL morphology, maturation stage, cell cluster composition, and lineage transition dynamics.

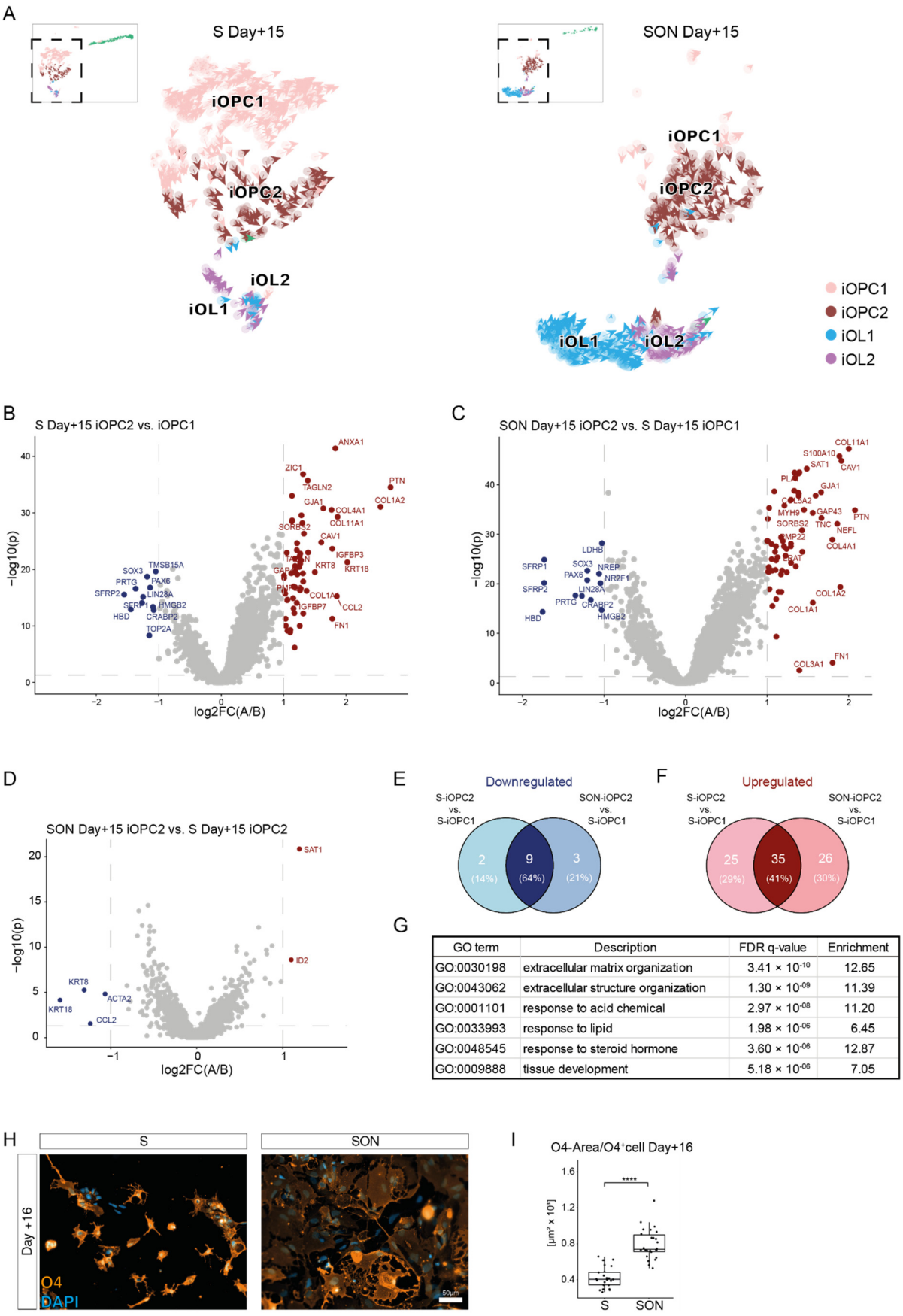

GO term	Description	FDR q-value	Enrichment
GO:0030198	extracellular matrix organization	3.41×10^{-10}	12.65
GO:0043062	extracellular structure organization	1.30×10^{-09}	11.39
GO:0001101	response to acid chemical	2.97×10^{-08}	11.20
GO:0033993	response to lipid	1.98×10^{-06}	6.45
GO:0048545	response to steroid hormone	3.60×10^{-06}	12.87
GO:0009888	tissue development	5.18×10^{-06}	7.05

Figure 6. Characterization of iOPC subcluster formation induced by S- and SON-directed differentiation reveals profound differences in expression of extracellular matrix components. (**A**) Zoom-out

of oligodendroglial lineage clusters of RNA velocity vectors projected on UMAP dimension plot of iOPC1, iOPC2, iOL1, and iOL2 clusters of S Day + 15 and SON Day + 15. For a complete dimension plot including neuronal linage, see Figure S6A,B. (**B**) Differential gene expression (DGE) analysis of S-iOPC2 subcluster and S-iOPC1 subcluster illustrated with volcano plot. The average log2 fold change (log2FC) is shown on the *x*-axis and the negative log10 *p*-value (−log10(*p*)) on the *y*-axis. Genes significantly upregulated (red) and downregulated (blue) in S-iOPC2 compared with S-iOPC1 are colored. The top 20 differentially expressed genes are labeled for up- and downregulation accordingly. (**C**) DGE analysis of SON-iOPC2 subcluster and S-iOPC1 subcluster illustrated with a volcano plot. Genes significantly upregulated (red) and downregulated (blue) in SON-iOPC2 compared with S-iOPC1 are colored. (**D**) DGE analysis of SON-iOPC2 subcluster and S-iOPC2 subcluster illustrated with a volcano plot. Genes significantly upregulated (red) and downregulated (blue) in SON-iOPC2 are colored. (**E**) Upregulated genes within iOPC subclusters shown in a Venn diagram. (**F**) Downregulated genes within iOPC subclusters shown in a Venn diagram. (**G**) Pathway enrichment analysis of iOPC subcluster comparison. (**H**) Representative images of $O4^+$ iOPCs after microbead purification. (**I**) Quantification of cell sizes of $O4^+$ iOPCs illustrated with a box-and-whisker plot. Dots correspond to analyzed fields of view (n = 25–26 per condition). Statistical analysis by two-sided *t*-test. **** $p < 0.0001$.

4. Discussion

In our comparative study, we confirmed that S-, SO- and SON-directed conversion are all sufficient to rapidly generate oligodendroglial lineage cells from hiPSCs. As a result of the side-by-side analysis at the single-cell resolution, we showed that the application of SON generated more $O4^+$ late-stage iOPCs and more mature and complex MBP^+ iOLs than the application of S alone, supporting previous observations [11]. S alone was most effective in generating a mixed population of iOPCs (see below). In agreement with previous studies [36,37], we observed a higher level of expression of smaller-sized constructs. However, an intermediate selection step performed in our protocol normalized these differences and allowed us to compare TF combinations irrespective of construct size. As mentioned above, a more recent study that used a systematic screen for lineage-converting TFs found that SOX9 was capable of inducing oligodendroglial cells on its own [14]. Thus, similar to other SOX family members, both SOX9 and SOX10 can be considered as pioneering TFs in the oligodendroglial lineage that prime critical steps essential for stem cell conversion [38]. SOX9 operates genetically upstream of SOX10 in the oligodendroglial lineage and—despite the fact that SOX9 can generate myelinating iOLs in a 3D system [14]—it remains an open question whether SOX9 might generate more earlier stage iOPCs than SOX10 in a cell-autonomous setting such as the one applied in this study. We observed substantial differences in iOPC and iOL heterogeneity and dynamics of differentiation between S- and SON-directed oligodendroglial differentiation. Despite the finding that OPC marker genes such as *SOX9*, *ST8SIA1*, *CNP*, *ID2* and *ID4* reached similar levels in S- and SON-iOPCs, the expression level of oligodendroglial maturation markers such as *GALC* and *MOBP* was higher in SON-iOLs than in S-iOLs under the applied conditions. Moreover, the cell cluster composition differed dramatically: Mature iOLs, that express *PLP1, GALC, MBP, MOBP,* were far more abundant upon SON-directed differentiation but the iOPC cluster was larger and more diverse in the S-directed condition (see below).

To improve purity and scalability, we introduced the lentivirus-encoded lineage transcription factors at the level of iPSC cultivation followed by two puromycin selection steps, one before and one after initiation of iOPC/iOL differentiation; this protocol was robust for different iPSC lines obtained from six different human donors. The advantage of this approach is that less lentivirus is needed and only infected S/O/N-hiPSCs are proliferative and can be amplified, frozen, banked, and recovered en masse at the time needed. In the future, this approach will be particularly suited to enable larger-

scaled case-control comparisons and may allow also genetic and compound screenings requiring high numbers of dedicated cells. Nonetheless, epigenetic lentivirus silencing is a confounding factor [39]. The drop of FLAG$^+$ hiPSCs after doxycycline induction is likely due to the loss of cleavage efficiencies by single versus double P2A/T2A element-containing constructs [40].

In both conditions (S and SON), the lentiviral construct expression level was associated with a higher level of OL-lineage marker load. However, SON-directed differentiation caused a much higher marker load underlining a more maturating oligodendroglial differentiation compared to S-directed differentiation in line with previous work [11].

On the iOPC/iOL level, lentiviral construct transcriptome levels within the clusters were comparable between S and SON indicating that the expression levels are unlikely to cause cluster diversity and that this diversity is most likely attributed to the different TF combinations. However, expression levels were higher in iOL clusters compared to iOPC clusters and the neuronal cluster. Thus, it might be possible that higher expression levels sustain the directed differentiation. Thus, for genetic and chemical screens [41,42], safe harbor strategies may be a better choice to express OL-lineage-converting TFs and previous work could highlight that safe harbor strategies using SOX10 were sufficient to generate high yields of homogenous MBP$^+$ iOLs [19].

However, safe harbourstrategies will be complicated to apply in case-control comparisons, where many subjects/cell lines are to be compared. Nonetheless, a safe harbor-mediated CRISPR/Cas9-based genetic screen has been described for hiPSC-derived NGN2-directed iNeurons [41], showing the potential of this approach also for other cell types. Safe harbor strategies that apply CRISPR/Cas9 technology could also be applied to modify directed differentiation. In contrast to exogenous overexpression of TFs for directed differentiation, a recently published study applied CRISPR/Cas9-mediated activation of endogenous *Sox10*, *Olig2*, and *Nkx6.2* by specific gRNAs to differentiate mouse neural stem cells and mouse embryonic fibroblasts to O4$^+$ and MBP$^+$ oligodendroglial cells [43].

In this study and previous studies that used the same neuronal patterning approach [13,19], the expression of early-stage OPCs markers, such as *CSPG4* (*NG2*) and *PDGFRA*, was barely detectable in iOPCs. Thus, with both SON and S this directed differentiation approach can be assumed to bypass early OPC stages. Chemical differentiation approaches may therefore be preferable for examining early-stage OPCs over a longer time period [44,45]. A study that used such an approach applied scRNAseq on PDGFRA-enriched, chemically transformed OL-lineage cells and uncovered several stages of OPCs [46]. The scRNAseq analysis of our study revealed that directed oligodendroglial-lineage conversion also reflects several aspects of known OPC and OL development [9,47]. For example, we observed an upregulation of *ST8STIA1* (A2B5), *ID2*, *ID4*, and *SOX9* in iOPCs. In addition, we found increased expression of the oligodendroglial markers *CNP* and *PLP1* during differentiation. In addition, in more mature iOLs we found an enhanced expression of marker genes for OL differentiation, such as *MBP* and *MYRF* that are crucial for myelination [47].

To investigate hiPSC-based oligodendroglial lineage differentiation, we applied RNA velocity analysis, a technique that was developed for investigating differentiation processes in scRNAseq datasets to infer temporal changes without needing to obtain samples at several time points [23]. Thereby, we described the transcriptional dynamics during fate decisions in induced oligodendroglial differentiation and identified *MBP*, for example, as a velocity gene. Nevertheless, our data are based on 3′UTR-enriched single-cell transcriptome libraries, which limits their information content in RNA velocity analysis. Full-length scRNAseq protocols, which cover more splicing sites, would detect a higher variety of splicing variants and thus increase the number of potential velocity genes and might be beneficial to improve velocity analysis [31]. Nonetheless, the RNA velocity-based analyses in this study provided additional insights. With the help of graph-based analysis methods such as PAGA [34], we could visualize the oligoden-

droglial differentiation stream from iOPC to iOL1 and iOL2, which could be validated independently in S- and SON-directed differentiation and which would not have been identified with standard scRNAseq analysis. To generate a pseudo-timeline, we used gene-shared latent time instead of common similarity-based Markovian diffusion models, as suggested by Bergen et al., (2020). This approach improved the resulting timeline dramatically because the diffusion-based pseudo-timeline forced a unidirectional 'time flow' onto the dataset, which clearly did not fit the existence of two distinct lineages in one dataset. We used latent time analysis to highlight the 'time'-dependent up- and downregulation of several oligodendroglial stage markers and to estimate the maturation state of a single cell within the whole span of oligodendroglial differentiation. Hereby, we observed a higher latent time distribution with SON than with S, indicating that oligodendroglial differentiation was faster in the SON- than in the S-directed differentiation. RNA velocity also uncovered a second neuronal leakage stream that was more prominent in S-directed differentiation. This leakage stream indicated that not only NPCs with low construct expression but also parts of the S-iOPC1s differentiated towards a neuronal state. Thus, we found evidence that S-directed differentiation might allow some iOPCs to 'escape' towards the neuronal lineage during the differentiation process, and that SON-directed differentiation seems to be less volatile and more efficient regarding OL differentiation under the applied conditions.

Differential gene expression analysis revealed that S-iOPC2 and SON-iOPC2 were quite similar and showed a substantial overlap in their differentially expressed genes when compared with iOPC1. This finding hints at a similar differentiation path with S and SON, although efficiency was higher with SON, as reflected by the abundance of more mature oligodendroglial cells, i.e., iOPC2, iOL1, and iOL2. On the other hand, iOPC1 constitutes a population of 'escaping' cells, giving us the opportunity to investigate the transcriptional networks and signaling machinery necessary for different steps of the differentiation process. Pathway analysis indicated greater expression of extracellular matrix components in iOPC2 cells than in iOPC1 cells; this difference may reflect a maturation step, as indicated by the change in direction of the velocity vectors towards the OL stage, or may represent a slight deflection towards other glial lineages [46].

Oligodendroglial-lineage cells represent a heterogeneous cell population with a high spatio-temporal diversity [3,6]. A limitation of directed protocols is that they most likely generate only a subset of OPC/OL sub-lineages, depending on which TFs or combination of TFs they use. An advantage of directed conversion, however, is that human cells from a defined differentiation state can be generated in virtually unlimited amounts for various applications.

Our work highlights that applied TFs for generating iOPCs or iOLs should be chosen depending on the intended application or research question. Our analysis suggests that differentiation directed by S offers a useful tool for research on OPC biology and earlier stages of oligodendroglial differentiation, including research that addresses the effects of external cues promoting OPC and OL differentiation, i.e., in a 3D/spheroid culture system; the same might be true for SOX9 [14]. On the other hand, applications, and research with a focus on more mature iOLs might benefit from the use of SON. TF combinations such as SON are likely to be better suited to studying OL biology and myelination-associated aspects, given the much higher conversion rate and easier access to much higher numbers of mature OLs with such combinations. Further investigations are certainly needed to unleash the potential of future cell therapies with engineered iOLs in myelin diseases, but a better understanding of the nature of induced cells via different TF-directed protocols will certainly be helpful to achieve this goal. We believe that the molecular and analysis tools applied in this study to force and dissect human oligodendrocyte development may support the understanding of dynamic aspects of cell-autonomous versus non-cell-autonomous contributions in in vivo disease models in the future, i.e., via grafting of iOLs generated from normal and diseased donors into mouse brains. The paradigmatic study on human iPSC-derived glia/mouse chimeras already revealed oligodendroglia-cell-autonomous

contributions to childhood-onset schizophrenia [48]. More such in vivo studies are needed that combine patient-derived oligodendoglial cell types with sophisticated single-cell level analyses to further increase our knowledge of disorders with myelination deficits.

Supplementary Materials: The following are available online at https://www.mdpi.com/article/10.3390/cells11020241/s1, Figure S1: Detailed illustration of applied lentiviral construct and neural induction (related to Figure 1), Figure S2: SON-directed differentiation from different hiPSC lines and effect of intermediate selection (related to Figure 2), Figure S3: 50 most variable genes from co-clustering of iOPCs and iOLs with primary cells (related to Figure 3), Figure S4: Illustration of extended marker gene expression from scRNAseq (related to Figure 4), Figure S5: Ratio of unspliced/spliced mRNA variants and sample-independent main differentiation trajectory analysis (related to Figure 5), Figure S6: Differences in RNA velocity graph between iOPC1 and iOPC2 are not based on different expression of directing TFs (related to Figure 6), Table S1: hiPSC lines in this study, Table S2: media, media supplements for cell cultivation and coating, Table S3: List of primary antibodies for immunostainings (related to Figure 1, Figure 2, Figure 6, Figures S1 and S2). Table S4: Abundance of cell clusters, gene marker expressing cells per samples and cluster. Related to Figure 3, Figure 4 and Figure S4. Table S5: Statistical analysis of cell clusters abundance per sample, abundance of gene expressing cells by sample and abundance of gene expressing cells per cluster split by sample. Related to Figure 3, Figure 4 and Figure S4. Table S6: Average expression of cell clusters. Related to Figure 3, Figure 4 and Figure S4. Table S7: Statistical analysis of normalized gene expression by cell cluster and by cell cluster split by sample. Related to Figure 3, Figure 4 and Figure S4. Table S8: Differential gene expression between iOPC1 and iOPC2. Related to Figure 6. Table S9: Hypergeometric gene ontology term enrichment analysis of iOPC1 and iOPC2. Related to Figure 6. Tables S4–S9 provide detailed datasets as separate Excel files.

Author Contributions: Conceptualization, F.J.R. and M.J.R.; methodology, F.J.R., M.S., S.G. and M.C.W.; investigation, F.J.R., M.S., V.H., D.D. and S.G.; formal analysis, F.J.R., M.S., J.B.W., N.K., M.J.Z., and M.J.R.; visualization, F.J.R., M.S., J.B.W. and M.J.R.; resources, M.C.W., P.F., M.J.Z., and M.J.R.; funding acquisition, F.J.R., A.S., P.F. and M.J.R.; writing—first draft, F.J.R., M.S. and M.J.R.; writing—review and editing, F.J.R., M.S., J.B.W., V.H., D.D., S.G., L.V.G., M.C.W., M.J.Z., A.S., P.F. and M.J.R.; supervision, M.J.R. All authors have read and agreed to the published version of the manuscript.

Funding: F.J.R. and M.S. were fellows of the International Max Planck Research School for Translational Psychiatry (IMPRS-TP). This research was funded by Munich Clinician Scientist Program (F.J.R.: Track 2–FöFoLePlus: 2020/009), Friedrich-Baur-Stiftung (F.J.R.: 68/19) and Verein zur Förderung von Wissenschaft und Forschung an der Medizinischen Fakultät der Ludwig-Maximilians-Universität München e.V. (F.J.R.), and by the Deutsche Forschungsgemeinschaft (M.J.R.; Az. RO 4076/3-1 and -2).

Institutional Review Board Statement: The study was conducted according to the guidelines of the Declaration of Helsinki and approved by the local ethics committee of the Faculty of Medicine, LMU Munich, Germany (17-880, 29.03.2018).

Informed Consent Statement: Informed consent was obtained from all subjects involved in the study.

Data Availability Statement: scRNAseq data (GEO: GSE179516) and codes for transcriptomic analyses (GitHub: https://github.com/MariusStephan/scRNAseq_S-SON, last accessed 1 December 2021) are publicly available.

Acknowledgments: The authors thank Jacquie Klesing, Board-certified Editor in the Life Sciences (ELS), for editing assistance with the manuscript. We like to acknowledge initial support regarding the implementation of RNA velocity analyses by Sven Falk, Friedrich-Alexander-University Erlangen-Nuremberg, Erlangen, Germany.

Conflicts of Interest: The authors declare conflict of interest. N.K., S.G., M.C.W. and M.J.R. are part-time employees and M.C.W. and M.J.R. are co-founders of Systasy Bioscience GmbH, Munich, Germany. The funders had no role in the design of the study; in the collection, analyses, or interpretation of data; in the writing of the manuscript, or in the decision to publish the results.

References

1. Micu, I.; Plemel, J.R.; Caprariello, A.V.; Nave, K.-A.; Stys, P.K. Axo-Myelinic Neurotransmission: A Novel Mode of Cell Signalling in the Central Nervous System. *Nat. Rev. Neurosci.* **2018**, *19*, 49–58. [CrossRef]
2. Simons, M.; Nave, K.-A. Oligodendrocytes: Myelination and Axonal Support. *Cold Spring Harb. Perspect. Biol.* **2015**, *8*, a020479. [CrossRef] [PubMed]
3. Dimou, L.; Simons, M. Diversity of Oligodendrocytes and Their Progenitors. *Curr. Opin. Neurobiol.* **2017**, *47*, 73–79. [CrossRef] [PubMed]
4. Zonouzi, M.; Berger, D.; Jokhi, V.; Kedaigle, A.; Lichtman, J.; Arlotta, P. Individual Oligodendrocytes Show Bias for Inhibitory Axons in the Neocortex. *Cell Rep.* **2019**, *27*, 2799–2808.e3. [CrossRef] [PubMed]
5. Jäkel, S.; Agirre, E.; Mendanha Falcão, A.; van Bruggen, D.; Lee, K.W.; Knuesel, I.; Malhotra, D.; Ffrench-Constant, C.; Williams, A.; Castelo-Branco, G. Altered Human Oligodendrocyte Heterogeneity in Multiple Sclerosis. *Nature* **2019**, *566*, 543–547. [CrossRef] [PubMed]
6. Spitzer, S.O.; Sitnikov, S.; Kamen, Y.; Evans, K.A.; Kronenberg-Versteeg, D.; Dietmann, S.; de Faria, O.; Agathou, S.; Káradóttir, R.T. Oligodendrocyte Progenitor Cells Become Regionally Diverse and Heterogeneous with Age. *Neuron* **2019**, *101*, 459–471.e5. [CrossRef]
7. Schmitt, A.; Simons, M.; Cantuti-Castelvetri, L.; Falkai, P. A New Role for Oligodendrocytes and Myelination in Schizophrenia and Affective Disorders? *Eur. Arch. Psychiatry Clin. Neurosci.* **2019**, *269*, 371–372. [CrossRef]
8. Chanoumidou, K.; Mozafari, S.; Baron-Van Evercooren, A.; Kuhlmann, T. Stem Cell Derived Oligodendrocytes to Study Myelin Diseases. *Glia* **2020**, *68*, 705–720. [CrossRef]
9. Goldman, S.A.; Kuypers, N.J. How to Make an Oligodendrocyte. *Development* **2015**, *142*, 3983–3995. [CrossRef]
10. Raabe, F.J.; Galinski, S.; Papiol, S.; Falkai, P.G.; Schmitt, A.; Rossner, M.J. Studying and Modulating Schizophrenia-Associated Dysfunctions of Oligodendrocytes with Patient-Specific Cell Systems. *NPJ Schizophr.* **2018**, *4*, 23. [CrossRef]
11. Ehrlich, M.; Mozafari, S.; Glatza, M.; Starost, L.; Velychko, S.; Hallmann, A.-L.; Cui, Q.-L.; Schambach, A.; Kim, K.-P.; Bachelin, C.; et al. Rapid and Efficient Generation of Oligodendrocytes from Human Induced Pluripotent Stem Cells Using Transcription Factors. *Proc. Natl. Acad. Sci. USA* **2017**, *114*, E2243–E2252. [CrossRef] [PubMed]
12. Pawlowski, M.; Ortmann, D.; Bertero, A.; Tavares, J.M.; Pedersen, R.A.; Vallier, L.; Kotter, M.R.N. Inducible and Deterministic Forward Programming of Human Pluripotent Stem Cells into Neurons, Skeletal Myocytes, and Oligodendrocytes. *Stem Cell Rep.* **2017**, *8*, 803–812. [CrossRef] [PubMed]
13. García-León, J.A.; Kumar, M.; Boon, R.; Chau, D.; One, J.; Wolfs, E.; Eggermont, K.; Berckmans, P.; Gunhanlar, N.; de Vrij, F.; et al. SOX10 Single Transcription Factor-Based Fast and Efficient Generation of Oligodendrocytes from Human Pluripotent Stem Cells. *Stem Cell Rep.* **2018**, *10*, 655–672. [CrossRef] [PubMed]
14. Ng, A.H.M.; Khoshakhlagh, P.; Rojo Arias, J.E.; Pasquini, G.; Wang, K.; Swiersy, A.; Shipman, S.L.; Appleton, E.; Kiaee, K.; Kohman, R.E.; et al. A Comprehensive Library of Human Transcription Factors for Cell Fate Engineering. *Nat. Biotechnol.* **2021**, *39*, 510–519. [CrossRef] [PubMed]
15. Chanoumidou, K.; Hernández-Rodríguez, B.; Windener, F.; Thomas, C.; Stehling, M.; Mozafari, S.; Albrecht, S.; Ottoboni, L.; Antel, J.; Kim, K.-P.; et al. One-Step Reprogramming of Human Fibroblasts into Oligodendrocyte-like Cells by SOX10, OLIG2, and NKX6.2. *Stem Cell Rep.* **2021**, *16*, 771–783. [CrossRef]
16. Okita, K.; Yamakawa, T.; Matsumura, Y.; Sato, Y.; Amano, N.; Watanabe, A.; Goshima, N.; Yamanaka, S. An Efficient Nonviral Method to Generate Integration-Free Human-Induced Pluripotent Stem Cells from Cord Blood and Peripheral Blood Cells. *Stem Cells* **2013**, *31*, 458–466. [CrossRef]
17. Danecek, P.; McCarthy, S.A.; Consortium, H.; Durbin, R. A Method for Checking Genomic Integrity in Cultured Cell Lines from SNP Genotyping Data. *PLoS ONE* **2016**, *11*, e0155014. [CrossRef]
18. Bock, C.; Kiskinis, E.; Verstappen, G.; Gu, H.; Boulting, G.; Smith, Z.D.; Ziller, M.; Croft, G.F.; Amoroso, M.W.; Oakley, D.H.; et al. Reference Maps of Human ES and IPS Cell Variation Enable High-Throughput Characterization of Pluripotent Cell Lines. *Cell* **2011**, *144*, 439–452. [CrossRef]
19. García-León, J.A.; García-Díaz, B.; Eggermont, K.; Cáceres-Palomo, L.; Neyrinck, K.; Madeiro da Costa, R.; Dávila, J.C.; Baron-Van Evercooren, A.; Gutiérrez, A.; Verfaillie, C.M. Generation of Oligodendrocytes and Establishment of an All-Human Myelinating Platform from Human Pluripotent Stem Cells. *Nat. Protoc.* **2020**, *15*, 3716–3744. [CrossRef]
20. Schindelin, J.; Arganda-Carreras, I.; Frise, E.; Kaynig, V.; Longair, M.; Pietzsch, T.; Preibisch, S.; Rueden, C.; Saalfeld, S.; Schmid, B.; et al. Fiji: An Open-Source Platform for Biological-Image Analysis. *Nat. Methods* **2012**, *9*, 676–682. [CrossRef]
21. Longair, M.H.; Baker, D.A.; Armstrong, J.D. Simple Neurite Tracer: Open Source Software for Reconstruction, Visualization and Analysis of Neuronal Processes. *Bioinformatics* **2011**, *27*, 2453–2454. [CrossRef]
22. Romagnoli, D.; Boccalini, G.; Bonechi, M.; Biagioni, C.; Fassan, P.; Bertorelli, R.; De Sanctis, V.; Di Leo, A.; Migliaccio, I.; Malorni, L.; et al. DdSeeker: A Tool for Processing Bio-Rad DdSEQ Single Cell RNA-Seq Data. *BMC Genom.* **2018**, *19*, 960. [CrossRef]
23. La Manno, G.; Soldatov, R.; Zeisel, A.; Braun, E.; Hochgerner, H.; Petukhov, V.; Lidschreiber, K.; Kastriti, M.E.; Lönnerberg, P.; Furlan, A.; et al. RNA Velocity of Single Cells. *Nature* **2018**, *560*, 494–498. [CrossRef]

24. Satija, R.; Farrell, J.A.; Gennert, D.; Schier, A.F.; Regev, A. Spatial Reconstruction of Single-Cell Gene Expression Data. *Nat. Biotechnol.* **2015**, *33*, 495–502. [CrossRef] [PubMed]
25. Hafemeister, C.; Satija, R. Normalization and Variance Stabilization of Single-Cell RNA-Seq Data Using Regularized Negative Binomial Regression. *Genome Biol.* **2019**, *20*, 296. [CrossRef] [PubMed]
26. McInnes, L.; Healy, J.; Melville, J. UMAP: Uniform Manifold Approximation and Projection for Dimension Reduction. *arXiv* **2020**, arXiv:1802.03426.
27. Zhang, Y.; Chen, K.; Sloan, S.A.; Bennett, M.L.; Scholze, A.R.; O'Keeffe, S.; Phatnani, H.P.; Guarnieri, P.; Caneda, C.; Ruderisch, N.; et al. An RNA-Sequencing Transcriptome and Splicing Database of Glia, Neurons, and Vascular Cells of the Cerebral Cortex. *J. Neurosci.* **2014**, *34*, 11929–11947. [CrossRef]
28. Love, M.I.; Huber, W.; Anders, S. Moderated Estimation of Fold Change and Dispersion for RNA-Seq Data with DESeq2. *Genome Biol.* **2014**, *15*, 550. [CrossRef]
29. Stuart, T.; Butler, A.; Hoffman, P.; Hafemeister, C.; Papalexi, E.; Mauck, W.M.; Hao, Y.; Stoeckius, M.; Smibert, P.; Satija, R. Comprehensive Integration of Single-Cell Data. *Cell* **2019**, *177*, 1888–1902.e21. [CrossRef]
30. Eden, E.; Navon, R.; Steinfeld, I.; Lipson, D.; Yakhini, Z. GOrilla: A Tool for Discovery and Visualization of Enriched GO Terms in Ranked Gene Lists. *BMC Bioinform.* **2009**, *10*, 48. [CrossRef]
31. Bergen, V.; Lange, M.; Peidli, S.; Wolf, F.A.; Theis, F.J. Generalizing RNA Velocity to Transient Cell States through Dynamical Modeling. *Nat. Biotechnol.* **2020**, *38*, 1408–1414. [CrossRef]
32. Wolf, F.A.; Angerer, P.; Theis, F.J. SCANPY: Large-Scale Single-Cell Gene Expression Data Analysis. *Genome Biol.* **2018**, *19*, 15. [CrossRef]
33. Soneson, C.; Srivastava, A.; Patro, R.; Stadler, M.B. Preprocessing Choices Affect RNA Velocity Results for Droplet ScRNA-Seq Data. *PLoS Comput. Biol.* **2021**, *17*, e1008585. [CrossRef]
34. Wolf, F.A.; Hamey, F.K.; Plass, M.; Solana, J.; Dahlin, J.S.; Göttgens, B.; Rajewsky, N.; Simon, L.; Theis, F.J. PAGA: Graph Abstraction Reconciles Clustering with Trajectory Inference through a Topology Preserving Map of Single Cells. *Genome Biol.* **2019**, *20*, 59. [CrossRef]
35. Gossen, M.; Freundlieb, S.; Bender, G.; Müller, G.; Hillen, W.; Bujard, H. Transcriptional Activation by Tetracyclines in Mammalian Cells. *Science* **1995**, *268*, 1766–1769. [CrossRef]
36. Nectow, A.R.; Nestler, E.J. Viral Tools for Neuroscience. *Nat. Rev. Neurosci.* **2020**, *21*, 669–681. [CrossRef]
37. Sweeney, N.P.; Vink, C.A. The Impact of Lentiviral Vector Genome Size and Producer Cell Genomic to Gag-Pol MRNA Ratios on Packaging Efficiency and Titre. *Mol. Ther. Methods Clin. Dev.* **2021**, *21*, 574–584. [CrossRef] [PubMed]
38. Dodonova, S.O.; Zhu, F.; Dienemann, C.; Taipale, J.; Cramer, P. Nucleosome-Bound SOX2 and SOX11 Structures Elucidate Pioneer Factor Function. *Nature* **2020**, *580*, 669–672. [CrossRef] [PubMed]
39. Hoffmann, D.; Schott, J.W.; Geis, F.K.; Lange, L.; Müller, F.-J.; Lenz, D.; Zychlinski, D.; Steinemann, D.; Morgan, M.; Moritz, T.; et al. Detailed Comparison of Retroviral Vectors and Promoter Configurations for Stable and High Transgene Expression in Human Induced Pluripotent Stem Cells. *Gene Ther.* **2017**, *24*, 298–307. [CrossRef] [PubMed]
40. Liu, Z.; Chen, O.; Wall, J.B.J.; Zheng, M.; Zhou, Y.; Wang, L.; Ruth Vaseghi, H.; Qian, L.; Liu, J. Systematic Comparison of 2A Peptides for Cloning Multi-Genes in a Polycistronic Vector. *Sci. Rep.* **2017**, *7*, 2193. [CrossRef]
41. Tian, R.; Gachechiladze, M.A.; Ludwig, C.H.; Laurie, M.T.; Hong, J.Y.; Nathaniel, D.; Prabhu, A.V.; Fernandopulle, M.S.; Patel, R.; Abshari, M.; et al. CRISPR Interference-Based Platform for Multimodal Genetic Screens in Human IPSC-Derived Neurons. *Neuron* **2019**, *104*, 239–255.e12. [CrossRef]
42. Herholt, A.; Galinski, S.; Geyer, P.E.; Rossner, M.J.; Wehr, M.C. Multiparametric Assays for Accelerating Early Drug Discovery. *Trends Pharmacol. Sci.* **2020**, *41*, 318–335. [CrossRef]
43. Matjusaitis, M.; Wagstaff, L.J.; Martella, A.; Baranowski, B.; Blin, C.; Gogolok, S.; Williams, A.; Pollard, S.M. Reprogramming of Fibroblasts to Oligodendrocyte Progenitor-like Cells Using CRISPR/Cas9-Based Synthetic Transcription Factors. *Stem Cell Rep.* **2019**, *13*, 1053–1067. [CrossRef]
44. Wang, S.; Bates, J.; Li, X.; Schanz, S.; Chandler-Militello, D.; Levine, C.; Maherali, N.; Studer, L.; Hochedlinger, K.; Windrem, M.; et al. Human IPSC-Derived Oligodendrocyte Progenitor Cells Can Myelinate and Rescue a Mouse Model of Congenital Hypomyelination. *Cell Stem Cell* **2013**, *12*, 252–264. [CrossRef] [PubMed]
45. Douvaras, P.; Wang, J.; Zimmer, M.; Hanchuk, S.; O'Bara, M.A.; Sadiq, S.; Sim, F.J.; Goldman, J.; Fossati, V. Efficient Generation of Myelinating Oligodendrocytes from Primary Progressive Multiple Sclerosis Patients by Induced Pluripotent Stem Cells. *Stem Cell Rep.* **2014**, *3*, 250–259. [CrossRef] [PubMed]
46. Chamling, X.; Kallman, A.; Fang, W.; Berlinicke, C.A.; Mertz, J.L.; Devkota, P.; Pantoja, I.E.M.; Smith, M.D.; Ji, Z.; Chang, C.; et al. Single-Cell Transcriptomic Reveals Molecular Diversity and Developmental Heterogeneity of Human Stem Cell-Derived Oligodendrocyte Lineage Cells. *Nat. Commun.* **2021**, *12*, 652. [CrossRef] [PubMed]
47. Elbaz, B.; Popko, B. Molecular Control of Oligodendrocyte Development. *Trends Neurosci.* **2019**, *42*, 263–277. [CrossRef]
48. Windrem, M.S.; Osipovitch, M.; Liu, Z.; Bates, J.; Chandler-Militello, D.; Zou, L.; Munir, J.; Schanz, S.; McCoy, K.; Miller, R.H.; et al. Human IPSC Glial Mouse Chimeras Reveal Glial Contributions to Schizophrenia. *Cell Stem Cell* **2017**, *21*, 195–208.e6. [CrossRef]

Inventory of Supplemental Information

- Supplemental Figures
- Supplemental Tables
- Supplemental References

A

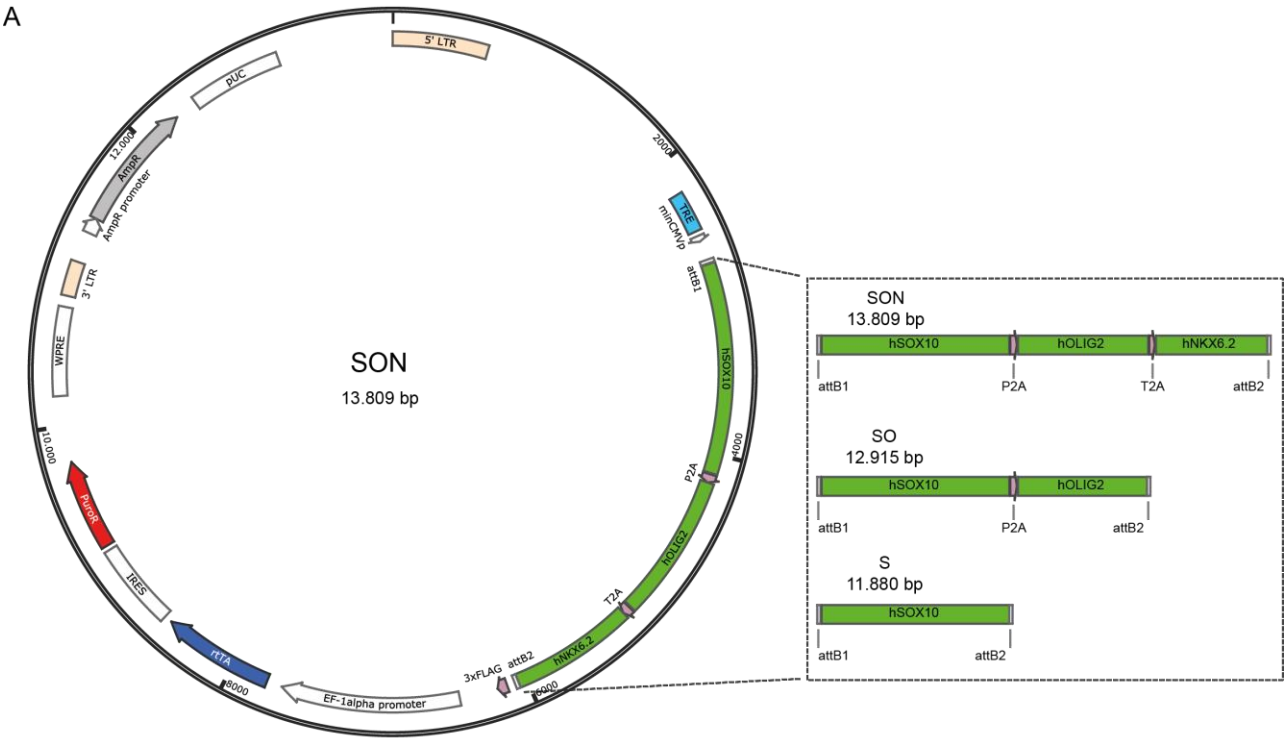

B

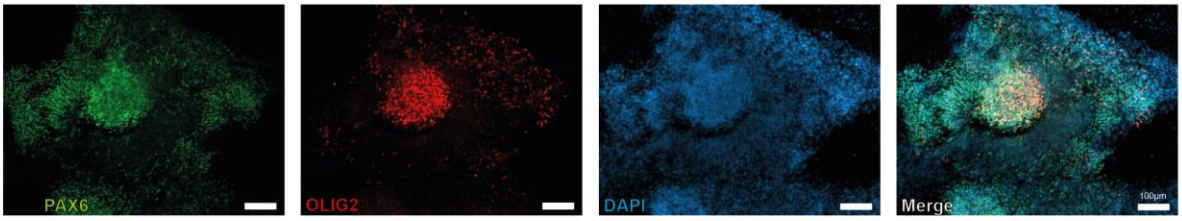

Figure S1. Detailed illustration of applied lentiviral construct and neural induction. Related to Figure 1.

(A) Schematic overview of the applied lentiviral vector containing constitutive expression units for the reversed tetracycline transactivator (rtTA) and puromycin N-acetyl-transferase (PuroR) and a tetracycline response element (TRE) for the doxycycline-dependent overexpression of the TFs. Magnification illustrates the different TFs combinations using SON, SO and S that are linked by the self-cleavage sites P2A and T2A. Plasmid maps of the constructs (S, SO, SON) are available in the supplemental files.

(B) Representative images of PAX6^{+} (green), OLIG2^{+} (red) neural precursor cells (NPC) 12 days after neural induction. Scale bar: 100µm.

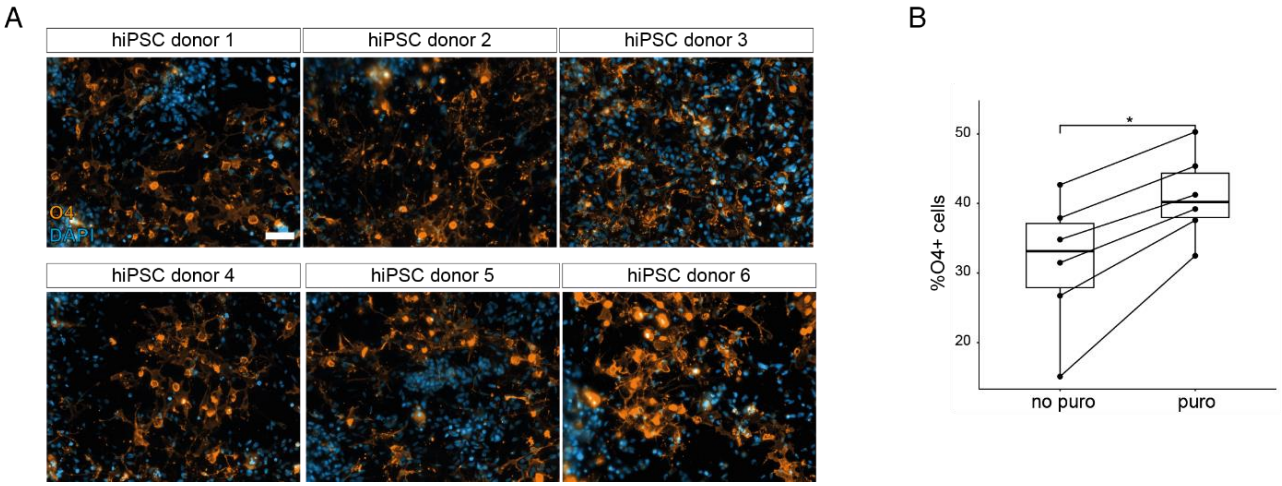

Figure S2. SON-directed differentiation from different hiPSC lines and effect of intermediate selection. Related to Figure 2.

(A) Illustration of $O4^+$ cells (orange) from six different hiPSC lines of independent donors 10days of SON-directed differentiation with intermediate puromycin selection (puro). Scale bar: 50µm.

(B) Quantification of $O4^+$ cells after 10 days of SON-directed differentiation with and without intermediate puromycin selection between Day+2 and Day+4. 13 analysed fields of view for each condition, Dots correspond to mean percentage of $O4^+$ cells per condition. Lines connects both conditions from one hiPSC cell line. Statistical analysis by Wilcoxon signed-rank test, *$p < 0.05$.

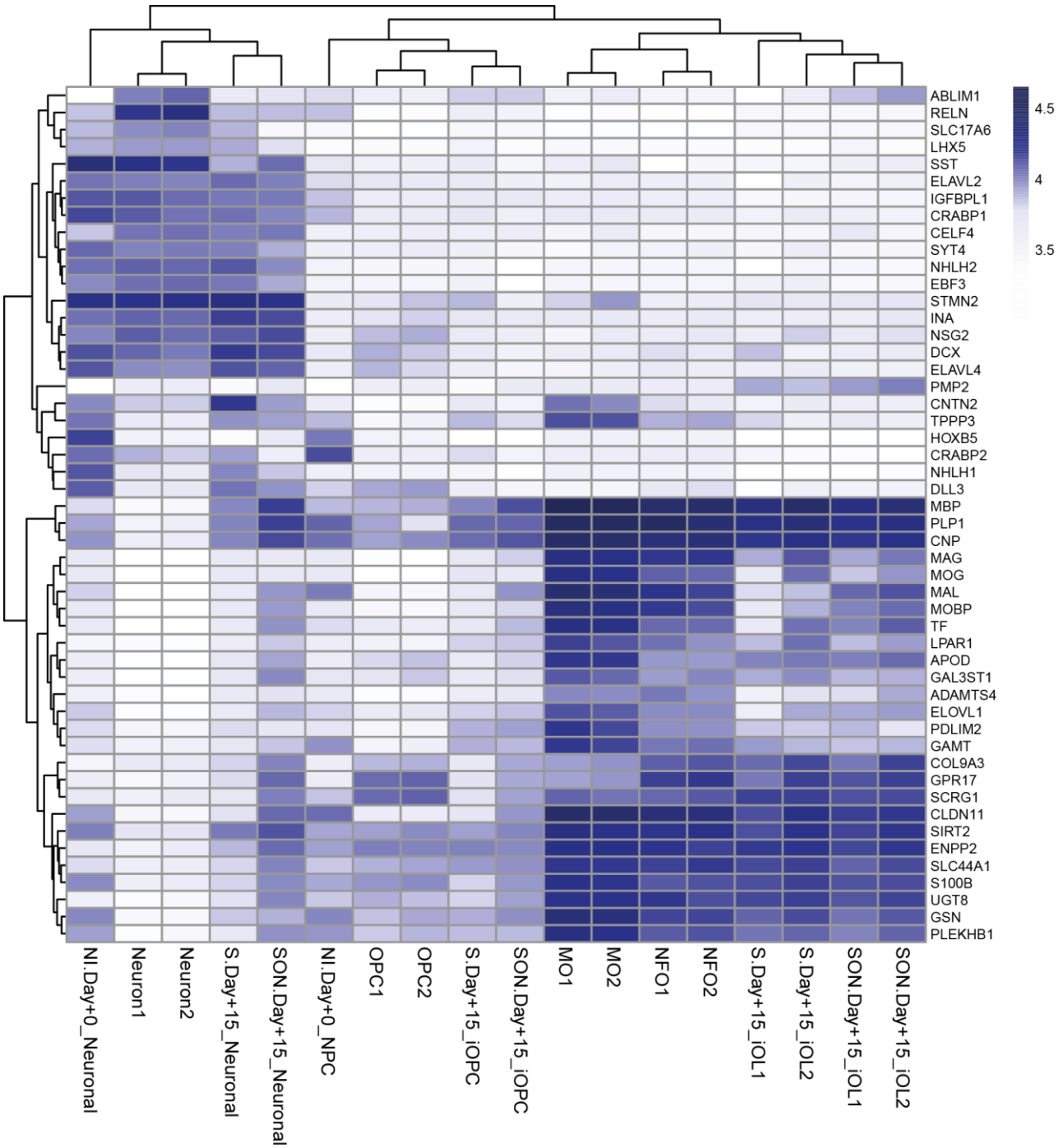

Figure S3. 50 most variable genes from co-clustering of iOPCs and iOLs with primary cells. Related to Figure 3.

Comparison of transcriptomes of hiPSC-derived cells with primary murine cells (Zhang et al., 2014). Expression heatmap of the 50 most variable genes in the analysis. Unsupervised hierarchical clustering based on Manhattan distances was performed on samples and genes and used for sorting of the heatmap. Abbreviations for primary reference samples: MO, myelinating oligodendrocytes; NFO, newly formed oligodendrocytes; OPC, oligodendrocyte precursor cells.

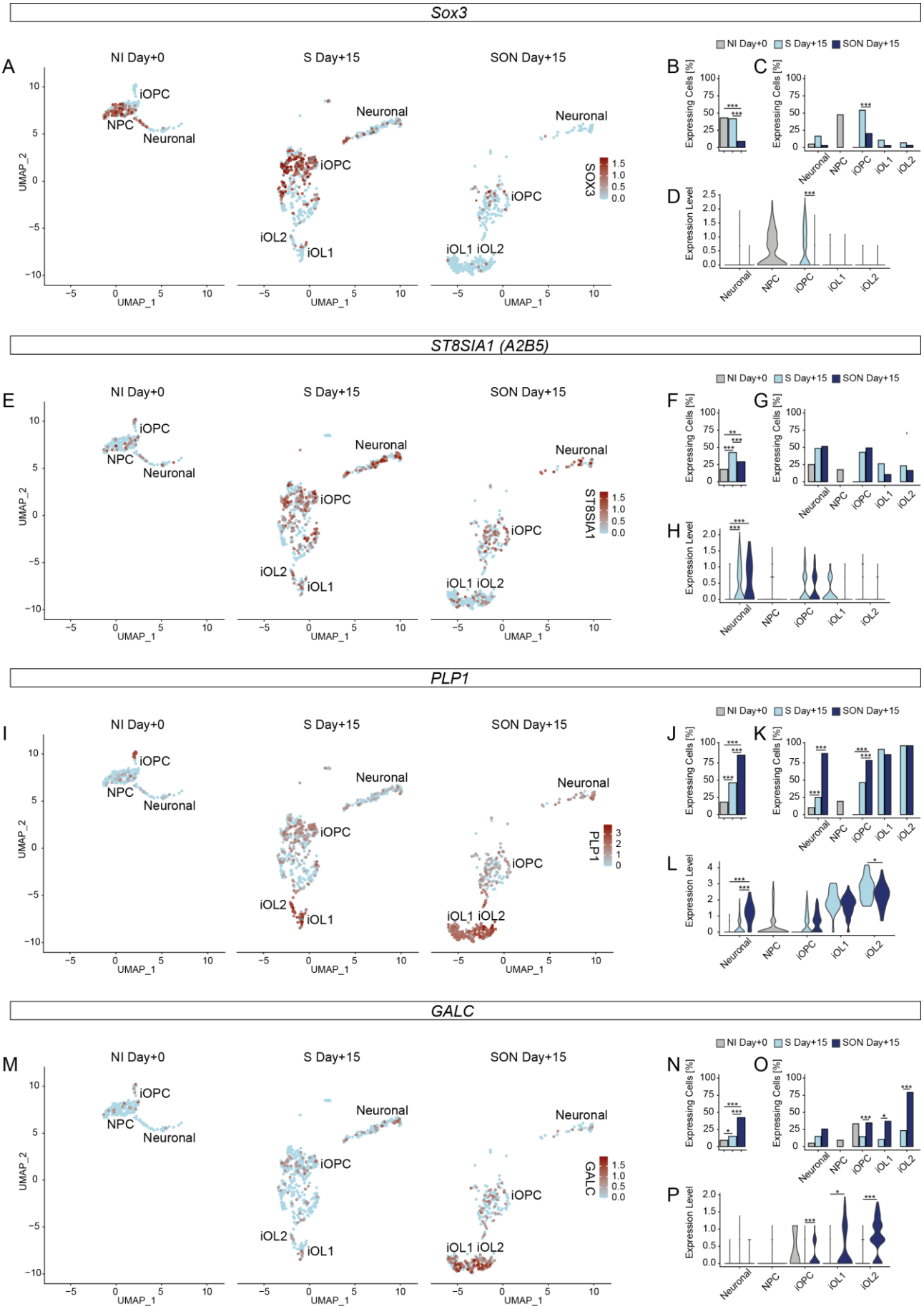
Sox3
A
NI Day+0
S Day+15
SON Day+15
iOPC
NPC
Neuronal
iOL2
iOL1
iOL1 iOL2
UMAP_1
UMAP_2
SOX3
B
C
D
NI Day+0
S Day+15
SON Day+15
Expressing Cells [%]
Expression Level
Neuronal
NPC
iOPC
iOL1
iOL2
ST8SIA1 (A2B5)
E
F
G
H
ST8SIA1
PLP1
I
J
K
L
GALC
M
N
O
P

Figure S4. Illustration of extended marker gene expression from scRNAseq. Related to Figure 4.
(**A, E, I, M**) UMAP representation of selected marker genes (**A**) *SOX3*, (**E**) *ST8SIA1* (also known as A2B5), (**I**) *PLP1*, (**M**) *GALC* from scRNAseq of baseline sample after neural induction (NI Day+0, n = 217 cells, one independent experiment) and samples after 15 days of directed differentiation by SOX10 (S Day+15, n = 577 cells, one independent experiment) and SOX10-OLIG2-NKX6.2 (SON Day+15, n = 400 cells, one independent experiment) with annotated cell clusters of neural precursor cells (NPC), neuronal cells, induced oligodendrocyte precursor cells (iOPCs), induced oligodendrocyte cluster 1 (iOL1) and induced oligodendrocyte cluster 2 (iOL2). Expression value per cell plotted according to the colour intensity of the respective scale bar as indicated.
(**B, F, J, N**) Bar plots illustrate the abundance of expressing cells for each sample. * (p-value < 0.05), ** (p-value < 0.01), *** (p-value < 0.001) based on Fisher's exact tests (details provided in Table S5).
(**C, G, K, O**) Bar plots illustrate the abundance of expressing cells for each cluster split by sample. * (p-value < 0.05), ** (p-value < 0.01), *** (p-value < 0.001) based on Fisher's exact tests (details provided in Table S5).
(**D, H, L, P**) Violin plots of the normalized expression per sample within the respective cell type cluster. * (p-value < 0.05), ** (p-value < 0.01), *** (p-value < 0.001) based on Wilcoxon signed-rank test (details provided in Table S7).

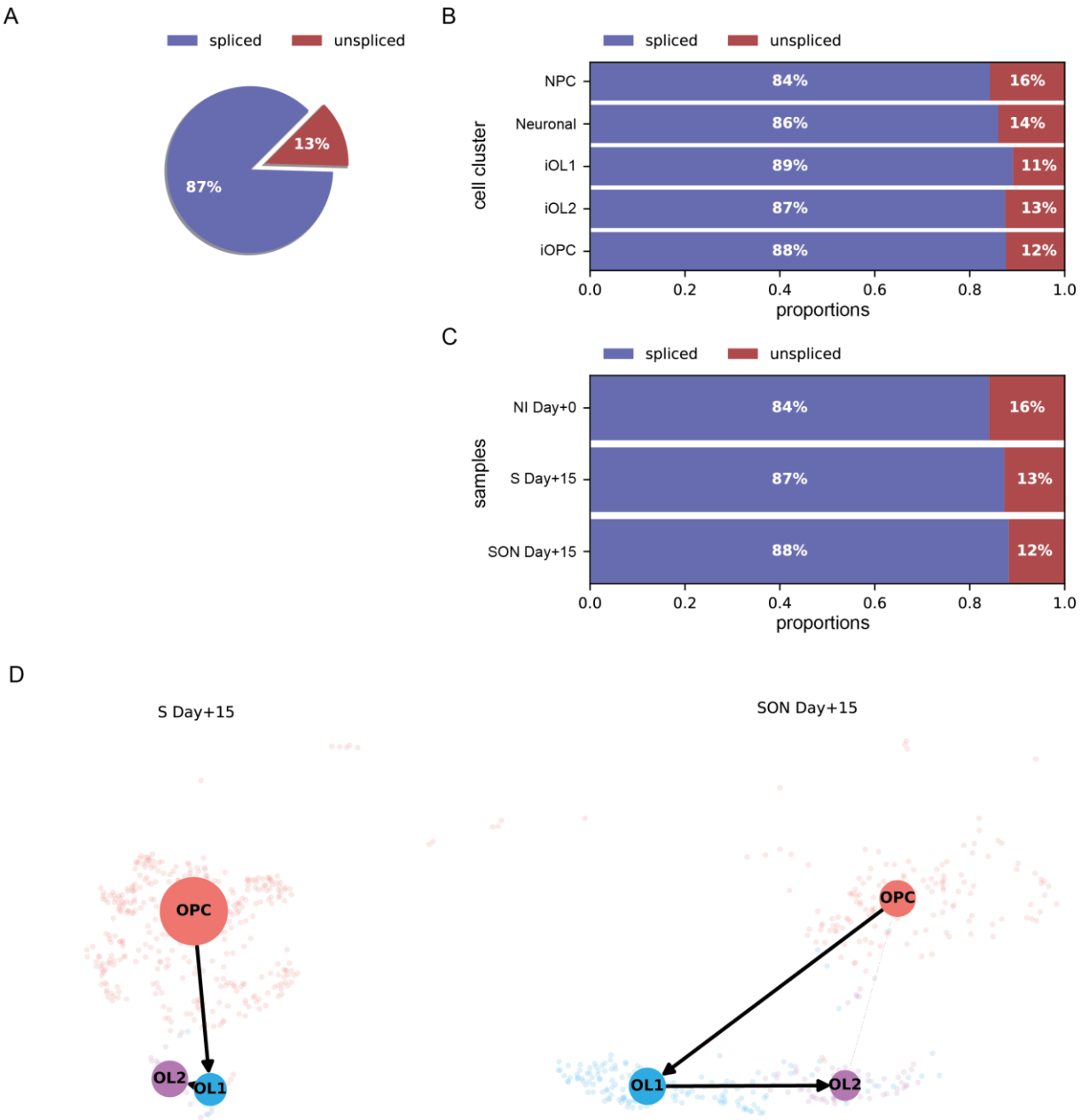

Figure S5. Ratio of unspliced/spliced mRNA variants and sample-independent main differentiation trajectory analysis. Related to Figure 5.

(A) Overall ratio of spliced vs. unspliced mRNA

(B) Cluster-dependent ratio of spliced vs. unspliced mRNA

(C) Sample-dependent ratio of spliced vs. unspliced mRNA

(D) Sample independent main differentiation trajectory analysis using Partition-based graph abstraction (PAGA) to illustrate cluster-to-cluster transitions within the S- and SON-promoted oligodendroglial differentiation.

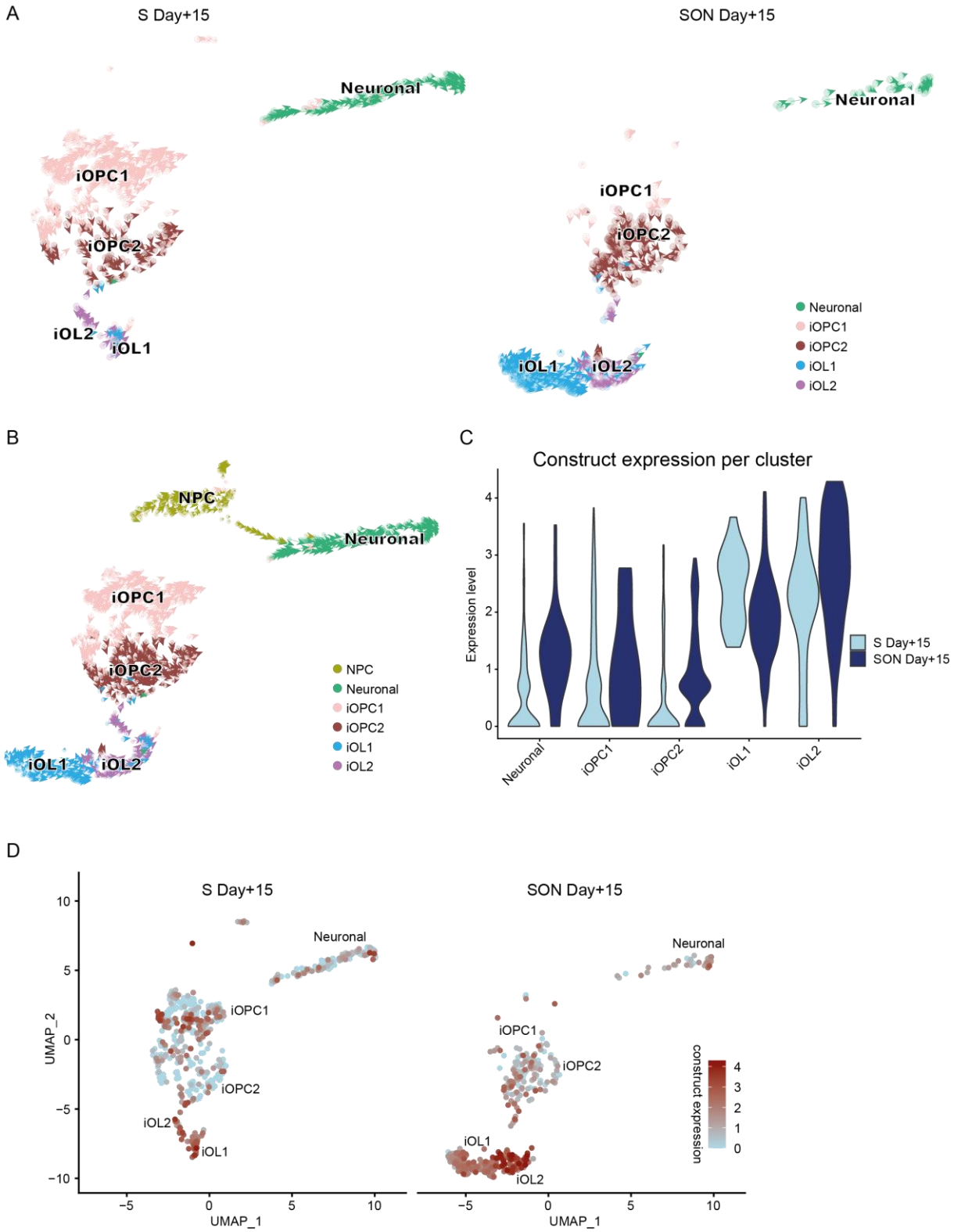

Figure S6. Differences of RNAvelocity between iOPC1 and iOPC2 are not based on different expression of directing TFs. Related to Figure 6.

(A) RNA velocity vectors projected on the single-cell UMAP-based dimension plot, indicating direction and speed of individual cells, including iOPC1 and iOPC2, in transcriptional space.

(B) Pooled Illustration of scVelocity of NI-, S- and SON-derived samples (NI Day+0, S Day+15, SON Day +15) including iOPC1 and iOPC2.

(C) Violin plots of normalized construct expression in Neuronal, iOPC1, iOPC2, iOL1 and iOL2 clusters split by S- and SON-sample (S Day+15, SON Day +15).

(D) Illustration of lentiviral construct expression from scRNAseq with UMAP dimension plot for S Day+15 and SON Day+15 with the normalized expression level indicated by colour. Related to Figure S6C.

Table S1. hiPSC lines in this study.

hiPSC cell line	ID LMU	Donor age	Donor sex	Passage
hiPSC donor 0	PSYLMUi001-A	27	male	P17
hiPSC donor 1	PSYLMUi002-A	24	male	P18
hiPSC donor 2	PSYLMUi003-A	19	male	P17
hiPSC donor 3	PSYLMUi004-A	31	male	P18
hiPSC donor 4	PSYLMUi006-A	52	male	P21
hiPSC donor 5	PSYLMUi023-A	47	male	P19
hiPSC donor 6	PSYLMUi027-A	53	male	P15

Table S2. Media, media supplements for cell cultivation and coating.

Item	Supplier	Cat.No.
iPS-Brew	Miltenyi Biotec	130-104-368
mTeSR1	Stem Cell	85850
ProFreeze CDM	Lonza	BEBP12-769E
DMEM/F-12 with GlutaMAX™ supplement	ThermoFisherScientific	31331028
N-2 Supplement (100x)	ThermoFisherScientific	17502048
B-27® Supplement (50X), without vitamin A	ThermoFisherScientific	12587010
Non-Essential Amino Acids Solution (NEAA)	ThermoFisherScientific	11140035
ß-Mercaptoethanol	ThermoFisherScientific	21985023
Insulin solution human	Sigma	I9278-5ML
SB431542	StemCell	72232
LDN193189 (HCl) - superstock	StemCell	72147
Retinoic acid (RA)	Sigma	R2625-50MG
SAG	Millipore	566660
PDGFaa	PeproTech	100-13A
IGF1	PeproTech	100-11
HGF	PeproTech	100-39
NT3	Peprotech	AF-450-03
Biotin	Sigma	B4639-100MG
dbcAMP	Sigma	D0627-250MG
T3	Sigma	T6397-100MG
Doxycycline	Clontech	NC0424034
Puromycin	ThermoFisherScientific	A1113803
ROCK-Inhibitor (Y-27632)	Selleckchem	S 1049
RevitaCell	ThermoFisherScientific	A2644501
Vitronectin	ThermoFisherScientific	A14700
Matrigel	BD Bioscience	354277
Poly-L-ornithine solution	Sigma	P4957
Laminin (mouse)	Sigma	T6397-100MG
EDTA	ThermoFisherScientific	15575-020
Accutase	Sigma	A6964
Anti-O4 microbeads	Miltenyi Biotec	130-096-670

Table S3. List of primary antibodies for immunostainings. Related to Figure 1, 2, 6, S1, S2.

Antigen	Dilution	Supplier	Cat.No.	Serotype	Host
O4	1:200	R&D Systems	MAB1326	IgM, monoclonal	mouse
MBP	1:50	Millipore	AB9348	IgG, polyclonal	chicken
MBP	1:200	Abcam	ab40390	IgG, polyclonal	rat

Pax 6	1:500	Millipore	AB2237	IgG, polyclonal	rabbit
Olig2 (H-10)	1:100	Santa Cruz	sc-515947	IgG, monoclonal	mouse
Flag-M2	1:100	Sigma	3165	IgG, monoclonal	mouse

Table S4: Abundance of cell clusters, gene marker expressing cells per samples and cluster. Provided separately as Excel file. Related to Figure 3, 4 and S4. Provided separately as Excel file.

Table S5: Statistical analysis of cell clusters abundance per sample, abundance of gene expressing cells by sample and abundance of gene expressing cells per cluster split by sample. Related to Figure 3, 4 and S4. Provided separately as Excel file.

Table S6: Average expression of cell clusters. Related to Figure 3, 4 and S4. Provided separately as Excel file.

Table S7: Statistical analysis of normalized gene expression by cell cluster and by cell cluster split by sample. Related to Figure 3, 4 and S4. Provided separately as Excel file.

Table S8: Differential gene expression between iOPC1 and iOPC2. Related to Figure 6. Provided separately as Excel file.

Table S9: Hypergeometric gene ontology term enrichment analysis of iOPC1 and iOPC2. Related to Figure 6. Provided separately as Excel file.

Supplemental References

Zhang, Y., Chen, K., Sloan, S.A., Bennett, M.L., Scholze, A.R., O'Keeffe, S., Phatnani, H.P., Guarnieri, P., Caneda, C., Ruderisch, N., et al. (2014). An RNA-sequencing transcriptome and splicing database of glia, neurons, and vascular cells of the cerebral cortex. J. Neurosci. Off. J. Soc. Neurosci. *34*, 11929–11947.

6. Paper II

iPSC-modelling reveals genetic associations and morphological alterations of oligodendrocytes in schizophrenia

Man-Hsin Chang [1,2,12], Jan Benedikt Waldeck [1,12], Marius Stephan [1,2,3], Nirmal Kannaiyan [1,3], Valéria de Almeida [1,4,5], Emanuel Boudriot [1,6], Temmuz Karali [1,7], Lukas Röll [1,6,7], Laura Fischer [6], Damianos Demetriou [1], Nadia Gabellini [1], Sabrina Galinski [1,3], Andrea Schmitt [1,8,9], Sergi Papiol [6,10], Daniel Keeser [1,7,11], Peter Falkai [1,6,8], Moritz J. Rossner [1,3,*] and Florian J. Raabe [1,6,*]

[1] Department of Psychiatry and Psychotherapy, LMU University Hospital, LMU Munich, 80336 Munich, Germany.
[2] International Max Planck Research School for Translational Psychiatry (IMPRS-TP), 80804 Munich, Germany.
[3] Systasy Bioscience GmbH, 81669 Munich, Germany.
[4] Department of Psychiatry, University of Münster, 48149 Münster, Germany.
[5] Center for Soft Nanoscience, University of Münster, 48149 Münster, Germany.
[6] Max Planck Institute of Psychiatry, 80804 Munich, Germany.
[7] NeuroImaging Core Unit Munich (NICUM), LMU University Hospital, LMU Munich, 80336 Munich, Germany.
[8] German Center for Mental Health (DZPG), partner site Munich/Augsburg, Munich, Germany.
[9] Laboratory of Neurosciences (LIM-27), Institute of Psychiatry, University of São Paulo (USP), São Paulo-SP 05403-903, Brazil.
[10] Institute of Psychiatric Phenomics and Genomics (IPPG), LMU University Hospital, LMU Munich, 80336 Munich, Germany.
[11] Munich Center for Neurosciences (MCN), LMU Munich, 82152 Planegg-Martinsried, Germany.
[12] These authors contributed equally: Man-Hsin Chang, Jan Benedikt Waldeck.

***** Correspondence: Moritz.Rossner@med.uni-muenchen.de,
Florian_Raabe@psych.mpg.de

ARTICLE OPEN

Check for updates

iPSC-modelling reveals genetic associations and morphological alterations of oligodendrocytes in schizophrenia

Man-Hsin Chang[1,2,12], Jan Benedikt Waldeck[1,12], Marius Stephan[1,2,3], Nirmal Kannaiyan[1,3], Valéria de Almeida[1,4,5], Emanuel Boudriot[1,6], Temmuz Karali[1,7], Lukas Röll[1,6,7], Laura Fischer[6], Damianos Demetriou[1], Nadia Gabellini[1], Sabrina Galinski[1,3], Andrea Schmitt[1,8,9], Sergi Papiol[6,10], Daniel Keeser[1,7,11], Peter Falkai[1,6,8], Moritz J. Rossner[1,3]✉ and Florian J. Raabe[1,6]✉

There is strong evidence for a genetically driven neuronal contribution in schizophrenia (SCZ). Although imaging and postmortem studies also provide evidence for white matter alterations with implications of the oligodendroglial lineage in SCZ, it is unclear whether these disturbances are a secondary consequence of neuronal deficits or also, at least in parts, genetically driven and cell-autonomous. Using human induced pluripotent stem cells (hiPSCs) in combination with gene set enrichment analysis, we investigated the cellular impact of SCZ genetics on the oligodendroglial lineage. We performed unsupervised clustering analysis of hiPSC-differentiated neural cells including oligodendrocytes (iOLs) and their precursor cells (iOPCs) with corresponding human postmortem cell types from single-cell RNA sequencing (scRNAseq) data and conducted a comparative gene set enrichment analysis. Subsequently, we stratified individuals based on white matter alteration using diffusion tensor imaging (DTI) within a translational cohort (N = 112) and then explored the cellular effects of SCZ risk with hiPSC modelling in a subset of SCZ patients (N = 8) with disturbed white matter integrity and unaffected healthy controls (N = 7). hiPSC-iOPCs/iOLs expression profiles strongly correlated with human postmortem OPCs/OLs based on scRNAseq, and their transcriptional signatures were highly enriched in the genetic associations of SCZ. The cellular assessment of patient-derived iOPCs/iOLs revealed morphological alterations, including significantly increased branch length and elevated junction number in mature iOLs from SCZ. Moreover, transcriptomic profiling revealed a dysregulation in oligodendroglial cell signaling and proliferation. In sum, hiPSC-modelling shows an impact of SCZ genetics on dedicated features of the oligodendroglial lineage.

Translational Psychiatry (2025)15:287 ; https://doi.org/10.1038/s41398-025-03509-x

INTRODUCTION

Schizophrenia (SCZ) is a severe psychiatric disorder with a prevalence of 0.4-0.7% [1], and characterized by positive (e.g., delusions and hallucinations), negative (e.g., anhedonia, lack of motivation and social withdrawal) and cognitive symptoms (e.g., learning and attention deficits) [2]. While current antipsychotics mainly improve positive symptoms effectively [3], negative and cognitive symptoms remain an unmet medical need and the pathogenesis of SCZ requires a better understanding.

A recent multicenter imaging study has revealed widespread white matter disturbances in SCZ and suggested, based on the configuration of the diffusion tensor imaging (DTI) parameters, that these alterations are most likely driven by impaired myelination [4]. Of note, myelination and white matter development take place during early postnatal time, maintain through adolescence and complete in young adulthood, a critical period of the development of the central nervous system, coincident with the onset of SCZ in the majority of patients [5, 6]. Furthermore, white matter impairments in SCZ patients are associated with declined cognitive performances, likely mediated by deficits in processing speed [7, 8]. Oligodendrocytes (OLs) and their precursor cells (OPCs) are critically involved in myelin sheath formation, promoting fast saltatory conduction of action potentials along the axon, and facilitating connectivity and thus effective information processing between various brain regions. Moreover, oligodendroglial cells also provide metabolic support to neuronal cells, building cell-cell contact to allow axon-glia signaling, and influencing neuronal excitability [9, 10].

Apart from neuronal cells, oligodendroglial lineage cells also participate in cognitive processes, including learning and memory consolidation [11, 12], and impairments of oligodendrocyte functions are linked to cognitive deficits in SCZ [13, 14].

[1]Department of Psychiatry and Psychotherapy, LMU University Hospital, LMU Munich, 80336 Munich, Germany. [2]International Max Planck Research School for Translational Psychiatry (IMPRS-TP), 80804 Munich, Germany. [3]Systasy Bioscience GmbH, 81669 Munich, Germany. [4]Department of Psychiatry, University of Münster, 48149 Münster, Germany. [5]Center for Soft Nanoscience, University of Münster, 48149 Münster, Germany. [6]Max Planck Institute of Psychiatry, 80804 Munich, Germany. [7]NeuroImaging Core Unit Munich (NICUM), LMU University Hospital, LMU Munich, 80336 Munich, Germany. [8]German Center for Mental Health (DZPG), partner site Munich/Augsburg, Munich, Germany. [9]Laboratory of Neurosciences (LIM-27), Institute of Psychiatry, University of São Paulo (USP), São Paulo-SP 05403-903, Brazil. [10]Institute of Psychiatric Phenomics and Genomics (IPPG), LMU University Hospital, LMU Munich, 80336 Munich, Germany. [11]Munich Center for Neurosciences (MCN), LMU Munich, 82152 Planegg-Martinsried, Germany. [12]These authors contributed equally: Man-Hsin Chang, Jan Benedikt Waldeck. ✉email: moritz.rossner@med.uni-muenchen.de; florian_raabe@psych.mpg.de

Received: 27 October 2023 Revised: 2 May 2025 Accepted: 4 August 2025
Published online: 16 August 2025

Postmortem studies have provided robust evidence for oligodendroglial alterations in SCZ, with reduced number of OLs, disturbed expression of OL-related genes and proteins, and altered myelination [13, 14]. Moreover, postmortem analyses indicate morphological changes in oligodendroglial cells from SCZ patients [15–17].

SCZ is a complex polygenic disorder with a multifactorial etiology with heritability estimates of about 79% [18]. Of note, post-hoc analyses based on genome-wide association studies (GWAS) in SCZ revealed the highest gene enrichment in cortical projection neurons and interneurons [19, 20]. However, moderate association of SCZ risk loci with gene sets from the oligodendroglial lineage were found with stronger effects from human postmortem data sets compared to mouse-derived transcriptomic data [19]. Pathway analysis that focused on glial lineages identified several risk-associated single nucleotide polymorphisms (SNPs) which are connected to genes that are expressed in OPCs/OLs [21, 22]. Post-hoc pathway and gene enrichment analyses of GWAS data face technical challenges for potential false-negative findings; i.e., transcriptomic data for GWAS-driven post-hoc analysis are based on human postmortem samples, which may not align with the most relevant cellular state or developmental stage, and murine expression profiles may differ in expression of critical genes [19, 20].

To investigate the cell-autonomous impact of SCZ on the oligodendroglial lineage in a human-derived model of living cells, we applied human induced pluripotent stem cell (hiPSC) modelling. The advantages of hiPSCs include their human origin and capability to differentiate into various cell types of interest, and to overcome the inaccessibility of living brain tissues in humans [23]. In a previous study, we successfully established a rapid and effective protocol for induced OL (iOL) differentiation [24] based on previous works [25, 26]. Here, we used scRNAseq data of hiPSC-derived late-stage iOPC/iOLs from our previous work [24] to conduct cell lineage-specific MAGMA gene enrichment analysis. Moreover, we investigated in a translational cohort of patient representatives with white matter disturbances based on DTI whether iOLs derived from individuals with SCZ display abnormal morphological characteristics and altered transcriptomic profiles compared to those derived from unaffected healthy controls.

MATERIALS AND METHODS

Ethics approval and consent to participate

This study was approved by the local ethics committee of the Ludwig Maximilian University Munich (votes 17–13, 17–880, 18–716, and 20–528). The entire study was conducted according to the Declaration of Helsinki and in accordance with the relevant guidelines and regulations. Written informed consent was obtained from all participants before taking part in the study.

Clustering analysis

Pseudo-bulked count data tables were generated for datasets of hiPSC-derived SON-directed (overexpression of *SOX10*, *OLIG2*, and *NKX6.2*) oligodendroglial cells retrieved from GEO (GSE179516) in our previous work [24] and human postmortem brain cells retrieved from GEO (GSE118257) [27] using Seurat v3 [28] without log transformation. hiPSC data genes were pre-filtered based on a differential expression analysis run on sctransform-normalized, unintegrated data using *PrepSCTFindMarkers*, and then *FindAllMarkers*. *PrepSCTFindMarkers* corrected counts for technical differences between samples. The *FindAllMarkers* was not run on the integrated count data due to the smoothing effect of integration procedures which leads to the underestimation of transcriptional variances. The data were evaluated using the Wilcoxon rank-sum test and the *p*-values were FDR adjusted with Bonferroni correction. Marker genes for downstream analysis were identified with a minimal $\log_2$(fold change) of 0.25 between the individual cluster and the background and a minimum abundance of 10% of expressing cells. This step reduced the noise level and focused the analysis on genes differentiating the cell populations of interest. The filtered, and pseudo-bulked datasets were merged without prior integration, since *DESeq2* expects raw count data and relies on a modelling approach to address technical variability [29]. Next, gene expression variability was calculated using the R package *DESeq2* [29] for variance stabilization, and *removeBatchEffect* was run to correct for technical differences between samples. For downstream analysis, the 2000 most variable genes were selected. A principal component analysis (PCA) was performed to find clusters of samples, and Manhattan distances between samples and features were computed and used for hierarchical clustering and plotted as heatmaps.

MAGMA gene enrichment analysis

MAGMA (Multi-marker Analysis of GenoMic Annotation, version 1.09) [30] was used to carry out formal enrichment analyses using the summary statistics of schizophrenia [20], bipolar disorder [31], and autism spectrum disorder [32] GWAS. Previously published single-cell RNA sequencing (scRNAseq) data from the SON-directed differentiation [24] were used to generate different gene sets (see Table S1) that characterize various cell and differentiation stages within the previously established protocol of directed oligodendroglial differentiation [24]: iPSC-derived neural precursor cells (iNPC), SON-induced OPCs (iOPC), SON-induced oligodendrocytes in different maturation stages iOL1 and iOL2 (more mature cluster), and iPSC-derived neurons (iNeuron) that escaped the directed oligodendroglial differentiation. After SNP-to-gene annotation, gene-level analyses (±10 kb) were carried out using the "SNPwise-mean" model. Gene-based *p*-values were obtained by combining the SNP *p*-values in a gene (±10 kb) into a gene test statistic (mean χ^2) corrected for linkage disequilibrium between SNPs. MAGMA competitive gene-set analysis tested, within a regression framework, if the gene-sets in differentiating stages have a stronger association with the target phenotype than randomly selected gene-sets with similar characteristics. For gene-set competitive testing, linear regression analyses were conditioned to gene size, log(gene size), gene density, log(gene density), inverse mac and log(inverse mac).

Magnetic resonance imaging (MRI) within clinical cohort

The clinical basis for this translational study were 58 patients with SCZ and 54 healthy controls (Ctrl) out of the *Multimodal Imaging in Chronic Schizophrenia Study* (MIMICSS), a pilot study of the *Munich Clinical Deep Phenotyping Study* [33], with processed DTI data out of a protocol of multimodal magnetic resonance imaging (mMRI). For detailed description of the MIMICSS cohort, please refer to the supplements of [33].

MRI acquisition. All MRI examinations were performed using a 3.0 T MR scanner (Siemens MAGNETOM Prisma, Siemens Healthineers AG, Erlangen, Germany) with a 32-channel head coil. T1-weighted scans were acquired using a magnetization-prepared rapid gradient echo (MP-RAGE) sequence with the following parameters: isotropic voxel size of 0.8 mm^3, 208 slices, a repetition time (TR) of 2500 ms, an echo time (TE) of 2.22 ms, a flip angle of 8°, and a field of view (FoV) of 256 mm. DTI was performed with 95 non-collinear diffusion-encoding directions using a monopolar diffusion scheme. The DTI parameters were as follows: TR of 5500 ms, TE of 99.20 ms, FoV of 224 mm, voxel size of 1.6 mm^3, slice thickness of 1.6 mm, and a multi-band acceleration factor of 3. Multiple diffusion weighting b-values were used (b = 0 s/mm^2 and 2000 s/mm^2).

Preprocessing and tensor fitting. Diffusion-weighted images (DWIs) were preprocessed using the *FMRIB Software Library* (FSL, version 6.0.7.6) [34]. The preprocessing pipeline included eddy current and motion correction of the DWIs using the eddy correct tool. Brain extraction was performed using the *Brain Extraction Tool* (BET) to exclude non-brain tissues. Subsequently, the diffusion tensor model was fitted at each voxel using the *DTIFIT* command, which involved the following parameters: input diffusion data, output basename for the files, brain mask, gradient directions file, and b-values file. The outputs from this step included fractional anisotropy (FA), three eigenvalues (L1, L2, L3), and eigenvectors.

Tract-based spatial statistics (TBSS). TBSS was utilized to perform voxelwise statistical analysis of the FA data following the standard FSL pipeline [35]. The TBSS analysis comprised several steps: (1) all FA images were aligned to a common space using the *tbss_1_preproc* script, (2) non-linear registration: the images were non-linearly registered to the *FMRIB58_FA* standard-space image using the *tbss_2_reg -T* command, (3) post-registration: a mean FA image was created and thinned to produce a mean FA skeleton representing the centers of all tracts common to the

group using the *tbss_3_postreg -S* command, and (4) thresholding: the mean FA skeleton was thresholded at FA > 0.2 using the tbss_4_prestats 0.2 command.

Statistics. Voxelwise statistical analysis was performed using the randomize tool with 5000 permutations to test for significant differences across groups, with multiple comparisons corrected using threshold-free cluster enhancement (TFCE). FA values from the skeleton were extracted for each subject for further analysis using the *fslstats* command, and then evaluated for normality using Shapiro-Wilk tests and QQ-plots and assessed for homogeneity of variances with Levene's test. Next, comparison between SCZ and Ctrl group was performed with t-test. The test results can be found in Table S2.

hiPSC cohort

hiPSCs utilized in this study were from translational patient representatives out of a characterized hiPSC cohort [36] that is part of deep phenotyped clinical cohorts within the Munich Mental Health Biobank [33] located at the Department of Psychiatry and Psychotherapy, LMU University Hospital, LMU Munich, Germany (for selection procedure, see results below). Diagnosis of patients with SCZ was assessed according to the *International Statistical Classification of Diseases and Related Health Problems, 10th revision (ICD-10)* in clinical settings. Guided by meta-analytical driven power calculations [37], we increased the number of included individual donors up to recommended 7/8 donors per group rather than analyzing multiple clones from very few donors to enhance the generalizability of our study.

These hiPSCs were created from peripheral blood mononuclear cells (PBMCs) following a previously established procedure [38]. Standard verification of hiPSCs involved confirming their pluripotency through immunocytochemistry (utilizing markers TRA1-60, NANOG, OCT4, and SOX2), assessing genomic integrity via digital karyotyping [39] (pipeline accessible at https://gitlab.mpcdf.mpg.de/luciat/cnv_detection.git, last accessed on June 28, 2021), and demonstrating successful differentiation into all three germ layers [40]. Additionally, the hiPSCs were screened for the absence of HIV, HCV, and CMV (by Synlab, Munich, Germany), and were confirmed to be free from mycoplasma infections (by Eurofins, Ebersberg, Germany). All lines were registered at the human pluripotent stem cell registry (hPSCreg®), register codes can be found in Table S2.

hiPSC cultivation

hiPSCs were cultured in feeder-free iPS-Brew medium (Miltenyi Biotec, Bergisch Gladbach, Germany, 130-104-368) on vitronectin (Thermo Fisher Scientific, Waltham, MA, USA, A14700)-coated plate.

Lentiviral infection and selection

hiPSCs with a concentration of 5×10^4 cells/cm^2 were seeded in iPSC-Brew medium supplemented with 1 µM ROCK inhibitor Y-27632 2HCl (Selleckchem, Houston, TX, USA, S1049). Lentiviral vectors containing doxycycline-inducible operator (tetO)-controlled SOX10-P2A-OLIG2-T2A-NKX6.2 (SON) plasmid and constitutively expressed reversed tetracycline transactivator (rtTA) followed by a puromycin selection cassette were used to infect hiPSCs. 48 hr after infection, cells were selected with 1 µg/ml puromycin (Thermo Fisher Scientific, A1113803).

Neural induction and oligodendroglial differentiation

Neural induction and oligodendroglial differentiation were performed as previously described [24]. In short: iPSC-Brew medium was changed to mTeSR1 medium (StemCell, Vancouver, Canada, 85850) at least one passage before neural induction. hiPSCs were singularized using Accutase (Sigma-Aldrich, St. Louis, USA, A6964) and seeded with a concentration of 2×10^4 cells/cm^2 in mTeSR1 medium supplemented with 1x RevitaCell (Thermo Fisher Scientific, A2644501) on Matrigel (BD Bioscience, San Jose, CA, USA, 354277)-coated 12- and 24-well plates. After two days, mTeSR1 medium was changed to N2B27 medium, comprising DMEM/F-12 with GlutaMAX™ (Thermo Fisher Scientific, 31331028), 1x N2 (Thermo Fisher Scientific, 17502048), 1x B27 (Thermo Fisher Scientific, 12587010), 1x NEAA (Thermo Fisher Scientific, 11140035), 50 µM mercaptoethanol (Thermo Fisher Scientific, 21985023) and 25 µg/ml insulin (Sigma-Aldrich, I9278), supplemented with 10 µM SB431542 (StemCell, 72232), 1 µM LDN193189 (StemCell, 72147) and 0.1 µM retinoic acid (RA) (Sigma-Aldrich, R2625). Full media change was performed daily for 12 days, 1 ml/well and 0.5 ml/well for 12- and 24-well plates, respectively. The volume of media was doubled four days after neural induction. Eight days after neural induction, N2B27 medium supplemented with 0.1 µM RA and 1 µM SAG (Millipore, Burlington, MA, USA, 566660) was used instead.

Day 12 hiPSC-derived neural precursor cells (iNPCs) were singularized using Accutase and seeded with a concentration of 1.5×10^5 cells/cm^2 in N2B27 medium supplemented with 1x RevitaCell, 0.1 µM RA and 1 µM SAG on poly-L-ornithine (Sigma-Aldrich, P4957) and laminin (Sigma-Aldrich, L2020)-coated plates. Next day, N2B27 medium was changed to OL differentiation medium which is N2B27 medium supplemented with 10 ng/ml PDGF-AA (PeproTech, Waltham, MA, USA, 100-13 A), 10 ng/ml IGF1 (PeproTech, 100-11), 5 ng/ml HGF (PeproTech, 100-39), 10 ng/ml NT3 (Peprotech, AF-450-03), 0.1 ng/ml biotin (Sigma-Aldrich, B4639), 1 mM dbcAMP (Sigma-Aldrich, D0627), 60 ng/ml T3 (Sigma-Aldrich, T6397). Full media change was performed every other day. From day +0 to +6, the medium was supplemented with 1 µg/ml doxycycline (Clontech, Shiga, Japan, NC0424034) to induce the overexpression of the transcription factors SOX10, OLIG2, and NKX6.2 (SON) promoting the differentiation of iOLs. From day +4 to +6, cells were additionally selected for the SON-construct using 1 µg/ml puromycin. Differentiated iOLs obtained from one parallel differentiation were examined by immunocytochemistry (ICC) on Day +10.

Immunocytochemistry

Cells seeded on glass coverslips were washed with PBS once and then fixed with 4% PFA for 10 min. After being washed with PBS three times, cells were permeabilized and blocked with 0.1% Triton-X (Sigma-Aldrich, T8787) and 5% goat serum (Thermo Fisher Scientific, 16210064) in PBS for 1 hr. To be noted, Triton-X was not used in all processes for O4 staining. Cells were incubated with primary antibodies in antibody solution (0.1% Triton-X and 1% goat serum in PBS) at 4 °C overnight. After three times of PBS wash, cells were incubated with secondary antibodies in antibody solution and protected from light for 1 hr. Cells were subsequently counterstained with DAPI (BD Bioscience, 564907) for 5 min and washed with PBS twice. Lastly, cells on coverslips were mounted to the microscope slides with a mounting medium. Cells were imaged using Axio Observer Z1 inverted fluorescence microscope (Zeiss, Oberkochen, Germany). Each PBS wash took 5 min. All steps were conducted at room temperature unless otherwise stated.

The following primary antibodies were used: mouse anti-O4 (1:200, R&D Systems, Minneapolis, MN, USA, MAB1326) and chicken anti-MBP (1:50, Millipore, AB9348). Secondary antibodies used: Alexa 555 goat anti-mouse IgM (1:500, Thermo Fisher Scientific, A21426) and Alexa Plus 488 goat anti-chicken (1:500, Thermo Fisher Scientific, A32931).

Image analysis

To perform quantitative image analysis, we developed a customized morphology analysis pipeline (for the applied macro script see **Code Availability**) with the BioVoxxel toolbox [41] based on Fiji, a distribution of ImageJ [42].

Image processing. Raw images were first converted to 8-bit and split into each channel (DAPI and O4, DAPI and MBP). To correct the bleed-through of DAPI signals in MBP images, regions of interest (ROIs) in both channels were defined. First, the extended particle analyzer was applied to MBP images, and only ROIs with a solidity < 0.7 were retained. Next, ROIs of MBP images having less than 60% overlap with ROIs of DAPI images were kept using the binary feature extractor, rendering the MBP images free of DAPI bleed-through. The uneven illumination was then adjusted through the pseudo-flat field correction for MBP and O4 channels. Next, all images were smoothed using the median filter, followed by a background subtraction for O4 and DAPI images with the sliding paraboloid method. The contrast of DAPI and O4 images was enhanced subsequently. Different thresholding approaches were used after optimizing for each channel: the Huang2 method was used on DAPI and MBP images; the Huang method [43] was used on O4 images. Finally, several binary operations were adopted: Erode, Open, Dilate and Watershed commands were used for DAPI images; Erode and Open commands for O4 images.

Image analysis and statistics. After processing of images, the percentages of O4-/MBP-positive ($O4^+/MBP^+$) cells were quantified by dividing the numbers of $O4^+/MBP^+$ cells colocalizing with DAPI by total $DAPI^+$ cells. The average cell size was determined by dividing the total area with a positive signal by the total cell number. For morphological analysis, *ridge detection* [44] and *skeletonize* [45] algorithms were used to quantify the branch length and junction number.

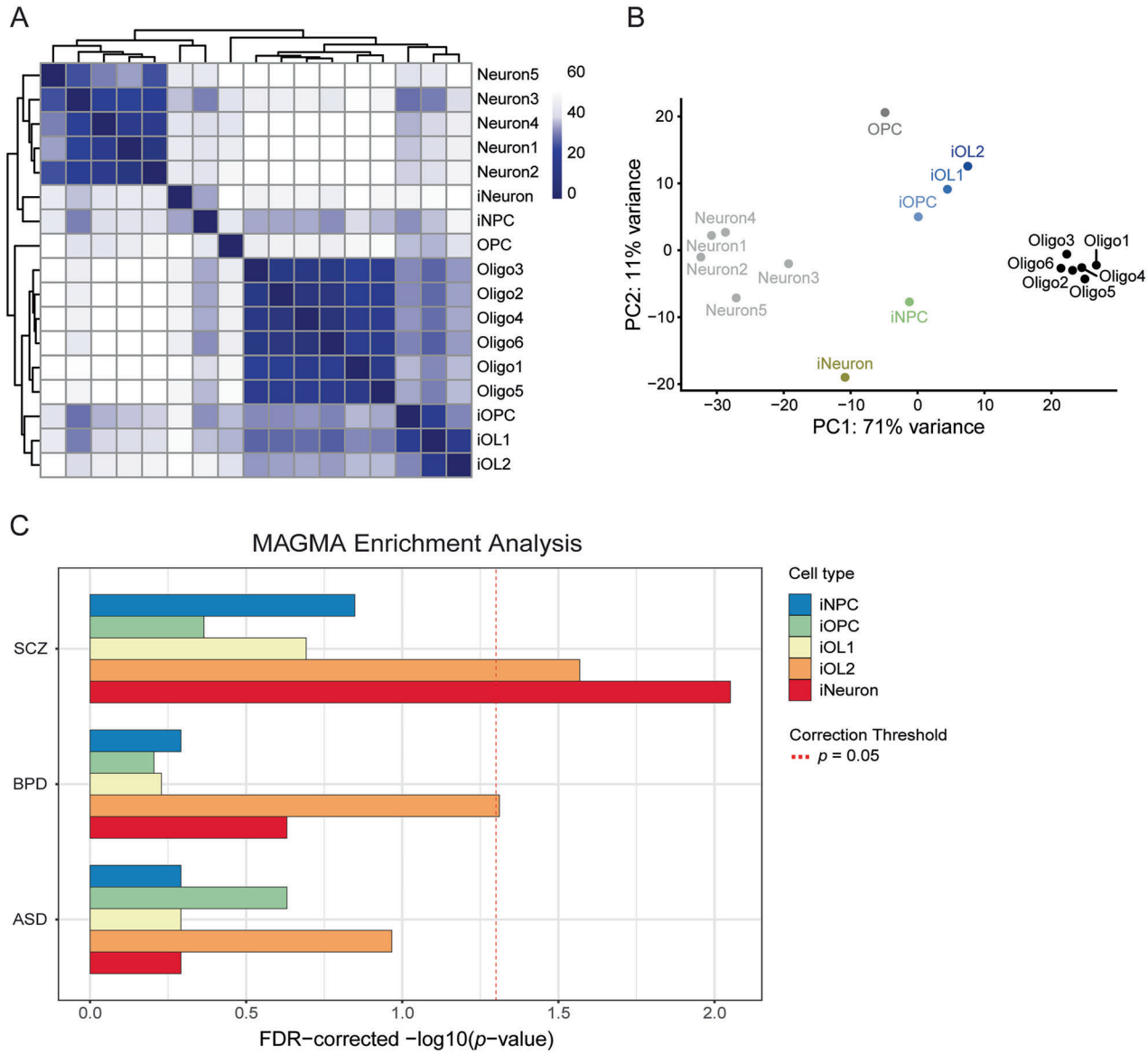

Fig. 1 hiPSC-derived induced oligodendrocyte precursor cells (iOPCs) and induced oligodendrocyte (iOLs) cluster with human postmortem OPCs and OLs, and genes of mature iOLs are enriched in schizophrenia (SCZ) GWAS. A Comparison of the transcriptome of hiPSC-derived oligodendroglial cells from Raabe et al. [24] with human postmortem brain cells from Jäkel et al. [27]. Heatmap of Manhattan sample distances and dendrograms from unsupervised hierarchical clustering of scRNAseq data. **B** Clustering of scRNAseq data with dimensionality reduction by PCA. hiPSC-derived cells are colored, whereas reference postmortem samples are in black and grey. **C** MAGMA gene-set enrichment analysis of different cell and differentiation stages in different psychiatric disorders based on scRNAseq data from a directed oligodendroglial differentiation [24]. SCZ, schizophrenia; BPD, bipolar disorder; ASD, autism spectrum disorder; OPCs, human postmortem oligodendrocyte precursor cells; Oligo1-6, clusters of human postmortem oligodendrocytes; Neuron1-5, clusters of human postmortem neurons; iOPC, hiPSC-derived OPC; iOL1-2, hiPSC-derived oligodendrocytes; iNPC, hiPSC-derived neural precursor cell; iNeuron, hiPSC-derived neurons.

All data are shown in mean ± SD. The n numbers in image analysis indicate the total images examined in each group, unequal n numbers resulted from the NA signals produced in some analyses. All statistical analyses were performed in R (version 4.2.3). Data were first transformed to normal distribution by optimal methods, such as Yeo-Johnson, Box-Cox, orderNorm, sqrt(x + a), and asinh(x) [46], and then the normalized data were evaluated for normality using Shapiro-Wilk tests and QQ-plots. Extreme outliers and homogeneity of variances were assessed with Levene's test, and homogeneity of covariances were assessed with Box's M test. To analyze morphological differences, we applied mixed-effects ANOVA, a recommended and widely used statistical method for handling complex experimental designs involving repeated measures and hierarchical data structures [47]. Mixed-effects models are particularly suited for experiments where data are nested at multiple levels, as they account for both between-group differences (SCZ vs. Ctrl) and within-group variability (individual variation of the iPSC lines). This approach provided the sensitivity needed to detect significant group-level effects despite variability among individual lines.

For further subanalysis, independent t-tests were performed on group-level averages, and effect sizes were calculated using Cohen's d [48]. Significance was defined as *, $p < 0.05$.

Bulk RNA sequencing (RNAseq) and gene set enrichment analysis (GSEA)

5×10^5 Day +10 iOLs were lysed in 350 µl Buffer RLT (Qiagen, Venlo, Netherlands, 74104) using QIAshredder homogenizer (Qiagen, 79656), and their RNAs were extracted by RNeasy Kits (Qiagen, 74104). cDNA synthesis was conducted using SMART-Seq® v4 Ultra® Low Input RNA Kit for Sequencing (Takara Bio, Kusatsu, Japan, 634893) and the library preparation was performed by Nextera XT DNA Library Preparation Kit (Illumina,

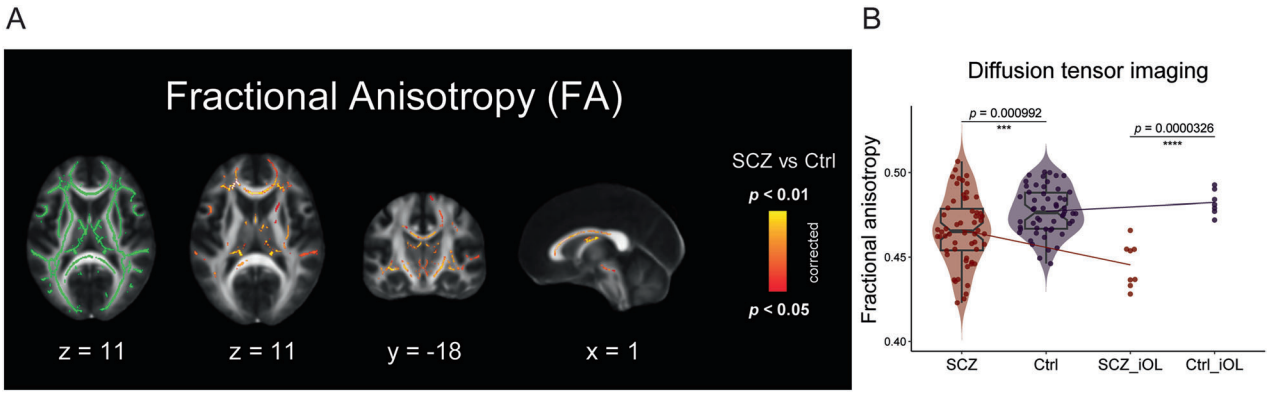

Fig. 2 Diffusion tensor imaging (DTI) reveals decreased fractional anisotropy (FA) in SCZ and allows patient stratification. **(A)** Investigation of the FA of the whole brain white matter skeleton with tract-based spatial statistics (TBSS) based on DTI in patients with SCZ (N = 58) compared to unaffected healthy controls (Ctrl; N = 54). Investigated areas are displayed in green on the left, areas with significant lower FA values in SCZ compared to Ctrl are depicted in a red-yellow scale from the second to fourth brain images. X, y, and z indicate the brain map coordinates. **(B)** Violin plots illustrate quantification of whole brain FA based on TBSS in SCZ patients and Ctrl. FA values of the patient and Ctrl representatives that are further investigated with iOL are individually illustrated on the right. Data = Mean ± SD. T-test: ***, $p < 0.001$; ****, $p < 0.0001$.

San Diego, CA, USA, FC131-1096). The sequencing was run in NovaSeq 6000 Sequencer (Illumina).

The quality of raw reads was examined using *FastQC* (version 0.11.9), and mapped to Ensembl GRCh38 human genome by *STAR aligner* (version 2.7.10a) [49]. Next, the mapped reads were counted for corresponding genes using *featureCounts* (Version 2.0.1) [50]. The data were subsequently analyzed with R package *DESeq2* [29] to find differentially expressed genes with the threshold set for *p*-value < 0.05 and $\log_2$FoldChange >= 1.5 or $\log_2$FoldChange <= −1.5.

Given the highly correlated structure of the transcriptomic data, not only the conventional false discovery rate (FDR) correction but also an alternative *p*-value correction based on estimating the effective number of tests using the *simpleM* method [51] implemented in R package *poolr* was used. The gene expression matrix was further used for revealing relevant pathways by gene set enrichment analysis (GSEA) [52] based on the full transcriptome.

RESULTS

hiPSC-derived iOPCs/iOLs cluster with human postmortem OPCs/OLs

To prove the validity of hiPSC-derived late-stage iOPCs and iOLs generated by the previously described protocol [24], we investigated whether their transcriptional profiles cluster with that of human postmortem OPCs and OLs [27]. Unsupervised clustering analyses demonstrate that iOLs and iOPCs are related to human postmortem OLs and OPCs, while hiPSC-derived induced neuronal cells (iNeurons) and neural precursor cells (iNPCs) segregate completely from the oligodendroglial lineage and co-cluster with human postmortem neurons (Fig. 1A), indicating that these two groups of cells display similar expression across all genes. Similarly, dimensional reduction with PCA separated two major sub-clusters, iOLs/iOPCs with human postmortem OLs/OPCs and iNeurons/iNPCs with human postmortem neurons, along PC1 by 71% variance (Fig. 1B). Furthermore, the hierarchical cluster analysis of the 50 genes whose expression varied most across samples showed higher correlated gene expression profiles in iOLs and mature OL subgroups (Oligo1-6), and displayed highly upregulated expression levels of *PLP1*, *QKI*, *MBP* and *CNP*, which are the marker genes for maturating OLs (Supplementary Fig. 1). These results confirm the strong similarity of the transcriptional profiles between iOPCs/iOLs and human postmortem OPCs/OLs.

MAGMA gene enrichment analysis indicates OL gene enrichment in SCZ

Most psychiatric disorders are characterized by a complex polygenic architecture, with hundreds to thousands common genetic variants contributing only with small effects to their etiology [53]. To investigate if gene expression profiles at different differentiation stages are associated with SCZ risk, we analyzed if cell-type specific gene sets, that we have obtained by in depth scRNAseq profiling of neural cells with a previously established oligodendroglial differentiation protocol [24], are enriched in genetic associations identified in SCZ GWAS [20]. Moreover, we included two more psychiatric disorders with high heritability estimates to our analysis: bipolar disorder (BPD) [31], and autism spectrum disorder (ASD) [32]. MAGMA gene enrichment analysis demonstrated that apart from neuronal genes, genes enriched in iOL2 were associated with SCZ (Fig. 1C, Table S1). Of note, iOL1 and iOL2 are two distinct iOL clusters, with iOL2 representing a cluster of more mature OLs [24]. Moreover, iOL2 genes were also associated with BPD risk, although with a less significant *p*-value.

Identification of SCZ patients with white matter disturbances

Patient stratification was performed within the translational *Multimodal Imaging in Chronic Schizophrenia Study* (MIMICSS), the pilot study of the *Munich Clinical Deep Phenotyping* (CDP) study [33], based on DTI imaging.

TBSS of DTI revealed an altered integrity of whole skeleton white matter tracts in SCZ patients (N = 58) compared to unaffected healthy controls (Ctrl, N = 54; Fig. 2A, Table S2). In detail, within the clinical cohort, the FA of patients with SCZ was reduced compared to Ctrl (Fig. 2B **left**, SCZ = 0.466 ± 0.02 vs. Ctrl. 0.477 ± 0.014, $p < 0.001$), indicating white matter pathology in SCZ. Based on the FA stratification within the clinical cohort, we further selected seven SCZ patients with reduced FA and eight unaffected healthy controls of whose hiPSCs were available from a characterized cohort of mental illness [36] (Table S3). Within this stratified translational hiPSC cohort, stronger discrepancy in FA values was shown between the investigated groups (Fig. 2B **right**, SCZ = 0.445 ± 0.013 vs. Ctrl = 0.482 ± 0.007, $p < 0.0001$).

Oligodendroglial differentiation

To investigate if the revealed genetic association of SCZ with OLs could contribute to cellular oligodendroglial effects, we examined iOPCs/iOLs derived from the stratified SCZ patients with presumed white matter disturbances compared to Ctrl (Fig. 3A, and B; Table S3). After neural induction and subsequently induced oligodendroglial differentiation with overexpression of the OL lineage transcription factors *SOX10*, *OLIG2* and *NKX6.2* (SON), we examined the number and the morphology of $O4^+$ late-stage iOPCs/premyelinating iOLs and MBP^+ mature iOLs using an automated image analysis pipeline (Fig. 3C). All cell lines derived

A

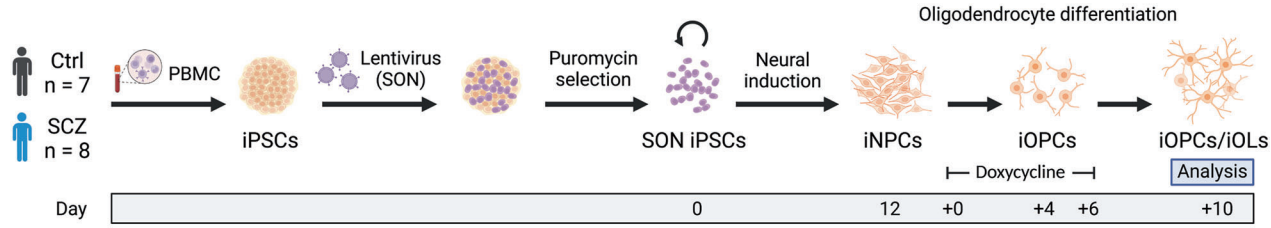

B

Sample ID	Sex	Age
Ctrl1	M	27
Ctrl2	M	35
Ctrl3	M	27
Ctrl4	M	33
Ctrl5	M	21
Ctrl6	F	34
Ctrl7	M	53
SCZ1	M	34
SCZ2	M	45
SCZ3	M	50
SCZ4	F	29
SCZ5	M	55
SCZ6	M	37
SCZ7	M	20
SCZ8	M	54

C

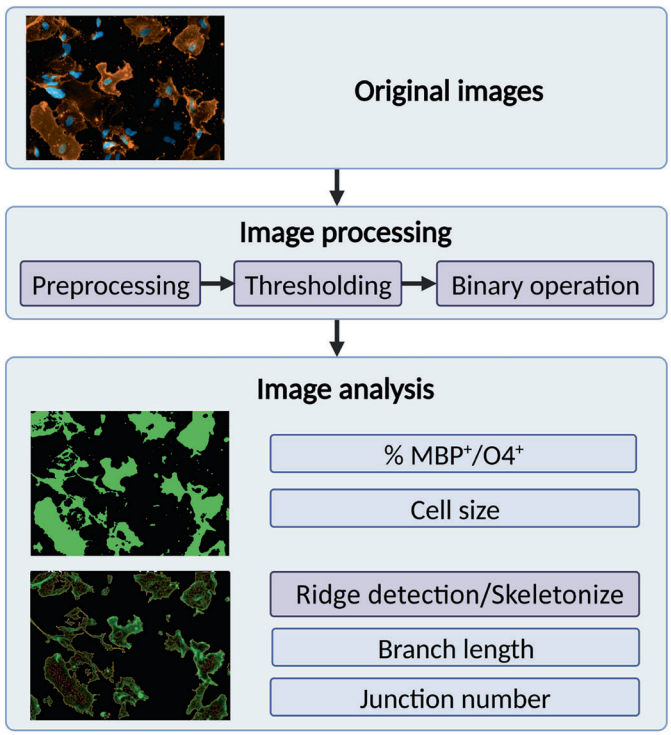

Fig. 3 Schematic overview of the experimental study design. A Overview scheme of directed iOL differentiation [24] from human peripheral blood mononuclear cell (PBMC)-derived iPSC-lines with initial neural induction to induced neural precursor cells (iNPC) and subsequent induced overexpression of the transcription factors *SOX10*, *OLIG2*, and *NKX6.2* (SON) to generate O4$^+$ induced oligodendrocyte precursor cells (iOPCs) and MBP$^+$ induced oligodendrocytes (iOL). **B** Basic cohort information. **C** Overview workflow of image analysis with Fiji. M, male; F, female; MBP, myelin basic protein.

from Ctrl and SCZ subjects were successfully differentiated into the oligodendroglial lineage, validated by the positive staining of O4 as a marker for OPCs (Supplementary Fig. 2). Maturation to iOLs was validated by the positive staining of myelin basic protein (MBP) for almost all cell lines from Ctrl and SCZ. However, one SCZ cell line (SCZ7) failed to differentiate into iOLs and was excluded from the morphological analyses of iOL (Supplementary Fig. 3).

No morphological changes of O4$^+$ iOPCs in SCZ

To investigate whether O4$^+$ iOPCs display numerical or morphological alterations between the groups, images of O4$^+$ iOPCs were processed by an automated imaging pipeline (Fig. 3C, Fig. 4A). However, neither the number (Fig. 4B) nor the average size (Fig. 4C) of O4$^+$ iOPCs was different between Ctrl and SCZ. Moreover, in the more detailed morphological quantification, we did not find significant differences in the average branch length (Fig. 4D) and the average junction number (Fig. 4E) using the image processing method *ridge detection* [44] nor by applying *skeletonize* [45] as quantification method of fine structures of the iOL morphology (Supplementary Fig. 4A-C, Supplementary Fig. 5A and B; see Table S2 for statistical parameters). Thus, by applying quantitative image analysis methods, we could not reveal significant numerical or morphological alterations in O4$^+$ iOPCs from SCZ patients compared to Ctrl.

Quantitative image analysis shows morphological alterations in MBP$^+$ iOLs from SCZ patients

To investigate whether maturating iOLs display numerical or morphological alteration, we applied a customized automated quantification pipeline to the images from MBP$^+$ mature iOLs (Fig. 3C; Fig. 5A). First, neither the average amount (Fig. 5B) nor the average cell size of MBP$^+$ iOLs (Fig. 5C) was significantly altered in SCZ cell lines. To further examine if there are morphological changes in processes and fine structures of iOLs from SCZ patients, we performed quantification analysis of the cellular morphology using the *ridge detection* approach [45]. We found significantly higher average branch length (Fig. 5D, 0.676 ± 0.151 vs. 0.624 ± 0.164, $p = 0.011$) and increased average junction

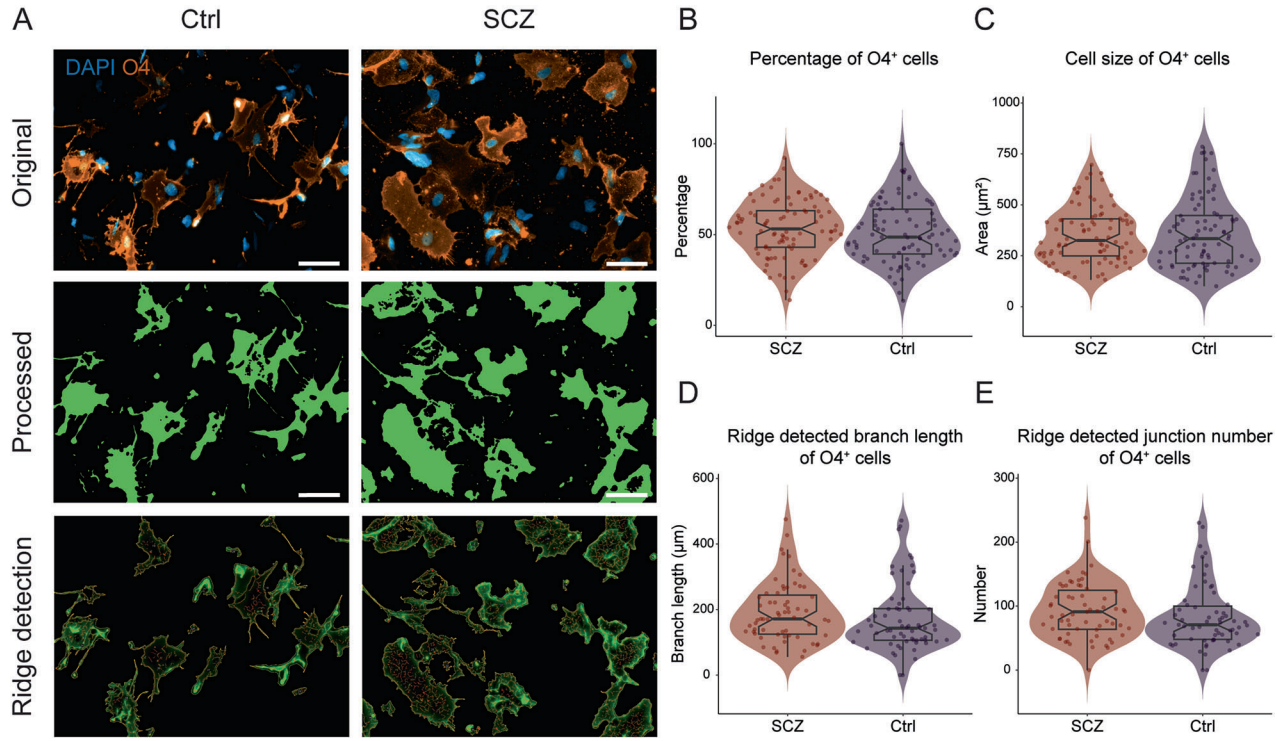

Fig. 4 Image analysis reveals neither alteration of total amount nor morphological changes in O4$^+$ oligodendrocyte precursor cells in SCZ. A Representative original (top), processed (middle), and *ridge detection* (bottom) images of O4$^+$ iOPCs from SCZ patients and Ctrl. Boxplots illustrate the **(B)** percentage of O4$^+$ cells (Ctrl, N = 7, n = 13 fields of view / cell line, vs. SCZ, N = 8, n = 10–13 fields of view / cell line) and the quantification of **(C)** average cell size (Ctrl, N = 7, n = 12–13 fields of view / cell line vs. SCZ, N = 8, n = 10–13 fields of view / cell line), as well as the morphological quantification with *ridge detection* of **(D)** average branch length and **(E)** average junction number (Ctrl, N = 7, n = 10 fields of view / cell line, vs. SCZ, N = 8, n = 8–10 fields of view / cell line). Data are based on biological independent hiPSC lines from 8 patients with SCZ and 7 Ctrl. Scale bar indicates 50 µm, Data = Mean ± SD. Mixed-effects ANOVA with group identity (SCZ-Ctrl) as the between-group factor.

number (Fig. 5E, 0.511 ± 0.162 vs. 0.409 ± 0.225, $p = 0.038$) in iOLs from SCZ patients compared to Ctrl (see Table S2 for statistical parameters). For technical validation, we performed the morphological quantification analysis with the *skeletonize* approach [44] as an alternative imaging analysis method and could confirm, although not completely equivalent, the detected morphological alterations with higher branch length (Supplementary Fig. 4D and E). Although an additional t-test comparison of group-level averages without accounting for the applied repeated measurements per individual did not reach significance, Cohen's d revealed a small effect size for branch length (Supplementary Fig. 5C, Table S2, Cohen's d = 0.37) and a medium effect size for junction number (Supplementary Fig. 5D, Table S2, Cohen's d = 0.52). Notably, while variation was observed across the hiPSC lines, the significant effects in MBP$^+$ iOLs were not driven by a few extreme cell lines but were instead representative of consistent group-level trends among hiPSC lines from patients with schizophrenia (Supplementary Fig. 5). In sum, our quantification analyses of MBP$^+$ iOLs suggest that SCZ exhibits altered cell morphology in maturating iOLs.

Transcriptomic analyses reveal disturbed pathways involved in cell signaling and replication in iOLs from SCZ patients

To investigate transcriptomic signatures in parallel to the morphological assessment, we performed bulk RNAseq of Day +10 iOLs. Dimensional reduction with PCA showed that the general genetic features of iOLs from SCZ patients and Ctrl did not differ (Fig. 6A). However, differential gene expression analysis identified 93 upregulated and downregulated genes in iOLs from SCZ patients compared to Ctrl with *p*-values < 0.05 (Fig. 6B, Table S4). Notably, only the upregulated gene *POTEM* remained significant after FDR correction, while 23 genes were significant after *p*-value adjustment applying the simpleM approach [51], that accounts for the elevated correlation within the transcriptomic data to estimate the effective number of tests. To gain more insights for the differentially expressed genes (DEGs), we conducted a Pubmed search with the keyword of the individual gene and oligodendrocyte and schizophrenia, respectively. Only few DEGs such as *APOE* were previously linked to oligodendrocyte (9 out of 93) and/or schizophrenia (18 out of 93), while the majority of DEGs have not yet been investigated for their roles in oligodendrocyte and schizophrenia (Table S5).

Given that individual genes may not fully reflect the effects of biological pathways alterations, we conducted a gene set enrichment analysis (GSEA) across all expressed genes to uncover the underlying biological information [52] of transcriptomic alterations in SCZ. For the GSEA, we applied the standard *q*-value threshold of 0.25. Most upregulated pathways in iOLs from SCZ patients are relevant to G protein-coupled receptors (GPCR) pathways, cell signaling or immune response (Fig. 6C, Table S6). While the top 10 downregulated pathways in iOLs from SCZ patients are all involved in DNA replication or cell cycles (Fig. 6D, Table S6). These findings reveal differences in expression profiles between iOLs from SCZ patients and Ctrl, and dysregulated pathways relevant to signaling mechanisms, DNA replication and cell cycle regulation are noteworthy.

DISCUSSION

In this study, we found evidence for the genetic impact of SCZ on mature iOLs and revealed morphological alterations in iOLs from patients with SCZ. First, unsupervised clustering of transcriptomes

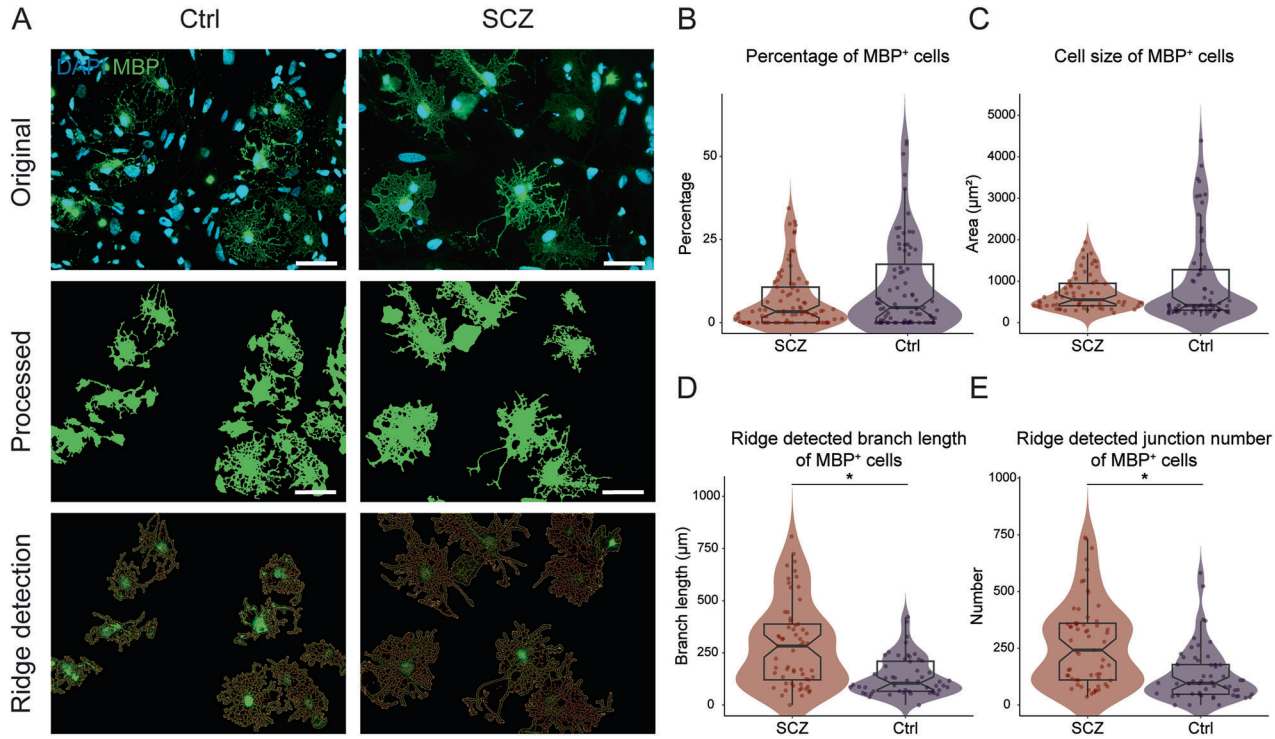

Fig. 5 Image analysis reveals morphological alterations of MBP$^+$ oligodendrocytes in SCZ. (A) Representative original (top), processed (middle), and *ridge detection* (bottom) images of MBP$^+$ iOLs from SCZ patients and Ctrl. Boxplots illustrate the **(B)** percentage of MBP$^+$ iOLs (Ctrl, N = 7, n = 9–11 fields of view / cell line, vs. SCZ, N = 7, n = 9–11 fields of view / cell line) and the **(C)** quantification of average cell size (Ctrl, N = 7, n = 8–11 fields of view / cell line, vs. SCZ, N = 7, n = 8–11 fields of view / cell line), and the morphological quantification with *ridge detection* of **(D)** average branch length and **(E)** average junction number (Ctrl, N = 7, n = 8–10 fields of view / cell line, vs. SCZ, N = 7, n = 8–10 fields of view / cell line). Data are based on biological independent hiPSC lines from 7 patients with SCZ and 7 Ctrl. Scale bar indicates 50 µm, Data = Mean ± SD. Mixed-effects ANOVA with group identity (SCZ-Ctrl) as the between-group factor: *, $p < 0.05$.

of hiPSC-derived iOPCs/iOLs and human postmortem OPCs/OLs revealed a high similarity underlining the validity of studying human oligodendroglial cells in vitro with hiPSC technology. Second, by performing gene set enrichment analyses, we found an enrichment of SCZ risk in maturating human iOLs, supporting previous findings with new technology [21, 22, 54]. This result implies that the polygenic architecture of schizophrenia could have a significant impact on OL genes, particularly those expressed on advanced stages of OL maturation. Of note, our performed gene enrichment analysis was based on hiPSC-derived cells, and that were analyzed with scRNAseq, but not single-nucleus RNA sequencing (snRNAseq) or perinuclear scRNAseq data from postmortem brains or mouse-derived samples [19, 20]. Postmortem and whole mouse brain tissues can only be processed for snRNAseq but not scRNAseq, because it is technically impossible to dissociate intact cells from postmortem brain tissues [55]. Consequently, our scRNAseq readouts of late-stage iOPCs/iOLs also contained broad cytoplasmic transcripts that could explain, at least in part, the differences between the results of our gene enrichment analysis and previous findings [19, 20]. Moreover, transcriptomic profiles from aged OLs obtained via postmortem sampling may not reflect the critical OL cell stage implicated in SCZ. Of note, in line with previous findings indicating an oligodendroglial contribution in BPD [56, 57], iOL2 genes were also slightly associated with BPD, that is genetically correlated with SCZ [58]. This result raises questions regarding the specificity of the oligodendroglial component in the genetic architecture of SCZ, suggesting a potential common mechanism for both disorders related to this cell type.

Notably, DTI imaging within our translational cohort confirmed the reduced whole brain FA as an indicator for white matter disturbances in line with a previous multicenter study of 4322 individuals that linked global FA alteration in SCZ to altered oligodendroglial microstructure [4]. Subsequently, we selected representative SCZ patient showing pronounced white matter disturbances and unaffected Ctrl samples with hiPSCs available from our translational cohort [33] for subsequent hiPSC modelling. With patient-derived iOPC/iOL monoculture from the imaging-based patient representatives, we aimed to investigate whether there are cell-autonomous disturbances of the oligodendroglial lineage in SCZ.

Interestingly, our automated morphological image analyses revealed altered morphological phenotypes in MBP$^+$ mature iOLs from SCZ patients, including longer branch length and increased junction numbers, but no measurable alterations were found in O4$^+$ late-stage iOPCs/premyelinating iOLs from SCZ patients. Importantly, only the mixed-effects ANOVA, that provides the sensitivity to detect group-level effects despite variability among individual lines, revealed the significance of morphological differences. In comparison, simpler methods such as t-tests on aggregated group-level averages did not yield statistically significant results. This discrepancy underscores the value of mixed-effects models in capturing subtle effects that might be masked by group-level variability. Thus, our findings suggest that joint polygenic mechanisms in SCZ drive cellular alterations in the oligodendroglial lineage in monocultures despite the genetic variability of the hiPSC donors [36].

However, it also highlights a limitation: mixed-effects models are more sensitive to sample size, and their robustness can be limited in studies with small cohorts. Although in line with a previous recommendation for the design of hiPSC cohort composition [37], future studies should aim to increase the sample size to address this limitation by encompassing both a greater number of patient-derived cell lines and technical

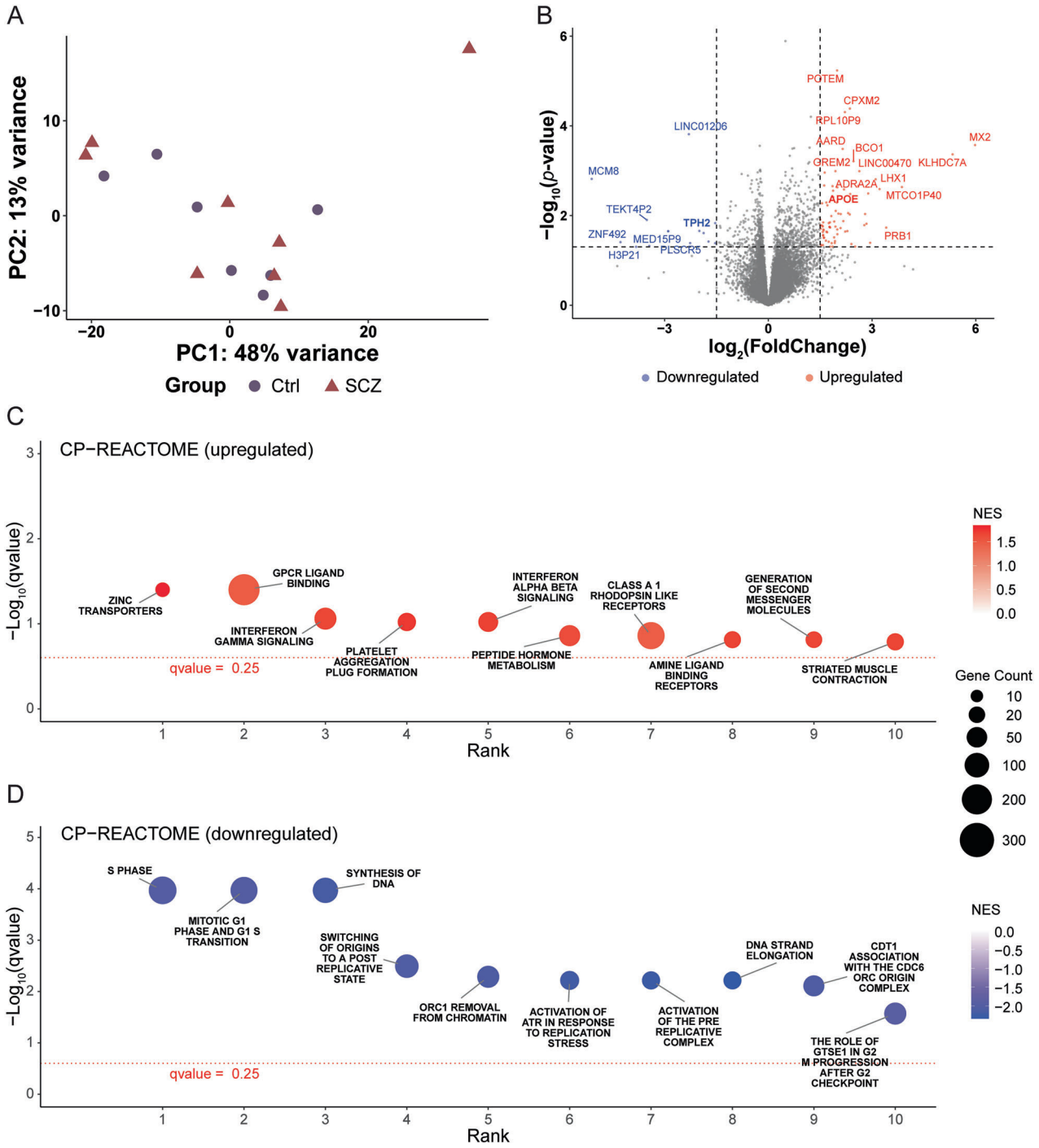

Fig. 6 Bulk RNA sequencing (RNAseq) analysis reveals significant differences in genetic profiles and pathways of SCZ oligodendrocytes. **(A)** Clustering of bulk RNAseq data with dimensionality reduction by principal component analysis (PCA). Ctrl iOLs are labeled by purple circle, and SCZ iOLs are labeled by magenta triangle **(B)** Volcano plot depicts the genes identified from differential expression analysis in SCZ iOLs versus Ctrl iOLs. Red and blue points label the genes with significantly increased or decreased expression respectively in SCZ iOLs, the dashed horizontal line corresponds to a cut-off significance threshold of p-value < 0.05, and the dashed vertical lines indicate the fold change thresholds ($\log_2$FoldChange >= 1.5 or $\log_2$FoldChange <= −1.5). Scatter plots of canonical pathway (CP) analysis show **(C)** the top 10 upregulated reactome pathways and **(D)** the top 10 downregulated reactome pathways. The number of differentially expressed genes in the pathway is represented by the circle size, and the colors of circle indicate the normalized enrichment score (NES). Data are based on biological independent hiPSC lines from 8 patients with SCZ and 7 Ctrl.

replicates. The scalability of our developed iOL differentiation protocol will allow to do this in the future [24]. Moreover, complementing morphological analyses with functional assays, such as studying myelination in more complex systems (e.g., nanofibers or neuroglial co-culturing systems in 2D, 3D, or chimeric models), could help confirm the biological relevance of the observed morphological alterations and provide a more comprehensive understanding of SCZ-associated changes in oligodendroglial function [59–61]. A further technical limitation is the presence of non-oligodendroglial cells within our directed

differentiations approach. Our previous technical study revealed around 8.8% neuronal cells present in SON-induced cells [24], suggesting the potential existence of cell types other than oligodendrocyte lineages in our cultures that could potentially influence the morphological and transcriptomic assessments of cell-autonomous effects of oligodendrocyte lineages. Furthermore, although the data were derived from biologically independent hiPSC lines from different patients with schizophrenia and the significant effects in MBP^+ iOLs reflected consistent group-level trends across these lines, it is important to note that the results were obtained from a single parallel oligodendroglial differentiation across the cohort.

Most previous results with postmortem samples showing OLs disturbances and white matter deficits in SCZ revealed the dysregulation of OL-relevant genes, declined number of OLs, and decreased volume of white matter, suggesting dysregulated oligodendrocytes and impaired myelination in the brains of adult and aged SCZ patients [4, 13, 14, 62]. A previous study also generated hiPSC-derived OLs from SCZ patients with a chemical differentiation protocol and found significantly decreased number of $O4^+$ cells after 85 days in culture [63]. Importantly, the in vitro model we used applies directed oligodendroglial differentiation with induced overexpression of lineage-determining transcription factors and may reflect different differentiation stages compared to the previous study [63]. Moreover, iPSC-based analysis investigates much earlier developmental stages compared to postmortem samples of SCZ. The increased branch length and junction numbers in SCZ iOLs likely represent an increased maturation speed that might misalign with trophic signals from developing axons, which might indirectly impact on the survival rate of OLs, known to be dependent on neuronal activity [64]. To what extent our findings of disturbed morphology of iOLs are in line with a previous study, which also revealed a prematuration phenotype in the migration of SCZ glial progenitor cells into the cortex using a humanized glial chimeric mouse model [65], should be addressed in future studies.

To investigate the transcriptomic underpinnings of the morphological alteration, we performed an RNAseq investigation. It should be noted that the DEG analysis was limited by the relatively small cohort size, and thus the identified individual genes may not fully reflect the effects of biological alteration associated with SCZ. Notably, only one gene, *POTEM*, reached significance by conservative FDR-adjusted *p*-value correction. Although not an established standard in RNAseq analysis, multiple testing correction using the simpleM approach accounting for the effective number of independent tests [51], that is becoming increasingly adopted in the field of biological psychiatry [66, 67], identified more than 20 DEGs, suggesting that overly conservative approaches may overlook disease signals in genetically complex and heterogeneous diseases such as SCZ.

To gain further insights into the biological dysfunctions contributed by the joint effects of certain gene sets in SCZ, a GSEA [52] was performed assessing all the expressed genes for pathway analysis. Thereby, several altered signaling pathways of the oligodendroglial lineage in SCZ were identified, in line with the prematuration hypothesis. The top downregulated pathways were related to replication and cell cycle regulation. Thus, the attenuation of these pathways could support a hypothesis of a prematuration phenotype in SCZ that would also fit with the abnormal morphological iOL phenotypes in SCZ as we have observed. The differential expression analysis identified several dysregulated genes in SCZ iOLs, while only a few among them were investigated in the context of oligodendrocyte and/or schizophrenia before. Among the dysregulated genes, *APOE* encodes the protein APOE which regulates lipid metabolism and myelination and plays an important role in synaptic plasticity and cognition [68]. *APOE* is not only involved in Alzheimer's disease [68] but also associated with SCZ, as studies have demonstrated its upregulation in SCZ [69].

Taken our observations together, we hypothesize that the irregular maturation of oligodendroglial cells in SCZ may impede the formation of normal neuronal networks, leading to a secondary loss of OLs and disrupted connections among brain regions and thus ultimately contributing to impaired cognitive functions. Nonetheless, we did not investigate the process of myelination and assess functions of neuronal networks, which could be addressed with electrophysiological tests of microcircuits in OLs co-cultured with neurons or in 3D cellular systems such as myelinating neurospheres or organoids [70, 71]. Another prematuration phenotype at the structural level has been described in a recent study in major depressive disorder that revealed morphological changes in a hiPSC-derived neuronal model with increased neurite length in selective serotonin reuptake inhibitor (SSRI)-non-responder subgroup [72]. Although this study is confined to a neuronal phenotype, it may relate to our study showing that a defined genetic background can cause a prematuration phenotype in a cellular model.

In summary, we validated iPSC-modelling as a robust tool for studying human oligodendroglial cells and demonstrated the importance of OLs in SCZ by revealing the enrichment of oligodendroglial genes in SCZ GWAS and morphological and transcriptomic dysregulation of SCZ-derived iOLs. These results suggest a failed maturation phenotype in oligodendroglial cells of patients with SCZ, which could contribute to the widely observed white matter pathology in SCZ. However, further investigations in escalated cohorts and functional assessments are needed to gain a more mechanical understanding of the pathophysiology of the widely observed oligodendroglial disturbances in SCZ.

DATA AVAILABILITY

Any patient-related materials that can be shared will be released via material transfer agreement and data processing agreement, conditional on proper ethics approval from the requesting institution. A subset of iPSC lines is subject to sharing constraints due to limited donor consent.

CODE AVAILABILITY

The developed, automated imaging pipeline for the morphological quantification of the oligodendroglial cells has been made publicly available (last update on 30th of April 2024): https://github.com/skoghoern/cell-coloc-and-morphology.

REFERENCES

1. Saha S, Chant D, Welham J, McGrath J. A systematic review of the prevalence of schizophrenia. PLoS Med. 2005;2:e141.
2. McCutcheon RA, Reis Marques T, Howes OD. Schizophrenia-An overview. JAMA Psychiatry. 2020;77:201–10.
3. Stępnicki P, Kondej M, Kaczor AA. Current concepts and treatments of schizophrenia. Molecules. 2018;23:2087.
4. Kelly S, Jahanshad N, Zalesky A, Kochunov P, Agartz I, Alloza C, et al. Widespread white matter microstructural differences in schizophrenia across 4322 individuals: results from the ENIGMA Schizophrenia DTI Working Group. Mol Psychiatry. 2018;23:1261–9.
5. Takahashi N, Sakurai T, Davis KL, Buxbaum JD. Linking oligodendrocyte and myelin dysfunction to neurocircuitry abnormalities in schizophrenia. Prog Neurobiol. 2011;93:13–24.
6. Millan MJ, Andrieux A, Bartzokis G, Cadenhead K, Dazzan P, Fusar-Poli P, et al. Altering the course of schizophrenia: progress and perspectives. Nat Rev Drug Discov. 2016;15:485–515.
7. Kochunov P, Coyle TR, Rowland LM, Jahanshad N, Thompson PM, Kelly S, et al. Association of white matter with core cognitive deficits in patients with schizophrenia. JAMA Psychiatry. 2017;74:958–66.
8. Seitz-Holland J, Wojcik JD, Cetin-Karayumak S, Lyall AE, Pasternak O, Rathi Y, et al. Cognitive deficits, clinical variables, and white matter microstructure in schizophrenia: a multisite harmonization study. Mol Psychiatry. 2022;27:3719–30.
9. Nave KA. Myelination and support of axonal integrity by glia. Nature. 2010;468:244–52.
10. Micu I, Plemel JR, Caprariello AV, Nave K-A, Stys PK. Axo-myelinic neurotransmission: a novel mode of cell signalling in the central nervous system. Nat Rev Neurosci. 2018;19:49–58.

11. Bacmeister CM, Barr HJ, McClain CR, Thornton MA, Nettles D, Welle CG, et al. Motor learning promotes remyelination via new and surviving oligodendrocytes. Nat Neurosci. 2020;23:819–31.
12. Steadman PE, Xia F, Ahmed M, Mocle AJ, Penning ARA, Geraghty AC, et al. Disruption of oligodendrogenesis impairs memory consolidation in adult mice. Neuron. 2020;105:150–64.e156.
13. Falkai P, Rossner MJ, Raabe FJ, Wagner E, Keeser D, Maurus I, et al. Disturbed oligodendroglial maturation causes cognitive dysfunction in schizophrenia: a new hypothesis. Schizophrenia Bull. 2023;49:1614–24.
14. Dietz AG, Goldman SA, Nedergaard M. Glial cells in schizophrenia: a unified hypothesis. Lancet Psychiatry. 2020;7:272–81.
15. Yu G, Su Y, Guo C, Yi C, Yu B, Chen H, et al. Pathological oligodendrocyte precursor cells revealed in human schizophrenic brains and trigger schizophrenia-like behaviors and synaptic defects in genetic animal model. Mol Psychiatry. 2022;27:5154–66.
16. Uranova NA, Vikhreva OV, Rachmanova VI, Orlovskaya DD. Ultrastructural alterations of myelinated fibers and oligodendrocytes in the prefrontal cortex in schizophrenia: a postmortem morphometric study. Schizophr Res Treat. 2011;2011:325789.
17. Vikhreva OV, Rakhmanova VI, Orlovskaya DD, Uranova NA. Ultrastructural alterations of oligodendrocytes in prefrontal white matter in schizophrenia: a post-mortem morphometric study. Schizophr Res. 2016;177:28–36.
18. Hilker R, Helenius D, Fagerlund B, Skytthe A, Christensen K, Werge TM, et al. Heritability of schizophrenia and schizophrenia spectrum based on the nationwide danish twin register. Biol Psychiatry. 2018;83:492–8.
19. Skene NG, Bryois J, Bakken TE, Breen G, Crowley JJ, Gaspar HA, et al. Genetic identification of brain cell types underlying schizophrenia. Nat Genet. 2018;50:825–33.
20. Trubetskoy V, Pardiñas AF, Qi T, Panagiotaropoulou G, Awasthi S, Bigdeli TB, et al. Mapping genomic loci implicates genes and synaptic biology in schizophrenia. Nature. 2022;604:502–8.
21. Goudriaan A, de Leeuw C, Ripke S, Hultman CM, Sklar P, Sullivan PF, et al. Specific glial functions contribute to schizophrenia susceptibility. Schizophrenia Bull. 2013;40:925–35.
22. Tansey KE, Hill MJ. Enrichment of schizophrenia heritability in both neuronal and glia cell regulatory elements. Transl Psychiatry. 2018;8:7.
23. Shi Y, Inoue H, Wu JC, Yamanaka S. Induced pluripotent stem cell technology: a decade of progress. Nat Rev Drug Discov. 2017;16:115–30.
24. Raabe FJ, Stephan M, Waldeck JB, Huber V, Demetriou D, Kannaiyan N, et al. Expression of lineage transcription factors identifies differences in transition states of induced human oligodendrocyte differentiation. Cells. 2022;11:241.
25. Ehrlich M, Mozafari S, Glatza M, Starost L, Velychko S, Hallmann AL, et al. Rapid and efficient generation of oligodendrocytes from human induced pluripotent stem cells using transcription factors. Proc Natl Acad Sci USA. 2017;114:e2243–52.
26. García-León JA, Kumar M, Boon R, Chau D, One J, Wolfs E, et al. SOX10 single transcription factor-based fast and efficient generation of oligodendrocytes from human pluripotent stem cells. Stem Cell Rep. 2018;10:655–72.
27. Jäkel S, Agirre E, Mendanha Falcão A, van Bruggen D, Lee KW, Knuesel I, et al. Altered human oligodendrocyte heterogeneity in multiple sclerosis. Nature. 2019;566:543–7.
28. Stuart T, Butler A, Hoffman P, Hafemeister C, Papalexi E, Mauck WM 3rd, et al. Comprehensive integration of single-cell data. Cell. 2019;177:1888–902.e1821.
29. Love MI, Huber W, Anders S. Moderated estimation of fold change and dispersion for RNA-seq data with DESeq2. Genome Biol. 2014;15:550.
30. de Leeuw CA, Mooij JM, Heskes T, Posthuma D. MAGMA: generalized gene-set analysis of GWAS data. PLoS Comput Biol. 2015;11:e1004219.
31. Mullins N, Forstner AJ, O'Connell KS, Coombes B, Coleman JRI, Qiao Z, et al. Genome-wide association study of more than 40,000 bipolar disorder cases provides new insights into the underlying biology. Nat Genet. 2021;53:817–29.
32. Grove J, Ripke S, Als TD, Mattheisen M, Walters RK, Won H, et al. Identification of common genetic risk variants for autism spectrum disorder. Nat Genet. 2019;51:431–44.
33. Krčmář L, Jäger I, Boudriot E, Hanken K, Gabriel V, Melcher J, et al. The multimodal Munich Clinical Deep Phenotyping study to bridge the translational gap in severe mental illness treatment research. Front Psychiatry. 2023;14:1179811.
34. Smith SM, Jenkinson M, Woolrich MW, Beckmann CF, Behrens TE, Johansen-Berg H, et al. Advances in functional and structural MR image analysis and implementation as FSL. Neuroimage. 2004;23:S208–219.
35. Smith SM, Jenkinson M, Johansen-Berg H, Rueckert D, Nichols TE, Mackay CE, et al. Tract-based spatial statistics: voxelwise analysis of multi-subject diffusion data. Neuroimage. 2006;31:1487–505.
36. Raabe FJ, Hausruckinger A, Gagliardi M, Ahmad R, Almeida V, Galinski S, et al. Polygenic risk for schizophrenia converges on alternative polyadenylation as molecular mechanism underlying synaptic impairment. bioRxiv [Preprint]. 2024 https://www.biorxiv.org/content/10.1101/2024.01.09.574815v1.
37. Germain PL, Testa G. Taming human genetic variability: transcriptomic meta-analysis guides the experimental design and interpretation of iPSC-Based disease modeling. Stem Cell Rep. 2017;8:1784–96.
38. Okita K, Yamakawa T, Matsumura Y, Sato Y, Amano N, Watanabe A, et al. An efficient nonviral method to generate integration-free human-induced pluripotent stem cells from cord blood and peripheral blood cells. Stem Cell. 2013;31:458–66.
39. Danecek P, McCarthy SA, HipSci C, Durbin R. A method for checking genomic integrity in cultured cell lines from SNP genotyping data. PLoS ONE. 2016;11:e0155014.
40. Bock C, Kiskinis E, Verstappen G, Gu H, Boulting G, Smith ZD, et al. Reference Maps of human ES and iPS cell variation enable high-throughput characterization of pluripotent cell lines. Cell. 2011;144:439–52.
41. Brocher J biovoxxel/BioVoxxel-Toolbox: BioVoxxel Toolbox v2.6.0. Zenodo. 2023.
42. Schindelin J, Arganda-Carreras I, Frise E, Kaynig V, Longair M, Pietzsch T, et al. Fiji: an open-source platform for biological-image analysis. Nat Methods. 2012;9:676–82.
43. Huang L-K, Wang M-JJ. Image thresholding by minimizing the measures of fuzziness. Pattern Recognit. 1995;28:41–51.
44. Steger C. An unbiased detector of curvilinear structures. IEEE Trans Pattern Anal Mach Intell. 1998;20:113–25.
45. Arganda-Carreras I, Fernández-González R, Muñoz-Barrutia A, Ortiz-De-Solorzano C. 3D reconstruction of histological sections: Application to mammary gland tissue. Microsc Res Tech. 2010;73:1019–29.
46. Peterson RA. Finding optimal normalizing transformations via bestNormalize. R J. 2021;13:294–313.
47. Yu Z, Guindani M, Grieco SF, Chen L, Holmes TC, Xu X. Beyond t test and ANOVA: applications of mixed-effects models for more rigorous statistical analysis in neuroscience research. Neuron. 2022;110:21–35.
48. Bishara AJ, Hittner JB. Testing the significance of a correlation with nonnormal data: comparison of Pearson, Spearman, transformation, and resampling approaches. Psychol Methods. 2012;17:399–417.
49. Dobin A, Davis CA, Schlesinger F, Drenkow J, Zaleski C, Jha S, et al. STAR: ultrafast universal RNA-seq aligner. Bioinformatics. 2013;29:15–21.
50. Liao Y, Smyth GK, Shi W. featureCounts: an efficient general purpose program for assigning sequence reads to genomic features. Bioinformatics. 2014;30:923–30.
51. Gao X, Starmer J, Martin ER. A multiple testing correction method for genetic association studies using correlated single nucleotide polymorphisms. Genet Epidemiol. 2008;32:361–9.
52. Subramanian A, Tamayo P, Mootha VK, Mukherjee S, Ebert BL, Gillette MA, et al. Gene set enrichment analysis: a knowledge-based approach for interpreting genome-wide expression profiles. Proc Natl Acad Sci. 2005;102:15545–50.
53. Geschwind DH, Flint J. Genetics and genomics of psychiatric disease. Science. 2015;349:1489–94.
54. Stokowy T, Polushina T, Sønderby IE, Karlsson R, Giddaluru S, Le Hellard S, et al. Genetic variation in 117 myelination-related genes in schizophrenia: Replication of association to lipid biosynthesis genes. Sci Rep. 2018;8:6915.
55. Bakken TE, Hodge RD, Miller JA, Yao Z, Nguyen TN, Aevermann B, et al. Single-nucleus and single-cell transcriptomes compared in matched cortical cell types. PLoS ONE. 2018;13:e0209648.
56. Tkachev D, Mimmack ML, Ryan MM, Wayland M, Freeman T, Jones PB, et al. Oligodendrocyte dysfunction in schizophrenia and bipolar disorder. Lancet. 2003;362:798–805.
57. Valdés-Tovar M, Rodríguez-Ramírez AM, Rodríguez-Cárdenas L, Sotelo-Ramírez CE, Camarena B, Sanabrais-Jiménez MA, et al. Insights into myelin dysfunction in schizophrenia and bipolar disorder. World J Psychiatry. 2022;12:264–85.
58. Anttila V, Bulik-Sullivan B, Finucane HK, Walters RK, Bras J, Duncan L, et al. Analysis of shared heritability in common disorders of the brain. Science. 2018;360:eaap8757.
59. Chanoumidou K, Mozafari S, Baron-Van Evercooren A, Kuhlmann T. Stem cell derived oligodendrocytes to study myelin diseases. Glia. 2020;68:705–20.
60. von der Bey M, De Cicco S, Zach S, Hengerer B, Ercan-Herbst E. Three-dimensional co-culture platform of human induced pluripotent stem cell-derived oligodendrocyte lineage cells and neurons for studying myelination. STAR Protoc. 2023;4:102164.
61. Mozafari S, Starost L, Manot-Saillet B, Garcia-Diaz B, Xu YKT, Roussel D, et al. Multiple sclerosis iPS-derived oligodendroglia conserve their properties to functionally interact with axons and glia in vivo. Sci Adv. 2020;6:eabc6983.
62. Fields RD. White matter in learning, cognition and psychiatric disorders. Trends Neurosci. 2008;31:361–70.
63. McPhie DL, Nehme R, Ravichandran C, Babb SM, Ghosh SD, Staskus A, et al. Oligodendrocyte differentiation of induced pluripotent stem cells derived from subjects with schizophrenias implicate abnormalities in development. Transl Psychiatry. 2018;8:230.

64. Rafael GA, David AL. On myelinated axon plasticity and neuronal circuit formation and function. J Neurosci. 2017;37:10023.
65. Windrem MS, Osipovitch M, Liu Z, Bates J, Chandler-Militello D, Zou L, et al. Human iPSC glial mouse chimeras reveal glial contributions to schizophrenia. Cell Stem Cell. 2017;21:195–208.e196.
66. Zack GW, Rogers WE, Latt SA. Automatic measurement of sister chromatid exchange frequency. J Histochem Cytochem. 1977;25:741–53.
67. Yap CX, Henders AK, Alvares GA, Giles C, Huynh K, Nguyen A, et al. Interactions between the lipidome and genetic and environmental factors in autism. Nat Med. 2023;29:936–49.
68. Blumenfeld J, Yip O, Kim MJ, Huang Y. Cell type-specific roles of APOE4 in Alzheimer disease. Nat Rev Neurosci. 2024;25:91–110.
69. Dean B, Laws SM, Hone E, Taddei K, Scarr E, Thomas EA, et al. Increased levels of apolipoprotein E in the frontal cortex of subjects with schizophrenia. Biol Psychiatry. 2003;54:616–22.
70. Yoon SJ, Elahi LS, Paşca AM, Marton RM, Gordon A, Revah O, et al. Reliability of human cortical organoid generation. Nat Methods. 2019;16:75–78.
71. Arlotta P, Paşca SP. Cell diversity in the human cerebral cortex: from the embryo to brain organoids. Curr Opin Neurobiol. 2019;56:194–8.
72. Vadodaria KC, Ji Y, Skime M, Paquola AC, Nelson T, Hall-Flavin D, et al. Altered serotonergic circuitry in SSRI-resistant major depressive disorder patient-derived neurons. Mol Psychiatry. 2019;24:808–18.

ACKNOWLEDGEMENTS

The authors thank all participants for their contribution, Verena Huber for her support of establishing iOPC/iOL differentiation, Jan Brocher for his help to establish customized morphological quantification analysis based on the BioVoxxel toolbox, Stefanie Behrens for her support in RNA sequencing, and Jacquie Klesing, BMedSci (Hons), Board-certified Editor in the Life Sciences (ELS), for editing assistance with the manuscript. This research was supported by the Munich Clinician Scientist Program (MCSP), FöFoLe^{Plus} (Reg.-Nr. 009, 2020) of the Faculty of Medicine, LMU Munich, Munich, Germany, to FJR; by B. Braun-Stiftung (BBST-D-20-00032, 2020) to FJR; by Friedrich-Baur-Stiftung (2019) to FJR; by "Verein zur Förderung von Wissenschaft und Forschung an der Medizinischen Fakultät der Ludwig-Maximilians-Universität München e.V." to FJR; by Boehringer Ingelheim funds to MJR; by BMBF with the EraNet project GDNF UpReg (01EW2206) to PF and AS; by the EU HORIZON-INFRA-2024-TECH-01-04 project DTRIP4H 101188432 to PF, AS and FR; by European Union's Horizon Europe Research and Innovation Programme (Psych-STRATA, grant agreement No 101057454) to SP; The study was endorsed by the Federal Ministry of Education and Research (Bundesministerium für Bildung und Forschung [BMBF]) within the initial phase of the German Center for Mental Health (DZPG) (grant: 01EE2303A, 01EE2303F to PF, AS). The study was supported by the Supplement to BMBF funding for the German Centre for Mental Health (DZPG) by the Bavarian State Ministry for Science and the Arts with the Grant for the research project 'Improving Infrastructures for DZPG and NAKO Cohorts" to PF, and DK. MHC, MS, and FJR were supported by the International Max Planck Research School for Translational Psychiatry (IMPRS-TP), Munich, Germany. FJR was supported by the Else Kröner-Fresenius Foundation (Research College "Translational Psychiatry") for the Residency/Ph.D. track at IMPRS-TP.

AUTHOR CONTRIBUTIONS

MHC, JBW, MJR, FJR designed and conceptualized the study. FJR wrote ethical proposal and performed patient recruitment. TK, LF, LR, DK, and FJR analyzed MRI imaging and performed patient stratification. VA, SG, NG, and FJR performed hiPSC reprogramming. JBW, VA, DD, and FJR established the experimental methodology of oligodendroglial differentiation from iPSC. JBW and FJR performed oligodendroglial differentiation on cohort level. JBW and FJR established and performed automated image analysis. MHC, NJ and MJR performed the RNA sequencing and analysis. Analyses were performed by MHC, JBW, MS, EB, NJ, SP and FJR. Data visualization was performed by MHC, JBW, MS, EB, NJ, SP, MJR, and FJR. Resources were provided by AS, PF, and MJR. Funding acquisition was performed by PF, AS, MJR and FJR. First draft was written by MHC, JBW, and FJR with the help of all authors. All authors contributed to review and editing of subsequent drafts and approved the final manuscript. Supervision by MJR and FJR. Project management by FJR.

FUNDING

Open Access funding enabled and organized by Projekt DEAL.

COMPETING INTERESTS

The authors have declared that there are no conflicts of interest in relation to the subject of this study. General declaration of potential conflict of interests: PF received speaker fees by Boehringer-Ingelheim, Janssen, Otsuka, Lundbeck, Recordati, and Richter and was member of advisory boards of these companies and Rovi. MS, SG, NJ and MJR are shareholders of and/or employed by Systasy Bioscience GmbH. All other authors report no potential conflicts of interest.

ADDITIONAL INFORMATION

Supplementary information The online version contains supplementary material available at https://doi.org/10.1038/s41398-025-03509-x.

Correspondence and requests for materials should be addressed to Moritz J. Rossner or Florian J. Raabe.

Supplementary information

iPSC-modelling reveals genetic associations and morphological alterations of oligodendrocytes in schizophrenia

Chang, Waldeck *et al.*

Corresponding authors:

Moritz J. Rossner, Department of Psychiatry and Psychotherapy, LMU University Hospital, LMU Munich, Nußbaumstraße 7, 80336 Munich, Germany, Mail: moritz.rossner@med.uni-muenchen.de

Florian J. Raabe, Max Planck Institute of Psychiatry, Kraepelinstr. 2-10, 80804 Munich, Germany, Mail: florian_raabe@psych.mpg.de

Supplementary tables

Table S1. Lists of gene sets for MAGMA gene enrichment analysis
Generated gene sets from scRNAseq profiling by Raabe et al. [24], characterizing different cells and differentiation stages within the established directed oligodendroglial differentiation protocol. The *p*-value of the association of each gene with SCZ risk by MAGMA analysis is annotated. See separate excel file.

Table S2. Test statistics of DTI and ICC imaging analysis
See separate excel file.

Table S3. Cohort information with unique iPSC ID on hPSCreg

Sample ID	Unique iPSC ID - hPSCreg.eu	Sex	Age
Ctrl1	PSYLMUi002-A	Male	27
Ctrl2	PSYLMUi008-A	Male	35
Ctrl3	PSYLMUi009-A	Male	27
Ctrl4	PSYLMUi011-A	Male	33
Ctrl5	PSYLMUi003-A	Male	21
Ctrl6	PSYLMUi004-A	Female	34
Ctrl7	PSYLMUi006-A	Male	53
SCZ1	PSYLMUi035-A	Male	34
SCZ2	PSYLMUi018-A	Male	45
SCZ3	PSYLMUi023-A	Male	50
SCZ4	PSYLMUi026-A	Female	29
SCZ5	PSYLMUi027-A	Male	55
SCZ6	PSYLMUi029-A	Male	37
SCZ7	PSYLMUi030-A	Male	20
SCZ8	PSYLMUi031-A	Male	54

Table S4. Lists of DESeq differentially expressed genes
See separate excel file.

Table S5. Number of articles of DESeq genes from Pubmed search
See separate excel file.

Table S6. Lists of GSEA Reactome pathways
See separate excel file.

Supplementary figures

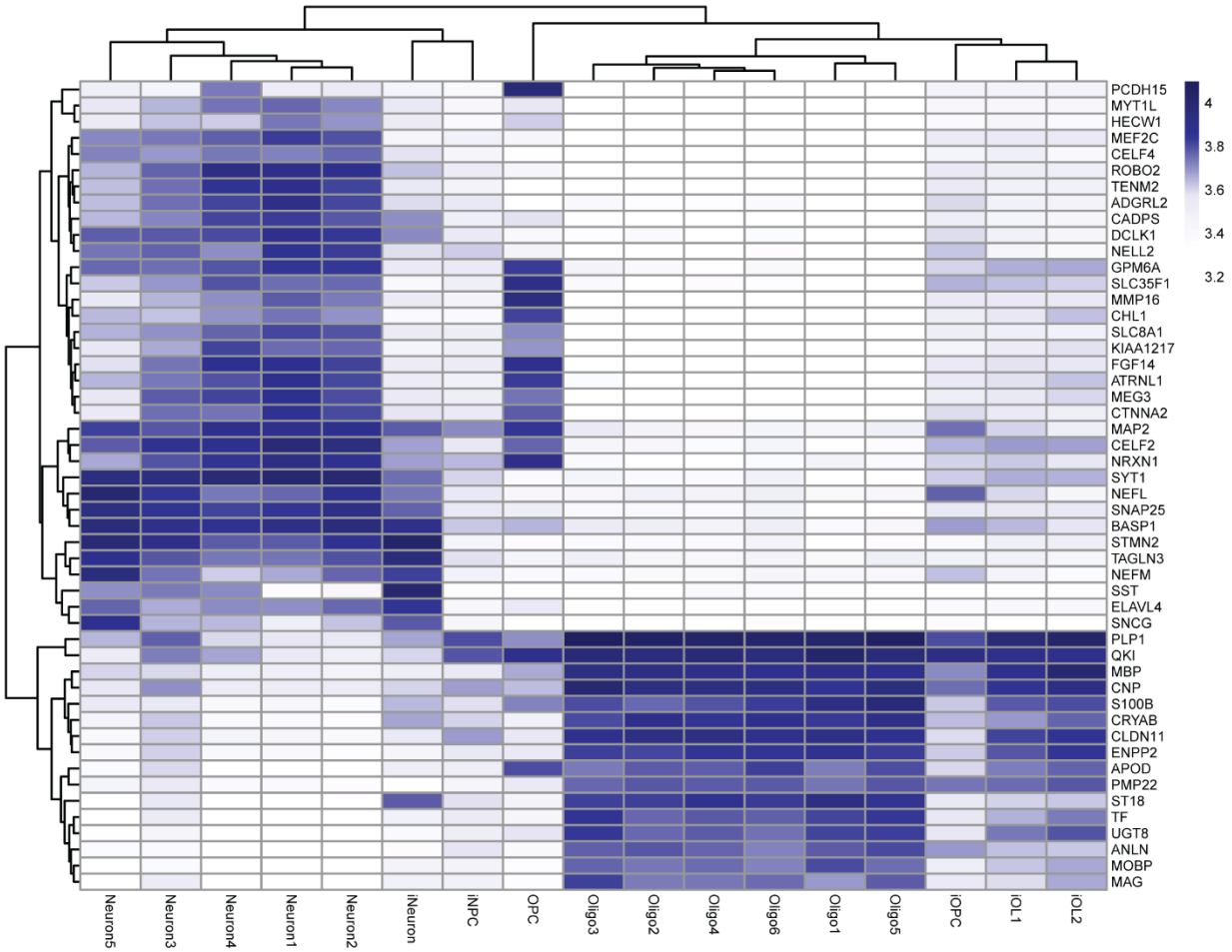

Figure S1. hiPSC-derived iOPCs and iOLs cluster with human postmortem OPCs and OLs. Heatmap of the top 50 gene hits from the clustering analysis of hiPSC-derived cells [24] with human postmortem brain cells [27]. Unsupervised hierarchical clustering was performed. *Abbreviations: OPCs, human postmortem oligodendrocyte precursor cells; Oligo1-6, human postmortem oligodendrocytes; Neuron1-5, human postmortem neurons; iOPC, hiPSC-derived OPC; iOL1-2, hiPSC-derived oligodendrocytes; iNPC, hiPSC-derived neural precursor cell; iNeuron, hiPSC-derived neurons.*

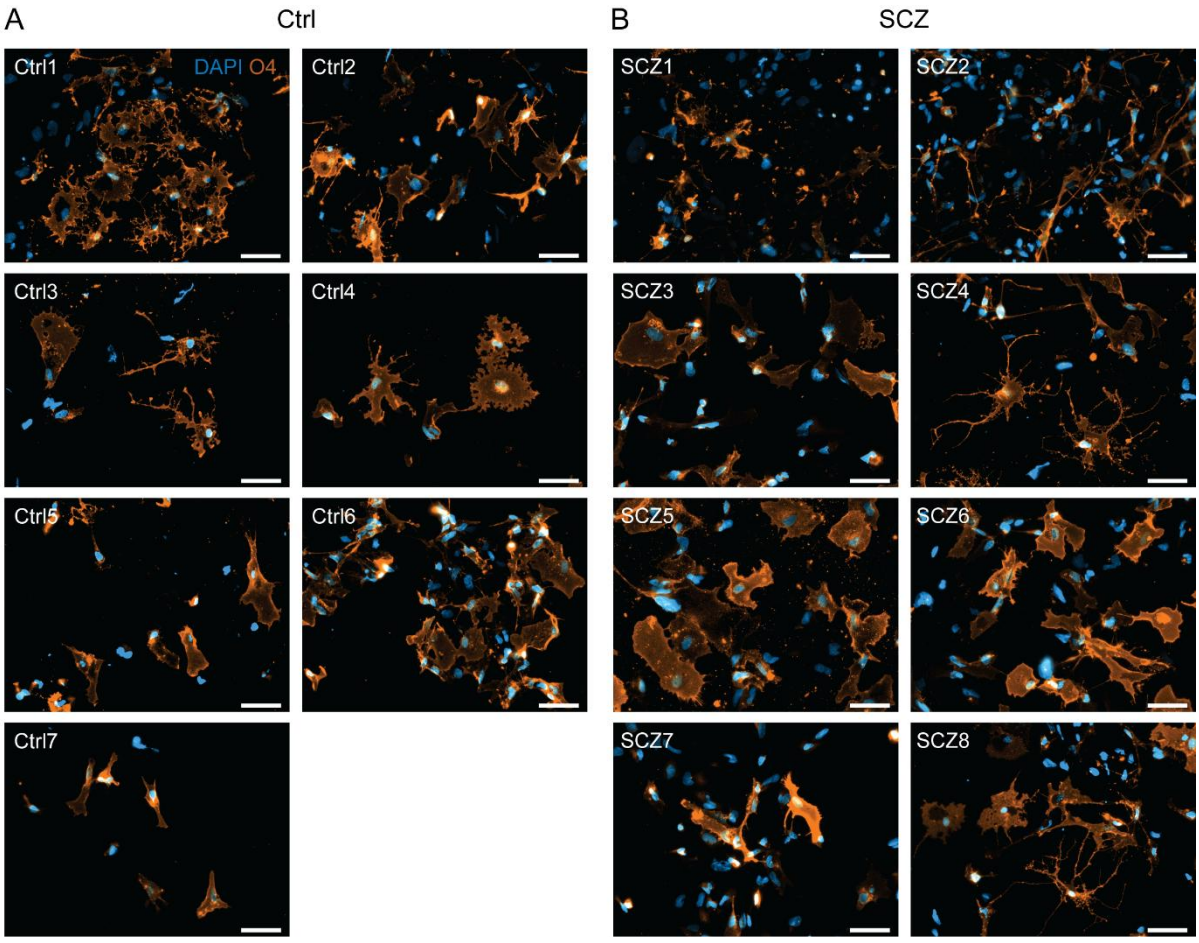

Figure S2. Oligodendroglial differentiation allows the generation of hiPSC-derived O4^{+} premature iOPCs.
(A) Representative images of control cell lines. **(B)** Representative images of SCZ cell lines. Scale bar indicates 50 µm.

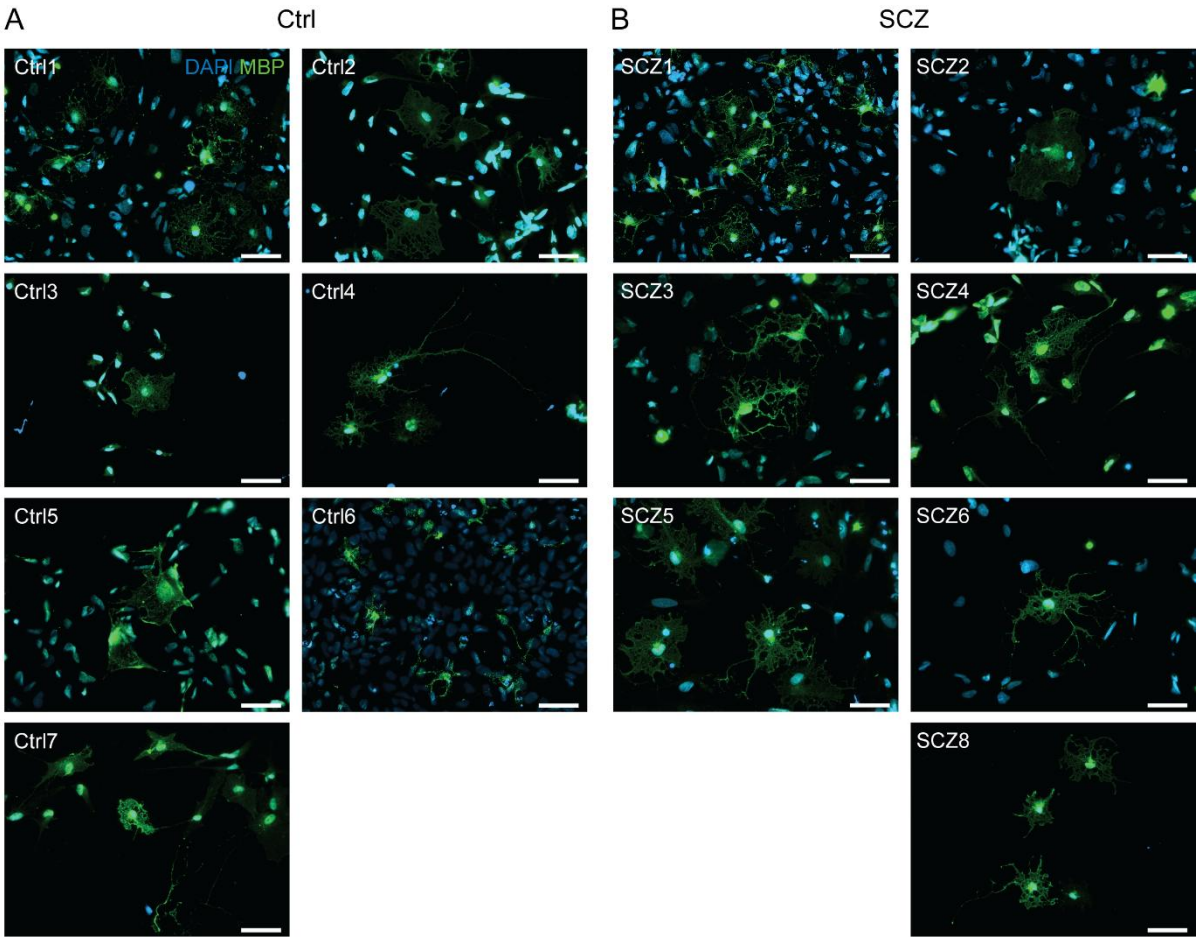

Figure S3. Oligodendroglial differentiation allows the generation of hiPSC-derived MBP$^+$ iOLs.
(A) Representative images of control cell lines. **(B)** Representative images of SCZ cell lines. Scale bar indicates 50 µm.

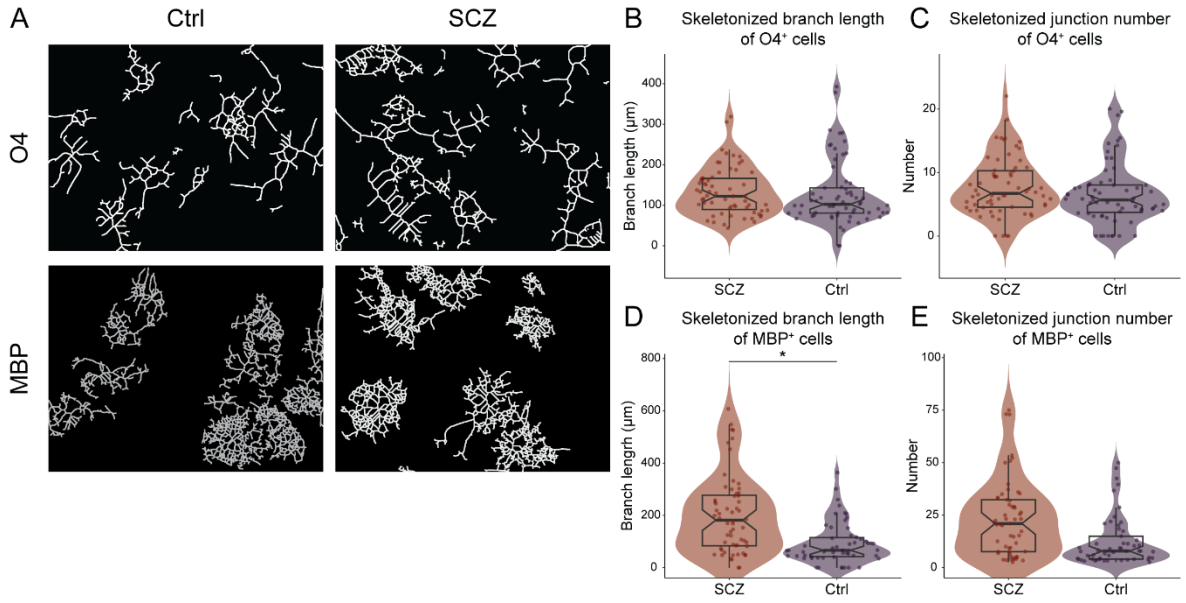

Figure S4. Validation of the morphological findings with an alternative morphological quantification analysis method.

(A) (Top) Representative image of O4$^+$ iOPCs from Ctrl and SCZ patients of **Figure 4A** after applying *skeletonize* as morphological quantification method. (Bottom) Representative image of MBP$^+$ iOLs from Ctrl and SCZ patients of **Figure 5A** after applying *skeletonize* as morphological quantification method. Boxplots illustrate quantification of **(B)** average branch length of O4$^+$ iOPCs and **(C)** average junction number of O4$^+$ iOPCs (Ctrl, N = 7, n = 10 fields of view / cell line, vs. SCZ, N = 8, n = 8-10 fields of view / cell line), and quantification of **(D)** average branch length of MBP$^+$ iOLs (Ctrl, n = 65 fields of view, N = 7, n = 8-10 fields of view / cell line, vs. SCZ, N = 7, n = 8-10 fields of view / cell line) and **(E)** average junction number of MBP$^+$ iOLs (Ctrl, N = 7, n = 8-10 fields of view / cell line, vs. SCZ, N = 7, n = 8-10 fields of view / cell line,). Data are based on biological independent hiPSC lines from 8 patients with SCZ and 7 Ctrl. Scale bar indicates 50 µm, Data = Mean ± SD. Mixed-effects ANOVA with group identity (SCZ-Ctrl) as the between-group factor: *, $p < 0.05$.

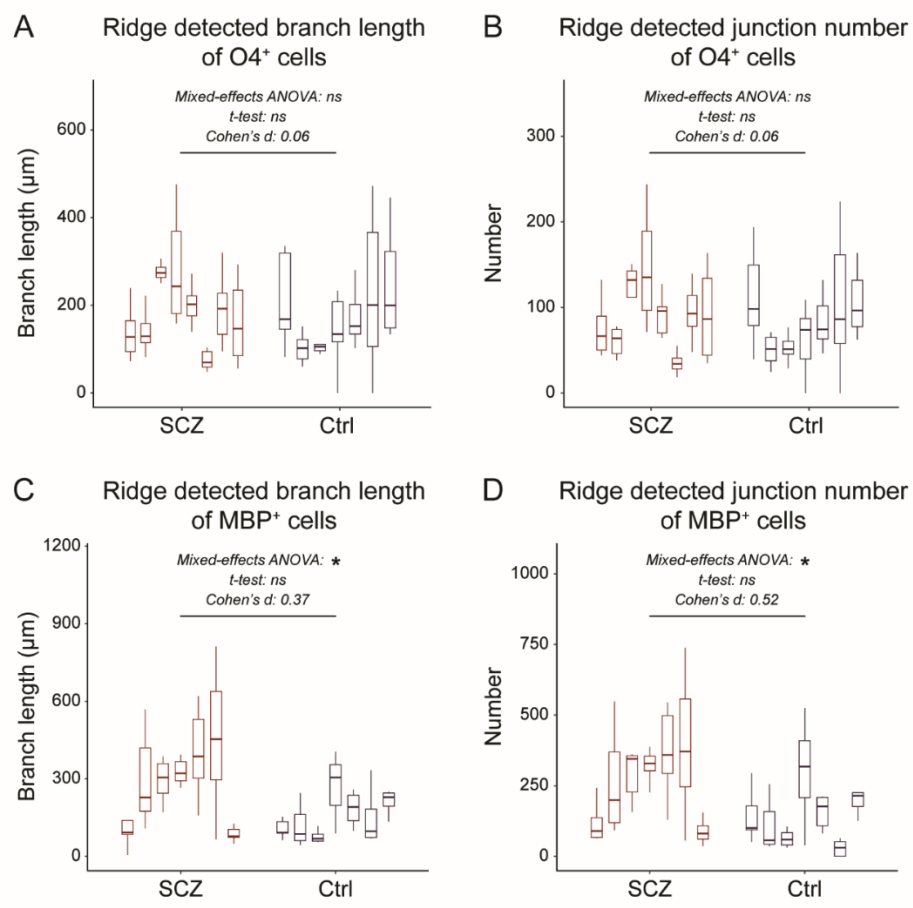

Figure S5. Morphological assessment across individual cell lines.
Boxplots illustrate **(A)** the branch length and **(B)** the junction number from each cell line of $O4^+$ iOPCs. A t-test and Cohen's d were used to compare the average values of each cell line on group level (Ctrl, N = 7, vs. SCZ, N = 8) and a mixed-effects ANOVA was performed to account for repeated measures across all images taken (Ctrl, n = 10 fields of view / cell line, vs. SCZ, n = 8-10 fields of view / cell line). Data are based on biological independent hiPSC lines from 8 patients with SCZ and 7 Ctrl. Boxplots illustrate **(C)** the branch length and **(D)** the junction number from each cell line of MBP^+ iOLs. A t-test and Cohen's d were used to compare the average values of each cell line (Ctrl, N = 7, vs. SCZ, N = 7) and a mixed-effects ANOVA was performed to account for repeated measures across all images taken (Ctrl, n = 8-10 fields of view / cell line, vs. SCZ, n = 8-10 fields of view / cell line). Data are based on biological independent hiPSC lines from 7 patients with SCZ and 7 Ctrl. ns, not significant; *, $p < 0.05$.

7. Literaturverzeichnis

1. Charlson FJ, Ferrari AJ, Santomauro DF, Diminic S, Stockings E, Scott JG, et al. Global Epidemiology and Burden of Schizophrenia: Findings From the Global Burden of Disease Study 2016. Schizophr Bull. 2018;44(6):1195-203.

2. Diseases GBD, Injuries C. Global burden of 369 diseases and injuries in 204 countries and territories, 1990-2019: a systematic analysis for the Global Burden of Disease Study 2019. Lancet. 2020;396(10258):1204-22.

3. Chong HY, Teoh SL, Wu DB, Kotirum S, Chiou CF, Chaiyakunapruk N. Global economic burden of schizophrenia: a systematic review. Neuropsychiatr Dis Treat. 2016;12:357-73.

4. McCutcheon RA, Reis Marques T, Howes OD. Schizophrenia-An Overview. JAMA Psychiatry. 2020;77(2):201-10.

5. Stepnicki P, Kondej M, Kaczor AA. Current Concepts and Treatments of Schizophrenia. Molecules. 2018;23(8).

6. Kahn RS, Sommer IE, Murray RM, Meyer-Lindenberg A, Weinberger DR, Cannon TD, et al. Schizophrenia. Nat Rev Dis Primers. 2015;1:15067.

7. Falkai P, Rossner MJ, Schulze TG, Hasan A, Brzozka MM, Malchow B, et al. Kraepelin revisited: schizophrenia from degeneration to failed regeneration. Mol Psychiatry. 2015;20(6):671-6.

8. Provencher HL, Mueser KT. Positive and negative symptom behaviors and caregiver burden in the relatives of persons with schizophrenia. Schizophr Res. 1997;26(1):71-80.

9. Orsolini L, Pompili S, Volpe U. Schizophrenia: A Narrative Review of Etiopathogenetic, Diagnostic and Treatment Aspects. J Clin Med. 2022;11(17).

10. Tandon R, Nasrallah H, Akbarian S, Carpenter WT, DeLisi LE, Gaebel W, et al. The schizophrenia syndrome, circa 2024: What we know and how that informs its nature. Schizophrenia Research. 2024;264:1-28.

11. Zamanpoor M. Schizophrenia in a genomic era: a review from the pathogenesis, genetic and environmental etiology to diagnosis and treatment insights. Psychiatr Genet. 2020;30(1):1-9.

12. Schmitt A, Falkai P, Papiol S. Neurodevelopmental disturbances in schizophrenia: evidence from genetic and environmental factors. J Neural Transm (Vienna). 2023;130(3):195-205.

13. DR W. The pathogenesis of schizophrenia: a neurodevelopmental theory. Neurology of Schizophrenia: Elsevier; 1986. p. 387-405.

14. Joo SW, Kim H, Jo YT, Ahn S, Choi YJ, Park S, et al. White matter impairments in patients with schizophrenia: A multisite diffusion MRI study. Prog Neuropsychopharmacol Biol Psychiatry. 2021;111:110381.

15. Kelly S, Jahanshad N, Zalesky A, Kochunov P, Agartz I, Alloza C, et al. Widespread white matter microstructural differences in schizophrenia across 4322 individuals: results from the ENIGMA Schizophrenia DTI Working Group. Mol Psychiatry. 2018;23(5):1261-9.

16. Castro-de-Araujo LFS, Allin M, Picchioni MM, McDonald C, Pantelis C, Kanaan RAA. Schizophrenia moderates the relationship between white matter integrity and cognition. Schizophrenia Research. 2018;199:250-6.

17. Faria AV, Zhao Y, Ye C, Hsu J, Yang K, Cifuentes E, et al. Multimodal MRI assessment for first episode psychosis: A major change in the thalamus and an efficient stratification of a subgroup. Hum Brain Mapp. 2021;42(4):1034-53.

18. Yamada S, Takahashi S, Malchow B, Papazova I, Stöcklein S, Ertl-Wagner B, et al. Cognitive and functional deficits are associated with white matter abnormalities in two independent cohorts of patients with schizophrenia. European Archives of Psychiatry and Clinical Neuroscience. 2022;272(6):957-69.

19. Kochunov P, Coyle TR, Rowland LM, Jahanshad N, Thompson PM, Kelly S, et al. Association of White Matter With Core Cognitive Deficits in Patients With Schizophrenia. JAMA Psychiatry. 2017;74(9):958-66.

20. Thomas MB, Raghava JM, Pantelis C, Rostrup E, Nielsen MO, Jensen MH, et al. Associations between cognition and white matter microstructure in first-episode antipsychotic-naive patients with schizophrenia and healthy controls: A multivariate pattern analysis. Cortex. 2021;139:282-97.

21. Seitz-Holland J, Wojcik JD, Cetin-Karayumak S, Lyall AE, Pasternak O, Rathi Y, et al. Cognitive deficits, clinical variables, and white matter microstructure in schizophrenia: a multisite harmonization study. Mol Psychiatry. 2022;27(9):3719-30.

22. Voineskos AN, Felsky D, Kovacevic N, Tiwari AK, Zai C, Chakravarty MM, et al. Oligodendrocyte genes, white matter tract integrity, and cognition in schizophrenia. Cereb Cortex. 2013;23(9):2044-57.

23. Li F, Lui S, Yao L, Ji GJ, Liao W, Sweeney JA, et al. Altered White Matter Connectivity Within and Between Networks in Antipsychotic-Naive First-Episode Schizophrenia. Schizophr Bull. 2018;44(2):409-18.

24. Yang M, Gao S, Zhang X. Cognitive deficits and white matter abnormalities in never-treated first-episode schizophrenia. Transl Psychiatry. 2020;10(1):368.

25. Raabe FJ, Slapakova L, Rossner MJ, Cantuti-Castelvetri L, Simons M, Falkai PG, et al. Oligodendrocytes as A New Therapeutic Target in Schizophrenia: From Histopathological Findings to Neuron-Oligodendrocyte Interaction. Cells. 2019;8(12).

26. Falkai P, Rossner MJ, Raabe FJ, Wagner E, Keeser D, Maurus I, et al. Disturbed Oligodendroglial Maturation Causes Cognitive Dysfunction in Schizophrenia: A New Hypothesis. Schizophr Bull. 2023;49(6):1614-24.

27. Kandel ER. Principles of neural science: Elsevier, Amsterdam, 1985, ISBN 0-444-00944-2. Journal of Affective Disorders. 1985;9(3):303.

28. Stadelmann C, Timmler S, Barrantes-Freer A, Simons M. Myelin in the Central Nervous System: Structure, Function, and Pathology. Physiological Reviews. 2019;99(3):1381-431.

29. Fields RD. Myelination: an overlooked mechanism of synaptic plasticity? Neuroscientist. 2005;11(6):528-31.

30. Nave KA, Asadollahi E, Sasmita A. Expanding the function of oligodendrocytes to brain energy metabolism. Curr Opin Neurobiol. 2023;83:102782.

31. Xin W, Chan JR. Myelin plasticity: sculpting circuits in learning and memory. Nat Rev Neurosci. 2020;21(12):682-94.

32. Simons M, Gibson EM, Nave KA. Oligodendrocytes: Myelination, Plasticity, and Axonal Support. Cold Spring Harb Perspect Biol. 2024;16(10).

33. de Faria O, Jr., Gonsalvez DG, Nicholson M, Xiao J. Activity-dependent central nervous system myelination throughout life. J Neurochem. 2019;148(4):447-61.

34. Jakovcevski I, Filipovic R, Mo Z, Rakic S, Zecevic N. Oligodendrocyte development and the onset of myelination in the human fetal brain. Front Neuroanat. 2009;3:5.

35. He L, Lu QR. Coordinated control of oligodendrocyte development by extrinsic and intrinsic signaling cues. Neurosci Bull. 2013;29(2):129-43.

36. Yu Y, Casaccia P, Lu QR. Shaping the oligodendrocyte identity by epigenetic control. Epigenetics. 2010;5(2):124-8.

37. Elbaz B, Popko B. Molecular Control of Oligodendrocyte Development. Trends Neurosci. 2019;42(4):263-77.

38. Yalçın B, Monje M. Microenvironmental interactions of oligodendroglial cells. Dev Cell. 2021;56(13):1821-32.

39. Kochunov P, Hong LE. Neurodevelopmental and Neurodegenerative Models of Schizophrenia: White Matter at the Center Stage. Schizophrenia Bulletin. 2014;40(4):721-8.

40. Paus T, Keshavan M, Giedd JN. Why do many psychiatric disorders emerge during adolescence? Nature Reviews Neuroscience. 2008;9(12):947-57.

41. Dietz AG, Goldman SA, Nedergaard M. Glial cells in schizophrenia: a unified hypothesis. Lancet Psychiatry. 2020;7(3):272-81.

42. Uranova NA, Vikhreva OV, Rachmanova VI, Orlovskaya DD. Ultrastructural alterations of myelinated fibers and oligodendrocytes in the prefrontal cortex in schizophrenia: a postmortem morphometric study. Schizophr Res Treatment. 2011;2011:325789.

43. Vikhreva OV, Rakhmanova VI, Orlovskaya DD, Uranova NA. Ultrastructural alterations of oligodendrocytes in prefrontal white matter in schizophrenia: A post-mortem morphometric study. Schizophr Res. 2016;177(1-3):28-36.

44. Yu G, Su Y, Guo C, Yi C, Yu B, Chen H, et al. Pathological oligodendrocyte precursor cells revealed in human schizophrenic brains and trigger schizophrenia-like behaviors and synaptic defects in genetic animal model. Mol Psychiatry. 2022;27(12):5154-66.

45. Schmitt A, Steyskal C, Bernstein H-G, Schneider-Axmann T, Parlapani E, Schaeffer EL, et al. Stereologic investigation of the posterior part of the hippocampus in schizophrenia. Acta neuropathologica. 2009;117:395-407.

46. Schmitt A, Tatsch L, Vollhardt A, Schneider-Axmann T, Raabe FJ, Roell L, et al. Decreased oligodendrocyte number in hippocampal subfield CA4 in schizophrenia: a replication study. Cells. 2022;11(20):3242.

47. Falkai P, Raabe F, Bogerts B, Schneider-Axmann T, Malchow B, Tatsch L, et al. Association between altered hippocampal oligodendrocyte number and neuronal circuit structures in schizophrenia: a postmortem analysis. Eur Arch Psychiatry Clin Neurosci. 2020;270(4):413-24.

48. Falkai P, Steiner J, Malchow B, Shariati J, Knaus A, Bernstein H-G, et al. Oligodendrocyte and interneuron density in hippocampal subfields in schizophrenia

and association of oligodendrocyte number with cognitive deficits. Frontiers in Cellular Neuroscience. 2016;10:78.

49. Sullivan PF, Kendler KS, Neale MC. Schizophrenia as a Complex Trait: Evidence From a Meta-analysis of Twin Studies. Archives of General Psychiatry. 2003;60(12):1187-92.

50. Polderman TJC, Benyamin B, de Leeuw CA, Sullivan PF, van Bochoven A, Visscher PM, et al. Meta-analysis of the heritability of human traits based on fifty years of twin studies. Nature Genetics. 2015;47(7):702-9.

51. Chou IJ, Kuo CF, Huang YS, Grainge MJ, Valdes AM, See LC, et al. Familial Aggregation and Heritability of Schizophrenia and Co-aggregation of Psychiatric Illnesses in Affected Families. Schizophr Bull. 2017;43(5):1070-8.

52. Hilker R, Helenius D, Fagerlund B, Skytthe A, Christensen K, Werge TM, et al. Heritability of Schizophrenia and Schizophrenia Spectrum Based on the Nationwide Danish Twin Register. Biol Psychiatry. 2018;83(6):492-8.

53. Trubetskoy V, Pardinas AF, Qi T, Panagiotaropoulou G, Awasthi S, Bigdeli TB, et al. Mapping genomic loci implicates genes and synaptic biology in schizophrenia. Nature. 2022;604(7906):502-8.

54. Tansey KE, Hill MJ. Enrichment of schizophrenia heritability in both neuronal and glia cell regulatory elements. Translational Psychiatry. 2018;8(1).

55. Rummel CK, Gagliardi M, Ahmad R, Herholt A, Jimenez-Barron L, Murek V, et al. Massively parallel functional dissection of schizophrenia-associated noncoding genetic variants. Cell. 2023;186(23):5165-82 e33.

56. Forrest MP, Zhang H, Moy W, McGowan H, Leites C, Dionisio LE, et al. Open Chromatin Profiling in hiPSC-Derived Neurons Prioritizes Functional Noncoding Psychiatric Risk Variants and Highlights Neurodevelopmental Loci. Cell Stem Cell. 2017;21(3):305-18 e8.

57. Baresic A, Nash AJ, Dahoun T, Howes O, Lenhard B. Understanding the genetics of neuropsychiatric disorders: the potential role of genomic regulatory blocks. Mol Psychiatry. 2020;25(1):6-18.

58. Hall J, Bray NJ. Schizophrenia Genomics: Convergence on Synaptic Development, Adult Synaptic Plasticity, or Both? Biological Psychiatry. 2022;91(8):709-17.

59. Raabe FJ, Hausruckinger A, Gagliardi M, Ahmad R, Almeida V, Galinski S, et al. Polygenic risk for schizophrenia converges on alternative polyadenylation as molecular mechanism underlying synaptic impairment. bioRxiv. 2024.

60. Bakken TE, Hodge RD, Miller JA, Yao Z, Nguyen TN, Aevermann B, et al. Single-nucleus and single-cell transcriptomes compared in matched cortical cell types. PLOS ONE. 2018;13(12):e0209648.

61. Goudriaan A, de Leeuw C, Ripke S, Hultman CM, Sklar P, Sullivan PF, et al. Specific glial functions contribute to schizophrenia susceptibility. Schizophr Bull. 2014;40(4):925-35.

62. Skene NG, Bryois J, Bakken TE, Breen G, Crowley JJ, Gaspar HA, et al. Genetic identification of brain cell types underlying schizophrenia. Nat Genet. 2018;50(6):825-33.

63. Bergstrom JJD, Fu MM. Dysregulation of myelination-related genes in schizophrenia. J Neurochem. 2024;168(9):2227-42.

64. Takahashi N, Sakurai T, Davis KL, Buxbaum JD. Linking oligodendrocyte and myelin dysfunction to neurocircuitry abnormalities in schizophrenia. Prog Neurobiol. 2011;93(1):13-24.

65. Roussos P, Haroutunian V. Schizophrenia: susceptibility genes and oligodendroglial and myelin related abnormalities. Front Cell Neurosci. 2014;8:5.

66. Takahashi K, Tanabe K, Ohnuki M, Narita M, Ichisaka T, Tomoda K, et al. Induction of pluripotent stem cells from adult human fibroblasts by defined factors. Cell. 2007;131(5):861-72.

67. Shi Y, Inoue H, Wu JC, Yamanaka S. Induced pluripotent stem cell technology: a decade of progress. Nat Rev Drug Discov. 2017;16(2):115-30.

68. Räsänen N, Tiihonen J, Koskuvi M, Lehtonen Š, Koistinaho J. The iPSC perspective on schizophrenia. Trends Neurosci. 2022;45(1):8-26.

69. Windrem MS, Osipovitch M, Liu Z, Bates J, Chandler-Militello D, Zou L, et al. Human iPSC Glial Mouse Chimeras Reveal Glial Contributions to Schizophrenia. Cell Stem Cell. 2017;21(2):195-208 e6.

70. McPhie DL, Nehme R, Ravichandran C, Babb SM, Ghosh SD, Staskus A, et al. Oligodendrocyte differentiation of induced pluripotent stem cells derived from subjects with schizophrenias implicate abnormalities in development. Transl Psychiatry. 2018;8(1):230.

71. Wang S, Bates J, Li X, Schanz S, Chandler-Militello D, Levine C, et al. Human iPSC-derived oligodendrocyte progenitor cells can myelinate and rescue a mouse model of congenital hypomyelination. Cell stem cell. 2013;12(2):252-64.

72. Douvaras P, Fossati V. Generation and isolation of oligodendrocyte progenitor cells from human pluripotent stem cells. Nature protocols. 2015;10(8):1143-54.

73. Krčmář L, Jäger I, Boudriot E, Hanken K, Gabriel V, Melcher J, et al. The multimodal Munich Clinical Deep Phenotyping study to bridge the translational gap in severe mental illness treatment research. Front Psychiatry. 2023;14:1179811.

Danksagung

An dieser Stelle möchte ich meinen tief empfundenen Dank all jenen aussprechen, die zum Gelingen dieser kumulativen Dissertation beigetragen haben. Ohne ihre vielfältige Unterstützung wäre die vorliegende Arbeit nicht möglich gewesen.

Zuallererst möchte ich meinem Betreuer, Dr. Dr. Florian Raabe, für die exzellente und umfassende Betreuung danken. Von den initialen Gesprächen 2019 bishin zu unzähligen Stunden gemeinsamer Datenauswertung und Diskussion – Florian begleitete mich stets mit unschätzbarem wissenschaftlichem Rat. Seine Fähigkeit, tiefgreifende Diskussionen anzustoßen, strukturiertes Arbeiten zu fördern und sein offenes Ohr für meine Anliegen prägten meine wissenschaftliche Entwicklung.

Ebenso danke ich dem gesamten Team des Labors für Molekulare Neurobiologie für die kollegiale Atmosphäre und gegenseitige Hilfsbereitschaft. Insbesondere Nadja Gabellini für ihre unermüdliche Unterstützung bei den Zellkulturen, gerade in kritischen Phasen. Mein Dank gilt auch Prof. Dr. Moritz Rossner für seinen erfahrenen wissenschaftlichen Führungsstil, seine konstruktiv-kritischen Fragen, die mich zur sorgfältigen Reflexion meiner Ergebnisse anregten, und seine stetige Ermutigung, neugierig zu bleiben und Fragen zu stellen.

Mein besonderer Dank gilt zudem meiner Doktormutter, Prof. Dr. Andrea Schmitt, ohne deren Unterstützung und Vertrauen dieses Projekt nicht möglich gewesen wäre. Sowie Herrn PD Dr. Dietmar Spengler, der durch sein Mitwirken im Betreuungskomitee zum Gelingen des Projekts beigetragen hat.

Die Forschungsarbeit wurde durch das FöFoLe-Programm der LMU München ermöglicht, wofür ich sehr dankbar bin. Besonderer Dank gilt hier Prof. Dr. Endres, der mich auf dieses Programm aufmerksam machte und zur Teilnahme inspirierte.

Schließlich gilt mein tiefster Dank meinen Freunden. Ihr unerschütterlicher Rückhalt, ihre Geduld und Verständnis, besonders in herausfordernden Phasen, waren eine immense Stütze.